University of Alberta

A Metabolic Basis for Vascular Remodeling in Pulmonary Arterial Hypertension

by

Gopinath Sutendra

A thesis submitted to the Faculty of Graduate Studies and Research
in partial fulfillment of the requirements for the degree of

Doctor of Philosophy
in
Experimental Medicine

Department of Medicine

Spring 2012
Edmonton, Alberta

Abstract

In Pulmonary Arterial Hypertension (PAH), pro-constrictive, pro-proliferative and anti-apoptotic diatheses converge to produce contraction and excessive proliferation of pulmonary artery smooth muscle cells (PASMC), a hallmark of PAH-vascular remodeling. The increased afterload causes right ventricular (RV) dysfunction and early death. The resistance to apoptosis is critical in PAH pathology, resembling the suppressed apoptosis in cancer, but its cause is unknown. We show that the apoptosis resistance is associated with a specific metabolic phenotype and remodeled mitochondria, the organelles in which metabolism and apoptosis regulation converge. Suppression of the mitochondria-based glucose oxidation (GO) and increased glycolysis (Gly) in the cytoplasm is associated with an anti-apoptotic state in many diseases including cancer. We show that reversing this mitochondrial remodeling in PAH PASMCs using dichloroacetate (DCA, an inhibitor of the mitochondrial pyruvate dehydrogenase kinase, PDK, the gatekeeper of carbohydrate influx in the mitochondria) resulted in increased GO/Gly ratio and induction of apoptosis in PAH but not normal cells, reversing the vascular remodeling in vivo. In addition, we investigated the role of fatty acids (FA), the other major mitochondrial fuel in this metabolic remodeling. FA oxidation (FAO) and GO, both occurring at the mitochondria, are kept in balance through the "Randle cycle" feedback: GO is activated (through PDK inhibition) when FAO is suppressed. We set to explore the role of FAO in the mitochondrial and vascular remodeling in PAH and we discovered that in mice which lack malonyl-CoA-decarboxylase (MCD), an enzyme that activates FAO in mitochondria, produced a normal phenotype that was completely resistant to PAH. We also showed that similar to DCA, the FAO inhibitor trimetazidine (TMZ), also reversed established PAH in-vivo. We then investigated the signals resulting in suppressed mitochondrial function. We show that the endoplasmic reticulum (ER; an

organelle that facilitates protein folding) and mitochondria unit was disrupted. Disruption of the unit resulted in decreased transfer of lipids and calcium from the ER to the mitochondria, resulting in mitochondrial suppression. In addition we showed that hypoxia induced ER stress, resulting in increased expression of the reticulon protein Nogo. Induction of Nogo resulted in an increased in the distance between the ER and mitochondria unit, mitochondrial suppression and apoptosis resistance. Nogo-deficient mice were resistant to the development of PAH. Finally, we explored the role of inflammation (which can also induce ER stress) in PAH and showed that treatment with Etanercept (a TNFα inhibitor) increased mitochondrial activity and attenuated an inflammatory rodent model of PAH. In conclusion, this work provides evidence for a generalized metabolic dysfunction in the pathogenesis of PAH which can be therapeutically targeted with mitochondrial activating drugs.

Acknowledgements

I would like to express my greatest thanks, gratitude and appreciation to my supervisor and mentor Dr. Evangelos Michelakis. His mentorship, both in science and life has helped shape me into the person I am today. Without the encouragement of my parents, Suren and Anandhi Sutendra, to instill a great inspiration for learning I never would have been able to achieve this level of education. The love and support from my wife Sheri and sons Naden and Tevan have helped in my completion of this PhD. Finally, I would like to thank all of the people who have helped in the publications resulting from this work. Specifically I would like to acknowledge Peter Dromparis and Sebastien Bonnet, who without their help and friendship, none of this would have occurred.

Table of Contents

Chapter Five

Chapter One

Introduction

Introduction

Pulmonary Arterial Hypertension (PAH) is clinically defined as an increase in mean pulmonary arterial (PA) pressure above 25 mmHg at rest or 30 mmHg upon exertion. The accompanied elevation in pulmonary vascular resistance (PVR) increases the afterload of the right ventricle (RV), eventually leading to RV dysfunction and premature death. Current therapies for PAH remain poor despite major advances in the field over the recent years [1-6]. A major limitation continues to be selectivity, as all therapies currently used for PAH therapy can affect the systemic vessels, which generally remain intact in PAH. In fact, all of the therapies currently used for PAH treatment (endothelin antagonists, sildenafil, prostacyclin analogues) were originally designed for use in the systemic vessels [7] and only upon their failure were tried in PAH where they have shown limited effectiveness [8].

Effective therapy for PAH is difficult, in part, because of the complexity of the disease. PAH shares many components of degenerative diseases (early loss of endothelial cells), neoplasia (apoptosis resistance and proliferation within the PA wall) and inflammation. Standard drug developments are designed to target single abnormal molecular pathways or develop selective vaccines in an attempt to reverse the disease. One example is the selectivity of imatinib (Gleevec) for chronic myelogenous leukemia (CML). CML has mutations in the *bcl-abl* gene resulting in dysregulated activity of tyrosine kinase [9-12]. Imatinib selectivity induces apoptosis and cell growth arrest in *Bcr-Abl*-positive leukemia cells [13, 14] and is therefore used as the primary therapy for CML. In many similarities to cancer, PAH does not have one specific abnormal pathway that can be therapeutically targeted, making drug development a difficult task. Many pathways in this disease are abnormal, suggesting that targeting one pathway would have limited effectiveness. Instead it may be most beneficial to target pathways where all of these abnormal molecular pathways converge (i.e. mitochondria, discussed below).

In addition, emerging therapies need to be selective to the pulmonary circulation. Therapies that are not selective to the pulmonary circulation (i.e. current therapies for PAH) may result in vasodilatation of the systemic vessels or induction of apoptotis in systemic arteries (which remain normal in PAH) or adversely affect the RV. One unique feature of the pulmonary circulation is hypoxic pulmonary vasoconstriction (HPV). While most systemic vessels dilate in response to hypoxia in an attempt to improve oxygen delivery, the pulmonary circulation contracts in order to maintain ventilation-perfusion match. The mechanism of HPV appears to be intrinsic to the mitochondria as these organelles are the major oxygen sensors of the cells. Interestingly mitochondrial diversity exists between systemic and pulmonary SMC potentially offering a therapeutic target selective to the pulmonary circulation [15]. In addition, inhaled drugs would also allow for selective delivery to the pulmonary circulation, however, developing such drugs could be challenging.

Finally, the right ventricle (RV) needs to be addressed in emerging therapies for PAH. Therapies that have negative inotropic or cardio-toxic effects on the RV, even though beneficial to the pulmonary circulation would be impractical. The ideal PAH therapy needs to be characterized by **1.)** selectivity, **2.)** targeting proximal molecular pathways unique to PAH, and **3.)** have a beneficial role on the RV. *This chapter will give a general overview of PAH and potential selective targets to the disease.*

1.1. PAH and Degeneration: Endothelial Cell Loss is an Early Event in PAH

It is now well recognized that endothelial dysfunction is an early event in the pathogenesis of PAH [16]. There are multiple factors responsible for endothelial cell dysfunction and apoptosis including; environmental factors (virus, inflammation, anorexigens, etc) and genetic factors (predisposition to loss-of-function mutations in bone morphogenetic protein receptor II, BMPRII). Endothelial dysfunction early in the pathogenesis of PAH results in increased vascular tone (decreased endothelial-derived

vasodilators (PGI_2 and NO)), increased PASMC proliferation (exposure of vascular media to growth factors (PDGF, EGF etc)) and has recently been implicated in the early loss of distal pulmonary arteries and capillaries [17].

Rescuing these endothelial cells early in the development of PAH would be ideal in preventing advancement of the disease, however its ability to reverse the disease may be limited. Where as, inducing apoptosis in proliferating PAEC and PASMC would be the ideal therapy in reversal of PAH (discussed below and the focus of Chapter 2). An emerging strategy early in the pathogenesis of PAH would be to promote regeneration of these 'lost' distal vessels. Stem cells are beginning to show promise in PAH as a recent study showed mesenchymal stem cells over-expressing eNOS, given intratracheally, attenuated monocrotaline-induced PAH [18]. Endothelial-like progenitor cells (ELPC) given to rats with established monocrotaline-PAH had improved survival [17]. In fact, in a recent clinical trial, endothelial precursor cells were given to 25 PAH patients with improvement shown in the clinical parameters of the 6 minute walk, pulmonary artery pressure, pulmonary vascular resistance and cardiac output [19]. The fact that these stem cells can be given selectively to the pulmonary circulation (via delivery through the jugular vein) and with positive early results suggests promise.

1.2. PAH and Similarities to Neoplasia

The resistance to apoptosis is a critical feature in PAH pathology. This includes well-described abnormalities involving the endothelium, smooth muscle cells (SMC), fibroblasts and the interstitial matrix within the vascular wall. The cause of the pro-proliferative and anti-apoptotic diathesis that occurs in PAH is unknown. Several mechanisms have been proposed, however, they do not appear to be related to each other. Loss-of-function mutations of the bone morphogenetic protein receptor-II, that have been identified in ~70% of familial PAH and ~10% of IPAH, results in resistance to apoptosis in PASMC [20, 21]. Interestingly, similar mutations have been seen in neoplastic

diseases [22]. In addition, the vascular media of PAH patients and animals also express the cancer marker survivin [23].

Endothelial dysfunction and apoptosis are well recognized in the early stages of PAH [16, 24, 25], resulting in an increase in vasoconstrictors (endothelin, thromboxane etc.) and a decrease in vasodilators (prostacyclin and nitric oxide). This eventually results to an increase in intracellular calcium (Ca^{++}) in PASMC, which not only increases vascular tone (vasoconstriction) but also increases PASMC proliferation [26]. Mitochondrial remodeling [27-30] and activation of the epidermal growth factor receptor [31] (EGFR) have been linked to the apoptosis resistance in PAH. As mentioned above, current PAH therapies are based on the "vasodilatation" hypothesis, however, it is now apparent that PAH is not a disease of vascular tone but an imbalance of enhanced vascular proliferation and apoptosis resistance, similar to neoplasia.

The PAH field is now beginning to expand potential therapies by targeting proliferation and apoptosis resistance in PAH. Interestingly, a number of experimental therapies have been shown to reverse established animal PAH by decreasing proliferation and inducing apoptosis in the vascular wall of PAs. Such diverse therapies include dichloroacetate (DCA) [29, 30], sildenafil [32], cyclosporine [28], imatinib [33], simvastatin [34], elastase inhibitors [35] and epidermal growth factor (EGF) receptor inhibitors [31]. Many of these therapies selectivity target the mitochondria, transcription factors intrinsic to the disease or abnormal receptor-mediated pathways. However, this dissertation will focus on mitochondria-targeting therapies as selective treatment for PAH.

1.3. Mitochondria and Apoptosis-Resistance

As in cancer [36, 37], the apoptosis resistance in PASMC may be due to mitochondrial remodeling. We have shown that the mitochondrial membrane potential ($\Delta\Psi m$) is hyperpolarized in both human and animal PAH [23, 27]. The *hyperpolarized*

mitochondrial ΔΨm may be marker for apoptosis resistance since mitochondrial depolarization is critical in initiating the intrinsic apoptotic-pathway. The mitochondrial transition pore (MTP) is a mega-channel complex, which includes the ΔΨm sensitive voltage-dependent anion channel (VDAC) [38]. When the mitochondrial ΔΨm is hyperpolarized, as in PAH PASMC, VDAC is closed. This confines pro-apoptotic mediators that can activate caspases (cytochrome c) or lyse nuclear DNA (apoptosis-inducing factor (AIF)) to the matrix of the mitochondria.

The *mitochondrial ΔΨm could also be an index for mitochondrial respiration*, as the proton efflux from the electron transport chain (ETC) contributes to ΔΨm [39]. The ETC is comprised of five-mega-complexes (I-V), which transfers electrons down a redox gradient. As electrons flow down the ETC, H^+ are transferred out of the inner mitochondrial membrane at complexes I, III and IV, creating the mitochondrial ΔΨm (~ -200mV). ATP synthase (complex V) uses the energy stored as ΔΨm to phosphorylate ADP into ATP. A small percentage of the electrons flowing down the ETC, results in the production of mitochondria-derived reactive oxygen species (mROS), mostly from complexes I and III. In the presence of mitochondrial manganese superoxide dismutase (MnSOD), superoxide is dismutated to the more stable H_2O_2, which can diffuse out of the mitochondria and regulate remote redox-sensitive targets like plasmalemmal voltage gated K^+ channels (Kv) [40, 41] or transcription factors, like hypoxia-inducible factor-1α (HIF1α) [42-44]. Oxidation of Kv channels (like Kv1.5, which is the most prominent Kv channel in PASMC [45]) by mROS results in their opening which leads to the efflux of K^+ down its concentration gradient. When the mitochondria are hyperpolarized, there is a decrease in mitochondrial respiration and consequently a decrease in the production of mROS. The inhibition/closure of Kv channels has two important effects. **First**, there is an accumulation of intracellular K^+ which results in **a)** tonic inhibition of caspases,[46] **b)**

inhibition on the formation of the apoptosome [47] and **c)** regulation of metabolic enzymes that can influence mitochondrial ΔΨm (like pyruvate dehydrogenase kinase (PDK)) [48]. **Second**, the PASMC plasma membrane depolarizes, opening voltage-gated Ca^{++} channels and increasing intracellular Ca^{++}. This results in **a)** vasoconstriction, **b)** proliferation and **c)** activation of critical transcription factors that promote apoptosis resistance and proliferative remodeling. For example, we recently showed that nuclear factor of activated T-cells (NFAT), which is regulated by Ca^{++} and metabolic signals, is activated in human and animal PAH [28]. Activation of NFAT results in downregulation of Kv1.5 and upregulation of the anti-apoptotic bcl-2. Inhibition of NFAT by VIVIT (*in-vitro*) or cyclosporine (*in-vivo*) reverses established PAH. In addition to NFAT, HIF-1α activation, which is also dependent on the mitochondrial signals, mROS [43] and the diffusible Krebs' cycle product α-ketoglutarate [49] has been shown to be activated in PAH PASMC [27].

In summary, the phenotype of PAH PASMC, which is similar to cancer, is characterized by hyperpolarized ΔΨm, decreased mROS, inhibition and down-regulation of Kv1.5, increased intracellular Ca^{++} and activation of critical transcription factors like NFAT and HIF-1α, which sustains the proliferative and apoptosis-resistant remodeling. In addition to apoptosis resistance, primary mitochondrial abnormalities could also alter cell metabolism, a change that is well documented in cancer.

1.4. Metabolism and PAH, Lessons from Cancer

Most solid tumors are characterized by enhanced glycolysis (Gly), a metabolic pathway that favors apoptosis-resistance. Glucose, the substrate for Gly, enters the cell via glucose transporters (GLUT) located on the plasma membrane where it is metabolized to pyruvate. In aerobic conditions, pyruvate is further metabolized in the mitochondria to acetyl-CoA through glucose oxidation (GO), a process that requires a

complex of enzymes on the inner mitochondrial membrane called pyruvate dehydrogenase (PDH). Acetyl-CoA can enter the Krebs' cycle and produces the electron donors NADH and FADH, which "donate" their electrons to the ETC producing ATP. In cancer, when the mitochondria are hyperpolarized, there is a decrease in mitochondrial respiration resulting in decreased oxidative phosphorylation (ATP production). To compensate, cells shift their metabolism from the mitochondria (the site of GO) to the cytoplasm (site of Gly), where pyruvate is metabolized to lactate by lactate dehydrogenase (LDH). Gly produces some ATP (net gain of 2 ATP/glucose) but is far less efficient than GO (~35 ATP/glucose). In an attempt to compensate, these cells **a)** increase the expression of critical enzymes in Gly (like hexokinase) and **b)** increase glucose uptake into the cell. For this purpose, positron emission tomography (PET) imaging is a powerful diagnostic tool for cancer detection and progression. Interestingly, PET imaging also reveals higher uptake of glucose in PAH lungs compared with controls [50].

In cancer, increased Gly also gives these cells a proliferative advantage, as many of the glycolytic enzymes directly suppress apoptosis [51]. PDK is a critical enzyme that inhibits PDH and pyruvate metabolism in the mitochondria, resulting in mitochondrial hyperpolarization. We have shown that inhibition of this enzyme with the orally available dicholoroacetate (DCA) depolarizes mitochondrial $\Delta\Psi m$, increases respiration and the GO/Gly ratio, and selectively induces apoptosis in a variety of cancer cell lines [37] and patients with glioblastoma (GBM; a highly aggressive form of brain cancer [36]). A similar metabolic profile has been identified in PAH cells [50, 52] with DCA reversing all established models of PAH in-vitro and in-vivo [29, 30, 52]. *This dissertation will expand on the role of metabolism in PAH in Chapter 2.*

The metabolic changes that occur in cancer and PAH could be explained by primary mitochondrial changes. For example, HIF1α, (which is regulated by

mitochondrial signals) can repress mitochondrial metabolism (GO, by increasing the expression of PDK) and promote Gly (by increasing the expression of GLUTs and glycolytic enzymes) [43]. Although mitochondrial remodeling is seen as an early event in PAH patho-biology, the cause for the initial remodeling is unknown.

A critical organelle that can directly regulate mitochondrial function, including $\Delta\Psi m$, is the endoplasmic reticulum (ER). The ER is a central organelle for lipid synthesis, protein folding and protein maturation. Recent evidence has shown that the ER and mitochondria form an intact and highly -regulated unit.

1.5. Endoplasmic Reticulum-Mitochondria Unit

The ER and mitochondria are in very close proximity to each other, in fact, there is strong evidence that the two organelles communicate [53]. The form of this communication is still a matter of debate, however, many mechanisms have been proposed. Anchoring proteins, mitochondrial-associated ER-membranes (MAM) and the localization of these organelles have all been identified as being critical in the ER-mitochondria unit. Regardless of the components in the ER-mitochondria network, the communication between the two organelles is important for the vital exchange of lipids, Ca^{++} and ATP. The mitochondrial-ATP is necessary for post-translational modifications and Ca^{++}-ATPase that occur at the ER, while the Ca^{++} and lipids produced by the ER are important for **a)** Ca^{++}-dependent enzymes and **b)** mitochondrial integrity. Therefore, a functional disruption of this unit could have multiple effects on protein folding, translation and trafficking (all of which occur in the ER) and cell signaling, energy production (i.e. metabolism) and apoptosis (which occur in the mitochondria). Functional disruption of the ER-mitochondria unit could occur through either **a)** direct alterations in MAM, **b)** critical proteins that regulate the exchange of lipids and Ca^{++} and **c)** directly reshaping the ER and increasing its distance from the mitochondria.

MAM consists of many proteins, including, metabolic enzymes, ion channels, molecular chaperones, vesicular-sorting proteins and electron transport chain proteins [reviewed in [54]]. Knock-down of the vesicular-sorting protein PACS-2 (phospho-acidic cluster sorting protein 2) results in uncoupling of the mitochondria from the ER and mitochondrial fragmentation [55]. In addition to mitochondrial fragmentation, PACS-2 depletion induces ER stress, but not apoptosis. In fact, in response to the apoptosis inducer staurosporine, PACS-2 deficient cells had increased survival rates and apoptosis resistance compared to controls cells [55]. Another MAM protein, mitofusin 2, stabilizes the contact between the ER and mitochondria. Knockdown of this protein results in ER-mitochondria uncoupling and decreased mitochondrial Ca^{++} uptake [56]. Finally, the Ca^{++}-binding chaperone proteins calnexin and calreticulin, components of MAM [57, 58], also contribute to Ca^{++} transport into the mitochondria [54]. Similar to mitofusin-2-deficient cells, fibroblasts isolated from calreticulin-deficient embryos have impaired Ca^{++} release [59, 60]. This suggests that targeting MAM proteins can directly disrupt the ER-mitochondria unit, decreasing mitochondrial Ca^{++} uptake and suppressing apoptosis.

Alternatively, the ER-mitochondrial unit can be disrupted by targeting other proteins that regulate Ca^{++} transfer and lipid biosynthesis [54]. For example, cells lacking the ER-regulated inositol-triphosphate receptor ($InsP_3R$) had diminished Ca^{++} uptake in the mitochondria resulting in mitochondrial and metabolic remodeling of lymphocytes [53]. $InsP_3R$-knock-out cells had decreased mitochondrial respiration, increased intracellular Ca^{++} and enhanced proliferation, similar to PAH PASMC.

Finally, the ER-mitochondria unit may also be disrupted by spatial separation of the two organelles, which can occur through direct changes in ER shape. Several proteins, including mitofusin-2 and the reticulon protein Nogo, can regulate ER shape [56, 61, 62]. For example, lack of mitofusin-2 results in decreased reticular ER [56], while over-expression of Nogo results in parallel or bundled ER tubules [62]. Since the

mitochondria-Ca^{++}-uniporter (MCU), the major regulator of mitochondrial Ca^{++} uptake, has a low affinity for Ca^{++} [63], it depends on large localized Ca^{++} pools facilitated by close ER-mitochondrial proximity [63]. Thus, changes in ER shape could directly contribute to the mitochondrial and metabolic remodeling that occurs in PAH.

In summary, alterations in MAM, critical proteins involved in Ca^{++} exchange or changes in ER shape may disrupt the communication between the ER and the mitochondria. In this case, it would be predicted that the decrease in ER-Ca^{++} to the mitochondria would result in mitochondrial hyperpolarization (in part due to inhibition of the Ca^{++}-sensitive PDH or the Krebs cycle enzymes α-ketoglutarate- and isocitrate-dehydrogenase [64, 65]), decreased mROS, decreased Kv channel expression and activity, increased intracellular Ca^{++} and activation of critical transcription factors (such as NFAT and HIF-1α), which all result in suppressed apoptosis and enhanced proliferation (i.e. the PAH phenotype). Although this cellular phenotype is common to human and all animal models of PAH, a comprehensive understanding of the pathogenesis of PAH remains elusive. Interestingly, many seemingly unrelated factors attributed to PAH pathogenesis also result in ER stress.

1.6. Endoplasmic Reticulum Stress

ER stress is associated with many diseases including, metabolic diseases like diabetes [66, 67] and developmental and neurological diseases, like Alzheimers [68]. The fact that PAH has recently been linked to diabetes [69], further supports a potential link between ER stress and PAH. Many of the pathologies of PAH are associated with ER stress. Genetic mutations to BMPRII, which characterize ~10% of PAH patients, can result in accumulation of unfolded protein aggregates and trigger ER stress [70]. Viruses, such as HIV [71, 72] and Herpes [73, 74], hypoxia or inflammation all of which contribute to a significant portion of PAH pathology are heavily implicated in ER stress [67]. Recently, notch-3 over-expression has been implicated in the pathogenesis PAH

[75] and ER stress [76]. Therefore, all forms of PAH may have a similar converging pathway resulting in ER stress potentially providing a therapeutic target towards the complexity of the disease.

ER stress functions to maintain homeostasis under instances of cellular stress. Initially, ER stress provides pro-survival signals and attenuates protein synthesis in an attempt to reduce the load of unfolded proteins. However, if cellular stress is excessive or irreversible, then ER stress initiates apoptosis (reviewed in [67]). In all cases, there are three components that result in the initial cascade of events. **1)** Activation of the transcription factor activating transcription factor-6 (ATF6), which binds to the ER stress response elements II and I and regulates the expression of many genes including reticulon proteins, such as Nogo [77]. **2)** Activation of the protein kinase PERK, which represses protein synthesis [68] and **3)** activation of the endonuclease IRE1 which activates the transcription factor XBP1 and regulates gene expression of many ER chaperone proteins [78]. Evidence suggests that activation of ATF6 may favor the proliferative and anti-apoptotic diathesis involved with ER stress [67]. Interestingly ATF6 has shown redox-sensitivity, potentially linking mitochondrial dysfunction to ATF6 activation.

1.7. ATF6 Regulation of Nogo, a Pro-Survival Pathway

Nogo is a reticulon protein that was first identified in the central nervous system [61]. Nogo exists in three isoforms, Nogo-A, B and C. While Nogo-A is produced by oligodendrocytes in the nervous system [61], Nogo-B is present in the vascular endothelium, SMCs and macrophages [79, 80]. There is emerging evidence that Nogo is expressed during ER stress as part of a rescue response, that could contribute toward cell survival [81]; whereas the absence of Nogo (or inadequate expression) during sustained ER stress might facilitate apoptosis. Nogo has been implicated in a number of diseases including Alzheimer's disease and cancer [82]. Although advances in Nogo signaling through its extracellular receptor have been made in recent years, our understanding of

the intracellular role of Nogo is lacking. One of the initial events during ER stress, regardless of the specific cause, is the activation of ATF6. It was recently shown that activation of ATF6 leads to more than a 9-fold increase in Nogo transcription, supporting the notion that Nogo is important during ER stress [77]. Recently, ATF6 was shown to be redox-sensitive [83-86]. The reducing agents DTT (dithiothreitol) and hypoxia both result in activation of ATF6 [83-86], supporting the notion that primary mitochondrial signals could result/sustain ATF6 activation and Nogo expression. *This dissertation will expand in Chapter 3 on the role of Nogo and the ER-mitochondria unit in PAH.*

1.8. PAH and Inflammation, An Emerging Concept

Recent evidence suggests a strong involvement of inflammation in PAH [87]. However, it still remains the most understudied aspect of the disease [88, 89]. Interestingly, PAH patients characterized with generalized activation of inflammation (connective tissue diseases (CTD), HIV) have the worst prognosis in clinical outcomes [90]. Some improvement has been seen in this subset of patients with immunosuppressive therapy further emphasizing the relevance of inflammation [91]. Several studies have identified several types of inflammatory infiltrates [92] (T-cells [93], B-cells [94], macrophages [94], neutrophils [95] and mast cells [96]) in the plexiform lesions of severe PAH patients. While these reports are compelling, they offer only correlative support for a role of chronic inflammation in disease progression and the precise role of inflammatory cells in the pathophysiology of PAH is still unknown. $CD4^+$ cells have been shown to have a protective role in PAH, as depletion of these cells caused significant PAH [95], however, injection of a soluble antigen enticing a Th2 response caused significant occlusive lesions, similar to those seen in PAH patients [97].

Many inflammatory cytokines are increased and associated in the pathogenesis of PAH. Interlukin-1 (IL-1) was excessively produced in monocrotaline-induced PAH rats [98]. Antagonizing the IL-1 receptor in these rats reduced PAH associated RV

hypertrophy [98]. The circulating cytokine fractalkine and its cognate receptor were both shown to be elevated in IPAH patients and were associated with heightened smooth muscle cell proliferation [99]. Circulating pro-inflammatory cytokines IL-4 [95], IL-6 [92], stromal-derived-factor-1 (SDF-1), monocyte chemoattractant protein-1 (MCP-1) and tumor necrosis factor-α (TNF-α) [100] are also elevated in PAH. The HIV Nef (negative factor) was recently found in endothelial cells from patients with HIV PAH [101] while human herpes virus 8 has been found in human plexogenic lesions [74]. Viral proteins may be able to influence vascular remodeling by triggering, in addition to ER-stress, inflammatory responses or have direct effects on vascular cells and the extracellular matrix [102].

We recently showed the transcription factor nuclear factor of activated T-cells (NFAT) is activated in circulating inflammatory cells and PASMCs in PAH patients [28]. NFAT can regulate the expression of many inflammatory mediator and cytokine genes [28, 103]. Interestingly, the levels of NFAT mRNA in the buffy coat of a small cohort of patients with PAH were higher than patients with secondary pulmonary hypertension and normal controls [28] suggesting that NFAT may be a potential biomarker for PAH. It is possible that many patients diagnosed with iPAH may have some underlying mild inflammation or viral infection. *This compelling evidence suggests that anti-inflammatory therapies need to be considered in treatment of PAH and will be the focus of Chapter 4 of this dissertation.*

1.9. A Generalized Metabolic Dysfunction in PAH

It is becoming increasingly recognized that PAH patients are associated with a generalized metabolic dysfunction, which includes insulin resistance[104]. However, the mechanisms resulting in the altered metabolism observed in PAH remains unknown. One explanation and the focus of this dissertation is suppressed mitochondrial function, which as explained above can result in the activation of many pro-proliferative and anti-

apoptotic transcription factors, like NFAT and HIF1α. However, there is increasing evidence that global changes to metabolism can also occur by inhibition of the master transcription factor peroxisome proliferator-activated receptor (PPAR). PPAR is a group of nuclear receptor proteins that function as master transcription factors in regulating the expression of many genes involved in differentiation, metabolism and cancer [105, 106]. PPARγ agonists were originally developed for the therapy of type 2 diabetes-mellitus. They have been shown to decrease vascular SMC proliferation by inhibiting the degradation of the CDK inhibitor p21[107]. In a recent study, insulin resistance and low plasma adiponectin levels were suggested as potential risk factors in PAH. In this study PPARγ agonists were shown to be beneficial in the treatment of a PAH model of $Apoe^{-/-}$ mice, with the PPARγ agonist rosiglitazone reversing PAH and increasing adiponectin levels[69]. More recently, it was shown that disruption of the PPARγ-mediated regulation of apelin resulted in apoptosis of PAEC and proliferation of PASMCs, further supporting the activation of PPARγ in PAH. [[108]. In addition, PPAR has also been linked to mitochondrial biogenesis[109], which could potentiate the overall mitochondrial suppression we discuss in this dissertation. Although mitochondrial suppression and inhibition of PPAR are both implicated in metabolic dysfunction and PAH, each component maybe regulated differently depending on the pathology of PAH. For example, PPAR inhibition may be critical in PAH associated with BMPRII mutations, while primary mitochondrial suppression may be the initial triggers in PAH associated with inflammation or viruses. Thus, targeted approaches to increase either mitochondrial function or PPAR activation may be viable selective PAH therapies.

As mentioned above, endothelial cell dysfunction is an early event in PAH. Interestingly, more aggressive, proliferative clones of endothelial cells have been shown to replace native damaged endothelial cells contributing to the plexiform lesions observed

in PAH [110]. These “replacement” endothelial cells also have a very similar metabolic prolife to cancer cells (i.e. glycolytic)[50], suggesting that metabolic-altering drugs that target either the mitochondria or PPAR may be selective to these cells as well.

Recent evidence also suggests that mitochondrial-targeting metabolic drugs may also be beneficial to RVH as well, which appears to follow a similar metabolic remodeling (i.e. a glycolytic shift) [111]. For example, DCA or fatty acid oxidation inhibitors, increased RV contractility [111, 112]. This suggests that targeting the mitochondria in PAH may be beneficial to both the remodeled PA vasculature and the RV. It is critical that emerging therapies for PAH must be beneficial to the PA-RV unit. Currently, the pyruvate dehydrogenase activator dichloroacetate (DCA), is being tested in a Phase I clinical trial at the University of Alberta and Imperial College (NCT01083524).

References

1. Archer S, Rich S (2000) Primary pulmonary hypertension: a vascular biology and translational research "Work in progress". Circulation 102: 2781-2791

2. Farber HW, Loscalzo J (2004) Pulmonary arterial hypertension. N Engl J Med 351: 1655-1665

3. Humbert M, Morrell NW, Archer SL, Stenmark KR, MacLean MR, Lang IM, Christman BW, Weir EK, Eickelberg O, Voelkel NF, Rabinovitch M (2004) Cellular and molecular pathobiology of pulmonary arterial hypertension. J Am Coll Cardiol 43: 13S-24S

4. McLaughlin VV, McGoon MD (2006) Pulmonary arterial hypertension. Circulation 114: 1417-1431

5. Rabinovitch M (2005) Cellular and molecular pathobiology of pulmonary hypertension conference summary. Chest 128: 642S-646S

6. Tuder RM, Marecki JC, Richter A, Fijalkowska I, Flores S (2007) Pathology of pulmonary hypertension. Clin Chest Med 28: 23-42, vii

7. Archer SL, Michelakis ED (2006) An evidence-based approach to the management of pulmonary arterial hypertension. Curr Opin Cardiol 21: 385-392

8. Macchia A, Marchioli R, Marfisi R, Scarano M, Levantesi G, Tavazzi L, Tognoni G (2007) A meta-analysis of trials of pulmonary hypertension: a clinical condition looking for drugs and research methodology. Am Heart J 153: 1037-1047

9. Deininger MW, Goldman JM, Melo JV (2000) The molecular biology of chronic myeloid leukemia. Blood 96: 3343-3356

10. Faderl S, Talpaz M, Estrov Z, O'Brien S, Kurzrock R, Kantarjian HM (1999) The biology of chronic myeloid leukemia. N Engl J Med 341: 164-172

11. Thijsen S, Schuurhuis G, van Oostveen J, Ossenkoppele G (1999) Chronic myeloid leukemia from basics to bedside. Leukemia 13: 1646-1674

12. Westbrook CA, Hooberman AL, Spino C, Dodge RK, Larson RA, Davey F, Wurster-Hill DH, Sobol RE, Schiffer C, Bloomfield CD (1992) Clinical significance of the BCR-ABL fusion gene in adult acute lymphoblastic leukemia: a Cancer and Leukemia Group B Study (8762). Blood 80: 2983-2990

13. Deininger MW, Goldman JM, Lydon N, Melo JV (1997) The tyrosine kinase inhibitor CGP57148B selectively inhibits the growth of BCR-ABL-positive cells. Blood 90: 3691-3698

14. Druker BJ, Tamura S, Buchdunger E, Ohno S, Segal GM, Fanning S, Zimmermann J, Lydon NB (1996) Effects of a selective inhibitor of the Abl tyrosine kinase on the growth of Bcr-Abl positive cells. Nat Med 2: 561-566

15. Michelakis ED, Hampl V, Nsair A, Wu X, Harry G, Haromy A, Gurtu R, Archer SL (2002) Diversity in mitochondrial function explains differences in vascular oxygen sensing. Circ Res 90: 1307-1315

16. Budhiraja R, Tuder RM, Hassoun PM (2004) Endothelial dysfunction in pulmonary hypertension. Circulation 109: 159-165

17. Zhao YD, Courtman DW, Deng Y, Kugathasan L, Zhang Q, Stewart DJ (2005) Rescue of monocrotaline-induced pulmonary arterial hypertension using bone marrow-derived endothelial-like progenitor cells: efficacy of combined cell and eNOS gene therapy in established disease. Circ Res 96: 442-450

18. Kanki-Horimoto S, Horimoto H, Mieno S, Kishida K, Watanabe F, Furuya E, Katsumata T (2006) Implantation of mesenchymal stem cells overexpressing endothelial nitric oxide synthase improves right ventricular impairments caused by pulmonary hypertension. Circulation 114: I181-185

19. Wang XX, Zhang FR, Shang YP, Zhu JH, Xie XD, Tao QM, Zhu JH, Chen JZ (2007) Transplantation of autologous endothelial progenitor cells may be beneficial in patients with idiopathic pulmonary arterial hypertension: a pilot randomized controlled trial. J Am Coll Cardiol 49: 1566-1571

20. Machado RD, Pauciulo MW, Thomson JR, Lane KB, Morgan NV, Wheeler L, Phillips JA, 3rd, Newman J, Williams D, Galie N, Manes A, McNeil K, Yacoub M, Mikhail G, Rogers P, Corris P, Humbert M, Donnai D, Martensson G, Tranebjaerg L, Loyd JE, Trembath RC, Nichols WC (2001) BMPR2 haploinsufficiency as the inherited molecular mechanism for primary pulmonary hypertension. Am J Hum Genet 68: 92-102

21. Lane KB, Machado RD, Pauciulo MW, Thomson JR, Phillips JA, 3rd, Loyd JE, Nichols WC, Trembath RC (2000) Heterozygous germline mutations in BMPR2, encoding a TGF-beta receptor, cause familial primary pulmonary hypertension. The International PPH Consortium. Nat Genet 26: 81-84

22. Howe JR, Bair JL, Sayed MG, Anderson ME, Mitros FA, Petersen GM, Velculescu VE, Traverso G, Vogelstein B (2001) Germline mutations of the gene encoding bone morphogenetic protein receptor 1A in juvenile polyposis. Nat Genet 28: 184-187

23. McMurtry MS, Archer SL, Altieri DC, Bonnet S, Haromy A, Harry G, Bonnet S, Puttagunta L, Michelakis ED (2005) Gene therapy targeting survivin selectively induces pulmonary vascular apoptosis and reverses pulmonary arterial hypertension. J Clin Invest 115: 1479-1491

24. Molteni A, Ward WF, Ts'ao CH, Port CD, Solliday NH (1984) Monocrotaline-induced pulmonary endothelial dysfunction in rats. Proc Soc Exp Biol Med 176: 88-94

25. Rabinovitch M, Bothwell T, Hayakawa BN, Williams WG, Trusler GA, Rowe RD, Olley PM, Cutz E (1986) Pulmonary artery endothelial abnormalities in patients with congenital heart defects and pulmonary hypertension. A correlation of light with scanning electron microscopy and transmission electron microscopy. Lab Invest 55: 632-653

26. Platoshyn O, Golovina VA, Bailey CL, Limsuwan A, Krick S, Juhaszova M, Seiden JE, Rubin LJ, Yuan JX (2000) Sustained membrane depolarization and pulmonary artery smooth muscle cell proliferation. Am J Physiol Cell Physiol 279: C1540-1549

27. Bonnet S, Michelakis ED, Porter CJ, Andrade-Navarro MA, Thebaud B, Bonnet S, Haromy A, Harry G, Moudgil R, McMurtry MS, Weir EK, Archer SL (2006) An abnormal mitochondrial-hypoxia inducible factor-1alpha-Kv channel pathway disrupts oxygen sensing and triggers pulmonary arterial hypertension in fawn hooded rats: similarities to human pulmonary arterial hypertension. Circulation 113: 2630-2641

28. Bonnet S, Rochefort G, Sutendra G, Archer SL, Haromy A, Webster L, Hashimoto K, Bonnet SN, Michelakis ED (2007) The nuclear factor of activated T cells in pulmonary arterial hypertension can be therapeutically targeted. Proc Natl Acad Sci U S A 104: 11418-11423

29. McMurtry MS, Bonnet S, Wu X, Dyck JR, Haromy A, Hashimoto K, Michelakis ED (2004) Dichloroacetate prevents and reverses pulmonary hypertension by inducing pulmonary artery smooth muscle cell apoptosis. Circ Res 95: 830-840

30. Michelakis ED, McMurtry MS, Wu XC, Dyck JR, Moudgil R, Hopkins TA, Lopaschuk GD, Puttagunta L, Waite R, Archer SL (2002) Dichloroacetate, a metabolic modulator, prevents and reverses chronic hypoxic pulmonary hypertension in rats: role of increased expression and activity of voltage-gated potassium channels. Circulation 105: 244-250

31. Merklinger SL, Jones PL, Martinez EC, Rabinovitch M (2005) Epidermal growth factor receptor blockade mediates smooth muscle cell apoptosis and improves survival in rats with pulmonary hypertension. Circulation 112: 423-431

32. Wharton J, Strange JW, Moller GM, Growcott EJ, Ren X, Franklyn AP, Phillips SC, Wilkins MR (2005) Antiproliferative effects of phosphodiesterase type 5 inhibition in human pulmonary artery cells. Am J Respir Crit Care Med 172: 105-113

33. Schermuly RT, Dony E, Ghofrani HA, Pullamsetti S, Savai R, Roth M, Sydykov A, Lai YJ, Weissmann N, Seeger W, Grimminger F (2005) Reversal of experimental pulmonary hypertension by PDGF inhibition. J Clin Invest 115: 2811-2821

34. Nishimura T, Vaszar LT, Faul JL, Zhao G, Berry GJ, Shi L, Qiu D, Benson G, Pearl RG, Kao PN (2003) Simvastatin rescues rats from fatal pulmonary hypertension by inducing apoptosis of neointimal smooth muscle cells. Circulation 108: 1640-1645

35. Cowan KN, Heilbut A, Humpl T, Lam C, Ito S, Rabinovitch M (2000) Complete reversal of fatal pulmonary hypertension in rats by a serine elastase inhibitor. Nat Med 6: 698-702

36. Michelakis ED, Sutendra G, Dromparis P, Webster L, Haromy A, Niven E, Maguire C, Gammer TL, Mackey JR, Fulton D, Abdulkarim B, McMurtry MS, Petruk KC (2010) Metabolic modulation of glioblastoma with dichloroacetate. Sci Transl Med 2: 31ra34

37. Bonnet S, Archer SL, Allalunis-Turner J, Haromy A, Beaulieu C, Thompson R, Lee CT, Lopaschuk GD, Puttagunta L, Harry G, Hashimoto K, Porter CJ, Andrade MA,

Thebaud B, Michelakis ED (2007) A mitochondria-K+ channel axis is suppressed in cancer and its normalization promotes apoptosis and inhibits cancer growth. Cancer Cell 11: 37-51

38. Zamzami N, Kroemer G (2001) The mitochondrion in apoptosis: how Pandora's box opens. Nat Rev Mol Cell Biol 2: 67-71

39. Duchen MR (1999) Contributions of mitochondria to animal physiology: from homeostatic sensor to calcium signalling and cell death. J Physiol 516 (Pt 1): 1-17

40. Weir EK, Lopez-Barneo J, Buckler KJ, Archer SL (2005) Acute oxygen-sensing mechanisms. N Engl J Med 353: 2042-2055

41. Michelakis ED, Thebaud B, Weir EK, Archer SL (2004) Hypoxic pulmonary vasoconstriction: redox regulation of O2-sensitive K+ channels by a mitochondrial O2-sensor in resistance artery smooth muscle cells. J Mol Cell Cardiol 37: 1119-1136

42. Callapina M, Zhou J, Schmid T, Kohl R, Brune B (2005) NO restores HIF-1alpha hydroxylation during hypoxia: role of reactive oxygen species. Free Radic Biol Med 39: 925-936

43. Denko NC (2008) Hypoxia, HIF1 and glucose metabolism in the solid tumour. Nat Rev Cancer 8: 705-713

44. Huang LE, Arany Z, Livingston DM, Bunn HF (1996) Activation of hypoxia-inducible transcription factor depends primarily upon redox-sensitive stabilization of its alpha subunit. J Biol Chem 271: 32253-32259

45. Archer SL, Souil E, Dinh-Xuan AT, Schremmer B, Mercier JC, El Yaagoubi A, Nguyen-Huu L, Reeve HL, Hampl V (1998) Molecular identification of the role of voltage-gated K+ channels, Kv1.5 and Kv2.1, in hypoxic pulmonary vasoconstriction and control of resting membrane potential in rat pulmonary artery myocytes. J Clin Invest 101: 2319-2330

46. Remillard CV, Yuan JX (2004) Activation of K+ channels: an essential pathway in programmed cell death. Am J Physiol Lung Cell Mol Physiol 286: L49-67

47. Cain K, Langlais C, Sun XM, Brown DG, Cohen GM (2001) Physiological concentrations of K+ inhibit cytochrome c-dependent formation of the apoptosome. J Biol Chem 276: 41985-41990

48. Knoechel TR, Tucker AD, Robinson CM, Phillips C, Taylor W, Bungay PJ, Kasten SA, Roche TE, Brown DG (2006) Regulatory roles of the N-terminal domain based on crystal structures of human pyruvate dehydrogenase kinase 2 containing physiological and synthetic ligands. Biochemistry 45: 402-415

49. MacKenzie ED, Selak MA, Tennant DA, Payne LJ, Crosby S, Frederiksen CM, Watson DG, Gottlieb E (2007) Cell-permeating alpha-ketoglutarate derivatives alleviate pseudohypoxia in succinate dehydrogenase-deficient cells. Mol Cell Biol 27: 3282-3289

50. Xu W, Koeck T, Lara AR, Neumann D, DiFilippo FP, Koo M, Janocha AJ, Masri FA, Arroliga AC, Jennings C, Dweik RA, Tuder RM, Stuehr DJ, Erzurum SC (2007) Alterations of cellular bioenergetics in pulmonary artery endothelial cells. Proc Natl Acad Sci U S A 104: 1342-1347

51. Kim JW, Dang CV (2005) Multifaceted roles of glycolytic enzymes. Trends Biochem Sci 30: 142-150

52. Sutendra G, Bonnet S, Rochefort G, Haromy A, Folmes KD, Lopaschuk GD, Dyck JRB, Michelakis ED (2010) Fatty acid oxidation and malonyl-CoA decarboxylase in the vascular remodeling of pulmonary hypertension. Science Translational Medicine 2

53. Cardenas C, Miller RA, Smith I, Bui T, Molgo J, Muller M, Vais H, Cheung KH, Yang J, Parker I, Thompson CB, Birnbaum MJ, Hallows KR, Foskett JK Essential regulation of cell bioenergetics by constitutive InsP3 receptor Ca2+ transfer to mitochondria. Cell 142: 270-283

54. Hayashi T, Rizzuto R, Hajnoczky G, Su TP (2009) MAM: more than just a housekeeper. Trends Cell Biol 19: 81-88

55. Simmen T, Aslan JE, Blagoveshchenskaya AD, Thomas L, Wan L, Xiang Y, Feliciangeli SF, Hung CH, Crump CM, Thomas G (2005) PACS-2 controls endoplasmic reticulum-mitochondria communication and Bid-mediated apoptosis. Embo J 24: 717-729

56. de Brito OM, Scorrano L (2008) Mitofusin 2 tethers endoplasmic reticulum to mitochondria. Nature 456: 605-610

57. Hayashi T, Su TP (2007) Sigma-1 receptor chaperones at the ER-mitochondrion interface regulate Ca(2+) signaling and cell survival. Cell 131: 596-610

58. Myhill N, Lynes EM, Nanji JA, Blagoveshchenskaya AD, Fei H, Carmine Simmen K, Cooper TJ, Thomas G, Simmen T (2008) The subcellular distribution of calnexin is mediated by PACS-2. Mol Biol Cell 19: 2777-2788

59. Mesaeli N, Nakamura K, Zvaritch E, Dickie P, Dziak E, Krause KH, Opas M, MacLennan DH, Michalak M (1999) Calreticulin is essential for cardiac development. J Cell Biol 144: 857-868

60. Nakamura K, Zuppini A, Arnaudeau S, Lynch J, Ahsan I, Krause R, Papp S, De Smedt H, Parys JB, Muller-Esterl W, Lew DP, Krause KH, Demaurex N, Opas M, Michalak M (2001) Functional specialization of calreticulin domains. J Cell Biol 154: 961-972

61. GrandPre TN, F. Vartanian, T. Strittmatter, SM. (2000) Identification of the Nogo inhibitor of axon regeneration as a Reticulon protein. Nature 403: 439-444

62. Voeltz GK, Prinz WA, Shibata Y, Rist JM, Rapoport TA (2006) A class of membrane proteins shaping the tubular endoplasmic reticulum. Cell 124: 573-586

63. Szanda G, Koncz P, Varnai P, Spat A (2006) Mitochondrial Ca2+ uptake with and without the formation of high-Ca2+ microdomains. Cell Calcium 40: 527-537

64. Szabadkai G, Duchen MR (2008) Mitochondria: the hub of cellular Ca2+ signaling. Physiology (Bethesda) 23: 84-94

65. Rizzuto R, Duchen MR, Pozzan T (2004) Flirting in little space: the ER/mitochondria Ca2+ liaison. Sci STKE 2004: re1

66. Ozcan U, Yilmaz E, Ozcan L, Furuhashi M, Vaillancourt E, Smith RO, Gorgun CZ, Hotamisligil GS (2006) Chemical chaperones reduce ER stress and restore glucose homeostasis in a mouse model of type 2 diabetes. Science 313: 1137-1140

67. Hotamisligil GS (2010) Endoplasmic reticulum stress and the inflammatory basis of metabolic disease. Cell 140: 900-917

68. Schroder M, Kaufman RJ (2005) ER stress and the unfolded protein response. Mutat Res 569: 29-63

69. Hansmann G, Wagner RA, Schellong S, Perez VA, Urashima T, Wang L, Sheikh AY, Suen RS, Stewart DJ, Rabinovitch M (2007) Pulmonary arterial hypertension is linked to insulin resistance and reversed by peroxisome proliferator-activated receptor-gamma activation. Circulation 115: 1275-1284

70. Sobolewski A, Rudarakanchana N, Upton PD, Yang J, Crilley TK, Trembath RC, Morrell NW (2008) Failure of bone morphogenetic protein receptor trafficking in pulmonary arterial hypertension: potential for rescue. Hum Mol Genet 17: 3180-3190

71. Sitbon O, Lascoux-Combe C, Delfraissy JF, Yeni PG, Raffi F, De Zuttere D, Gressin V, Clerson P, Sereni D, Simonneau G (2008) Prevalence of HIV-related pulmonary arterial hypertension in the current antiretroviral therapy era. Am J Respir Crit Care Med 177: 108-113

72. Sehgal PB, Mukhopadhyay S, Patel K, Xu F, Almodovar S, Tuder RM, Flores SC (2009) Golgi dysfunction is a common feature in idiopathic human pulmonary hypertension and vascular lesions in SHIV-nef-infected macaques. Am J Physiol Lung Cell Mol Physiol 297: L729-737

73. Voelkel NF, Cool CD, Flores S (2008) From viral infection to pulmonary arterial hypertension: a role for viral proteins? AIDS 22 Suppl 3: S49-53

74. Cool CD, Rai PR, Yeager ME, Hernandez-Saavedra D, Serls AE, Bull TM, Geraci MW, Brown KK, Routes JM, Tuder RM, Voelkel NF (2003) Expression of human herpesvirus 8 in primary pulmonary hypertension. N Engl J Med 349: 1113-1122

75. Li X, Zhang X, Leathers R, Makino A, Huang C, Parsa P, Macias J, Yuan JX, Jamieson SW, Thistlethwaite PA (2009) Notch3 signaling promotes the development of pulmonary arterial hypertension. Nat Med 15: 1289-1297

76. Takahashi K, Adachi K, Yoshizaki K, Kunimoto S, Kalaria RN, Watanabe A (2009) Mutations in NOTCH3 cause the formation and retention of aggregates in the endoplasmic reticulum, leading to impaired cell proliferation. Hum Mol Genet 19: 79-89

77. Belmont PJ, Tadimalla A, Chen WJ, Martindale JJ, Thuerauf DJ, Marcinko M, Gude N, Sussman MA, Glembotski CC (2008) Coordination of growth and endoplasmic reticulum stress signaling by regulator of calcineurin 1 (RCAN1), a novel ATF6-inducible gene. J Biol Chem 283: 14012-14021

78. Lee AH, Iwakoshi NN, Glimcher LH (2003) XBP-1 regulates a subset of endoplasmic reticulum resident chaperone genes in the unfolded protein response. Mol Cell Biol 23: 7448-7459

79. Yu J, Fernandez-Hernando C, Suarez Y, Schleicher M, Hao Z, Wright PL, DiLorenzo A, Kyriakides TR, Sessa WC (2009) Reticulon 4B (Nogo-B) is necessary for macrophage infiltration and tissue repair. Proc Natl Acad Sci U S A 106: 17511-17516

80. Acevedo L, Yu J, Erdjument-Bromage H, Miao RQ, Kim JE, Fulton D, Tempst P, Strittmatter SM, Sessa WC (2004) A new role for Nogo as a regulator of vascular remodeling. Nat Med 10: 382-388

81. Teng FY, Tang BL (2008) Cell autonomous function of Nogo and reticulons: The emerging story at the endoplasmic reticulum. J Cell Physiol 216: 303-308

82. Yan R, Shi Q, Hu X, Zhou X (2006) Reticulon proteins: emerging players in neurodegenerative diseases. Cell Mol Life Sci 63: 877-889

83. Haze K, Okada T, Yoshida H, Yanagi H, Yura T, Negishi M, Mori K (2001) Identification of the G13 (cAMP-response-element-binding protein-related protein) gene product related to activating transcription factor 6 as a transcriptional activator of the mammalian unfolded protein response. Biochem J 355: 19-28

84. Haze K, Yoshida H, Yanagi H, Yura T, Mori K (1999) Mammalian transcription factor ATF6 is synthesized as a transmembrane protein and activated by proteolysis in response to endoplasmic reticulum stress. Mol Biol Cell 10: 3787-3799

85. Nadanaka S, Okada T, Yoshida H, Mori K (2007) Role of disulfide bridges formed in the luminal domain of ATF6 in sensing endoplasmic reticulum stress. Mol Cell Biol 27: 1027-1043

86. Doroudgar S, Thuerauf DJ, Marcinko MC, Belmont PJ, Glembotski CC (2009) Ischemia activates the ATF6 branch of the endoplasmic reticulum stress response. J Biol Chem 284: 29735-29745

87. Tuder RM, Voelkel NF (1998) Pulmonary hypertension and inflammation. J Lab Clin Med 132: 16-24

88. Dorfmuller P, Perros F, Balabanian K, Humbert M (2003) Inflammation in pulmonary arterial hypertension. Eur Respir J 22: 358-363

89. Nicolls MR, Taraseviciene-Stewart L, Rai PR, Badesch DB, Voelkel NF (2005) Autoimmunity and pulmonary hypertension: a perspective. Eur Respir J 26: 1110-1118

90. McLaughlin VV, Presberg KW, Doyle RL, Abman SH, McCrory DC, Fortin T, Ahearn G (2004) Prognosis of pulmonary arterial hypertension: ACCP evidence-based clinical practice guidelines. Chest 126: 78S-92S

91. Sanchez O, Humbert M, Sitbon O, Simonneau G (1999) Treatment of pulmonary hypertension secondary to connective tissue diseases. Thorax 54: 273-277

92. Balabanian K, Foussat A, Dorfmuller P, Durand-Gasselin I, Capel F, Bouchet-Delbos L, Portier A, Marfaing-Koka A, Krzysiek R, Rimaniol AC, Simonneau G, Emilie D, Humbert M (2002) CX(3)C chemokine fractalkine in pulmonary arterial hypertension. Am J Respir Crit Care Med 165: 1419-1425

93. Caslin AW, Heath D, Madden B, Yacoub M, Gosney JR, Smith P (1990) The histopathology of 36 cases of plexogenic pulmonary arteriopathy. Histopathology 16: 9-19

94. Tuder RM, Groves B, Badesch DB, Voelkel NF (1994) Exuberant endothelial cell growth and elements of inflammation are present in plexiform lesions of pulmonary hypertension. Am J Pathol 144: 275-285

95. Taraseviciene-Stewart L, Nicolls MR, Kraskauskas D, Scerbavicius R, Burns N, Cool C, Wood K, Parr JE, Boackle SA, Voelkel NF (2007) Absence of T cells confers increased pulmonary arterial hypertension and vascular remodeling. Am J Respir Crit Care Med 175: 1280-1289

96. Heath D, Yacoub M (1991) Lung mast cells in plexogenic pulmonary arteriopathy. J Clin Pathol 44: 1003-1006

97. Daley E, Emson C, Guignabert C, de Waal Malefyt R, Louten J, Kurup VP, Hogaboam C, Taraseviciene-Stewart L, Voelkel NF, Rabinovitch M, Grunig E, Grunig G (2008) Pulmonary arterial remodeling induced by a Th2 immune response. J Exp Med 205: 361-372

98. Voelkel NF, Tuder RM, Bridges J, Arend WP (1994) Interleukin-1 receptor antagonist treatment reduces pulmonary hypertension generated in rats by monocrotaline. Am J Respir Cell Mol Biol 11: 664-675

99. Perros F, Dorfmuller P, Souza R, Durand-Gasselin I, Godot V, Capel F, Adnot S, Eddahibi S, Mazmanian M, Fadel E, Herve P, Simonneau G, Emilie D, Humbert M

(2007) Fractalkine-induced smooth muscle cell proliferation in pulmonary hypertension. Eur Respir J 29: 937-943

100. Hoeper MM, Welte T (2007) Systemic inflammation, COPD, and pulmonary hypertension. Chest 131: 634-635; author reply 635

101. Marecki JC, Cool CD, Parr JE, Beckey VE, Luciw PA, Tarantal AF, Carville A, Shannon RP, Cota-Gomez A, Tuder RM, Voelkel NF, Flores SC (2006) HIV-1 Nef is associated with complex pulmonary vascular lesions in SHIV-nef-infected macaques. Am J Respir Crit Care Med 174: 437-445

102. Spiekerkoetter E, Alvira CM, Kim YM, Bruneau A, Pricola KL, Wang L, Ambartsumian N, Rabinovitch M (2008) Reactivation of gammaHV68 induces neointimal lesions in pulmonary arteries of S100A4/Mts1-overexpressing mice in association with degradation of elastin. Am J Physiol Lung Cell Mol Physiol 294: L276-289

103. Macian F (2005) NFAT proteins: key regulators of T-cell development and function. Nat Rev Immunol 5: 472-484

104. Zamanian RT, Hansmann G, Snook S, Lilienfeld D, Rappaport KM, Reaven GM, Rabinovitch M, Doyle RL (2009) Insulin resistance in pulmonary arterial hypertension. Eur Respir J 33: 318-324

105. Michalik L, Auwerx J, Berger JP, Chatterjee VK, Glass CK, Gonzalez FJ, Grimaldi PA, Kadowaki T, Lazar MA, O'Rahilly S, Palmer CN, Plutzky J, Reddy JK, Spiegelman BM, Staels B, Wahli W (2006) International Union of Pharmacology. LXI. Peroxisome proliferator-activated receptors. Pharmacol Rev 58: 726-741

106. Belfiore A, Genua M, Malaguarnera R (2009) PPAR-gamma Agonists and Their Effects on IGF-I Receptor Signaling: Implications for Cancer. PPAR Res 2009: 830501

107. Wakino S, Kintscher U, Kim S, Yin F, Hsueh WA, Law RE (2000) Peroxisome proliferator-activated receptor gamma ligands inhibit retinoblastoma phosphorylation and G1--> S transition in vascular smooth muscle cells. J Biol Chem 275: 22435-22441

108. Alastalo TP, Li M, de Jesus Perez V, Pham D, Sawada H, Wang JK, Koskenvuo M, Wang L, Freeman BA, Chang HY, Rabinovitch M (2011) Disruption of PPARgamma/beta-catenin-mediated regulation of apelin impairs BMP-induced mouse and human pulmonary arterial EC survival. J Clin Invest 121: 3735-3746

109. Wenz T, Diaz F, Spiegelman BM, Moraes CT (2008) Activation of the PPAR/PGC-1alpha pathway prevents a bioenergetic deficit and effectively improves a mitochondrial myopathy phenotype. Cell Metab 8: 249-256

110. Michelakis ED (2006) Spatio-temporal diversity of apoptosis within the vascular wall in pulmonary arterial hypertension: heterogeneous BMP signaling may have therapeutic implications. Circ Res 98: 172-175

111. Fang YH, Piao L, Hong Z, Toth PT, Marsboom G, Bache-Wiig P, Rehman J, Archer SL (2011) Therapeutic inhibition of fatty acid oxidation in right ventricular hypertrophy: exploiting Randle's cycle. J Mol Med (Berl)

112. Nagendran J, Gurtu V, Fu DZ, Dyck JR, Haromy A, Ross DB, Rebeyka IM, Michelakis ED (2008) A dynamic and chamber-specific mitochondrial remodeling in right ventricular hypertrophy can be therapeutically targeted. J Thorac Cardiovasc Surg 136: 168-178, 178 e161-163

Chapter Two

Fatty Acid Oxidation and Malonyl-CoA Decarboxylase in the Vascular Remodeling of Pulmonary Hypertension

Abstract

Pulmonary arterial hypertension is caused by excessive growth of vascular cells that eventually obliterate the pulmonary arterial lumen, causing right ventricular failure and premature death. Despite some available treatments its prognosis remains poor, while the cause of the vascular remodeling remains unknown. The vascular smooth muscle cells that proliferate during pulmonary arterial hypertension are characterized by mitochondrial hyperpolarization, activation of the transcription factor NFAT and downregulation of the voltage-gated potassium channel Kv1.5, all of which suppress apoptosis. Here we show that mice lacking the gene for the metabolic enzyme malonyl-CoA decarboxylase (MCD) do not show pulmonary vasoconstriction during exposure to acute hypoxia and do not develop pulmonary arterial hypertension during chronic hypoxia, but have an otherwise normal phenotype. The lack of MCD results in an inhibition of fatty acid oxidation, which in turn promotes glucose oxidation and prevents the shift in metabolism toward glycolysis in the vascular media, which drives the development of pulmonary arterial hypertension in wild-type mice. Clinically used metabolic modulators that mimic the lack of MCD and its metabolic effects normalize the mitochondrial/NFAT/Kv1.5 abnormalities and the resistance to apoptosis in the proliferated smooth muscle cells, reversing the pulmonary hypertension induced by hypoxia or monocrotaline in mice and rats respectively. This study of fatty acid oxidation and MCD identifies a critical role for metabolism in both the normal pulmonary circulation (hypoxic pulmonary vasoconstriction) and pulmonary hypertension, pointing to several potential therapeutic targets for the treatment of this deadly disease.

Introduction

Increased proliferation and suppressed apoptosis in pulmonary vessel walls results in an obliterative remodeling that characterizes pulmonary arterial hypertension (PAH)[1]. The pathology of PAH is restricted to the pulmonary circulation; other vasculature is typically normal. Thus, therapies are needed that both reverse the vascular remodeling and are selective to the diseased pulmonary vascular bed. The cause of the proliferative and anti-apoptotic diathesis in PAH is unknown. Nevertheless several unrelated molecular abnormalities have been described: for example, loss-of-function mutations in the bone morphogenetic protein receptor II (BMPRII), hypoxia, viruses, dys-regulation of voltage-gated potassium channels (Kv), signaling abnormalities involving notch, epidermal growth factor, tyrosine kinase receptors or transcription factor abnormalities (NFAT, HIF-1α or PPAR) [1, 2]. The lack of understanding of the mechanisms underlying PAH limits the development of effective therapies.

In cancer, which is characterized by a similar anti-apoptotic diathesis and a multifactorial pathogenesis, a number of unrelated molecular and genetic abnormalities all result in increased glycolysis (GLY) and suppressed glucose oxidation (GO). This unique metabolic phenotype drives in part the resistance to apoptosis and might be due to a functional remodeling of mitochondria, which regulate both apoptosis and metabolism [3-6]. We speculated that a similar metabolic/mitochondrial remodeling in the pulmonary artery (PA) wall might be an integrative response to diverse molecular abnormalities, and its reversal will inhibit the resistance to apoptosis and the development of PAH.

Because the mitochondria of the smooth muscle cells in the pulmonary arteries (PASMC) are different than those of the systemic arterial smooth muscle cells (SASMC), mitochondria-targeting therapies might be selective for the pulmonary circulation [7, 8]. SASMC and PASMC have different levels of electron transport chain proteins, anti-oxidant enzymes, respiration rates and mitochondrial membrane potential [8]. It is not

known whether the basis for this difference is genetic (the resistance PAs, i.e. <300μm diameter, have different embryologic origin from the systemic arteries) or induced (the resistance PAs are exposed to a different redox environment, a result of higher oxygen concentrations; the PO_2 is >100mmHg in PAs and <50mmHg in the systemic microcirculation) [9]. Since mitochondria are important oxygen sensors, this difference may explain, at least in part, a critical difference between the pulmonary and systemic circulation: PAs constrict while systemic arteries dilate in hypoxia, a fundamental response in mammals [10]. Thus PASMC mitochondria may be a target for selective, pro-apoptotic/anti-proliferative therapies for PAH.

An increase in the GO to GLY ratio can be achieved pharmacologically with dichloroacetate (DCA), an inhibitor of the mitochondrial pyruvate dehydrogenase kinase (PDK) [11]. PDK tonically inhibits pyruvate dehydrogenase (PDH), a critical enzyme that promotes the coupling of GLY to GO because it promotes the entry of pyruvate into the mitochondria, where it enters the Krebs' cycle and completes GO rather than remaining in the cytoplasm for GLY. DCA treatment reverses both established PAH in several animal models [12-15] and cancer growth in xenotransplant models [3] and in patients with glioblastoma [4], by increasing the GO to GLY ratio and promoting mitochondria-dependent apoptosis. Genetic/molecular proof for this mechanism in PAH in vivo is lacking because the absence of PDH results, as would occur in knockout mice, in embryonic lethality.

While GO is suppressed upon PDH inhibition, energy production can still take place in the mitochondria via a switch in the fuel for oxidative phosphorylation from carbohydrates (pyruvate) to fatty acids. Fatty acids enter the mitochondria, oxidize to acetyl-CoA and feed the Krebs' cycle, as does pyruvate. A feedback mechanism in which PDH is critical, the Randle cycle, controls the relative balance between carbohydrate and fatty acid fuel supply to the mitochondria [16]: activation of fatty acid oxidation (FAO)

results in inhibition of PDH and vice versa, allowing for tissue-specific regulation of fuel supply to the mitochondria. The decrease in GO is associated with an increase in the dependence of cancer cell survival on FAO [6]. Can suppression of FAO result in PDH activation, increase in GO/GLY ratio and reversal of PAH?

A recently recognized key regulatory enzyme for FAO is malonyl-CoA decarboxylase (MCD) [17]. MCD decarboxylates malonyl-CoA to acetyl-CoA. Malonyl-CoA inhibits carnitine-palmitoyl transferase-1 (CPT1), the rate-limiting pathway for fatty acids into mitochondria. Thus inhibition of MCD increases malonyl-CoA, decreasing FAO, thus activating PDH and GO [18]. In the myocardium, lack of MCD promotes GO and improves cardiac efficiency during ischemia-reperfusion in $MCD^{-/-}$ mice [19, 20]. The limited FAO in these mice (which under normal conditions have a normal phenotype) keeps PDH tonically activated, promoting GO. We hypothesized that the enhanced GO in the $MCD^{-/-}$ PAs will limit the shift towards cytoplasmic GLY and its associated resistance to apoptosis, preventing vascular remodeling and PAH.

Results

MCD is present in the PAs of wild-type ($MCD^{+/+}$), but not $MCD^{-/-}$, mice and in both healthy and PAH human lungs obtained from transplant surgery (Fig. 2-1). Its presence in human PAs supports the relevance of our animal work to human disease.

2.1. $MCD^{-/-}$ mice lack hypoxic pulmonary vasoconstriction (HPV)

The pulmonary circulation shows a unique response to acute, moderate hypoxia (not anoxia) with the resistance PAs constricting (HPV) while systemic arteries dilate. Mitochondria are oxygen *sensors* and in response to hypoxia they alter the production of mitochondria-derived reactive oxygen species (mROS), which regulate important *effectors*, such as plasma-membrane potassium channels [10]. In response to acute hypoxia, normal PASMCs show mitochondrial hyperpolarization, decreased mROS and inhibition of redox-sensitive Kv channels, causing plasma membrane depolarization and

Ca^{2+} influx through voltage-dependent Ca^{2+} channels, leading to contraction [10]. Although PASMCs freshly isolated from $MCD^{+/+}$ resistance PAs showed these expected changes, $MCD^{-/-}$ PASMCs did not respond to acute hypoxia: they did not show mitochondrial hyperpolarization, did not show decreased mROS production (Fig. 2-2A), did not show Kv current inhibition (Fig. 2-2B), and only had a minimal increase in intracellular Ca^{2+} concentration (Fig. 2-2C). Although there was a slight decrease in K^+ current in baseline $MCD^{-/-}$ PASMC compared to baseline $MCD^{+/+}$ PASMC, this did not result in a significant difference in baseline intracellular Ca^{2+} (Fig. 2-2C). Intact resistance PAs from $MCD^{+/+}$ and $MCD^{-/-}$ mice in tissue baths constricted identically in response to phenylephrine, an α-adrenergic agonist that causes constriction by a mechanism not involving mitochondrial signaling. However, $MCD^{-/-}$ PAs did not show HPV, while $MCD^{+/+}$ PAs displayed HPV even without pre-constriction, which is often required to elicit a clear response to physiologic hypoxia ex vivo (Fig. 2-2D). Thus the lack of HPV was intrinsic to the sensor mechanism (mitochondria) and not due to deficiencies in the contractile machinery, as the response to phenylephrine remained intact in the $MCD^{-/-}$ PAs. We then used an air-sealed treadmill in which mice exercised during moderate ambient hypoxia. In this device, HPV increases the right ventricular afterload, decreasing cardiac output and impairing exercise performance, comparable to exercise in high altitude [21]. The $MCD^{-/-}$ mice ran further than the $MCD^{+/+}$ mice, in keeping with a lack of HPV in vivo (Fig. 2-2E).

2.2. $MCD^{-/-}$ mice do not develop chronic hypoxia-induced PAH

We then studied normoxic mice and mice exposed to four weeks of chronic normobaric hypoxia (CH), a standard PAH model [22]. We measured hemodynamics both invasively (with high-fidelity catheters advanced to the PAs in anesthetized animals) and noninvasively in non-anesthetized animals by measuring pulmonary artery acceleration time (PAAT) with echocardiography (PAAT is inversely related to mean PA

pressure). The CH-MCD$^{+/+}$ mice developed PAH, with increased mean PA pressure, decreased PAAT and increased right ventricular (RV) hypertrophy [measured by RV mass (RV/LV+septum weight) and RV free-wall thickness]; they also developed vascular remodeling, measured by % medial wall thickness in medium (100-300μm) and small-sized (<100μm) PAs (Fig. 2-3A, 2-3B and 2-4). However, in CH-MCD$^{-/-}$ mice, PA pressure, PAAT, RV mass and thickness and PA medial wall thickness remained unchanged, and they ran for a significantly longer distance on the treadmill than the CH-MCD$^{+/+}$ mice. All groups had similar systemic blood pressure and heart rate (Fig. 2-3A, 2-3B and 2-4).

We then measured standard metabolic parameters, mitochondrial membrane potential (ΔΨm) and mROS in freshly isolated resistance PAs from these mice. As expected, fatty acid (palmitate) oxidation was significantly decreased in normoxic MCD$^{-/-}$ compared to MCD$^{+/+}$ mice (Fig. 2-5A). The fact that MCD$^{-/-}$ mice were able to oxidize fatty acids is consistent with their normal phenotype in normoxic conditions. Although the MCD$^{+/+}$ PAs showed the expected increase in GLY and decrease in GO (increased GLY/GO ratio), this switch to a glycolytic phenotype did not occur in MCD$^{-/-}$ PAs (Fig. 2-5A). This CH-induced switch in metabolism was associated with increased ΔΨm and decreased mROS in the CH-MCD$^{+/+}$ but not CH-MCD$^{-/-}$ PAs (Fig. 2-5B and 2-6A).

Before investigating the mechanism for the increased ΔΨm, we studied how these primary metabolic differences relate to known molecular abnormalities in PAH. Although PASMC Kv channels can be inhibited by acute hypoxia, a significant downregulation in Kv channel abundance has been described in several PAH models [12-15, 23] including human PAH [24]. Since Kv1.5 regulates plasma-membrane potential in PASMC [25], its inhibition and down-regulation can affect contraction and proliferation, mainly as a result of an increase in Ca^{2+} influx [26]. In addition, Kv1.5 downregulation

will increase intracellular K^+ and contribute to inhibition of apoptosis via K^+ inhibition of caspases [27]. We have previously shown that the down-regulation of Kv1.5 in animal and human PAH is driven, at least in part, by the activation of the transcription factor NFATc2 (nuclear factor of activated T-cells) [28]. As expected, chronic hypoxia caused NFATc2 activation (nuclear localization) and downregulation of Kv1.5, as well as increased proliferation (PCNA) in the CH-$MCD^{+/+}$ but not the CH-$MCD^{-/-}$ mice PAs (Fig. 2-5C-D, 2-6B).

In keeping with the decreased Kv1.5 protein in vivo, isolated CH-$MCD^{+/+}$ PASMCs had reduced K^+ current compared to normoxic $MCD^{+/+}$ PASMCs, measured by standard patch-clamping. The majority of the reduced current was Kv, based on the sensitivity to 4-aminopyridine (Fig. 2-5E, 2-7A). In contrast, the K^+ current in CH-$MCD^{-/-}$ was similar to that in normoxic $MCD^{-/-}$ PASMCs. The CH-$MCD^{+/+}$ PASMCs showed the expected decrease in membrane potential and increased intracellular Ca^{2+} concentration which were not seen in CH-$MCD^{-/-}$ PASMCs (Figs. 2-5F, 2-7B). The increase in intracellular Ca^{2+} in CH-$MCD^{+/+}$ PASMC was reversed by exogenous H_2O_2 (t-butyl-H_2O_2) (Fig. 2-8). This suggests that the increase in intracellular Ca^{2+} is a result of suppressed primary mitochondria-derived mROS [mostly mitochondrial superoxide, which in the presence of manganese superoxide dismutase, dismutates to the more stable H_2O_2 which can reach extra-mitochondrial redox-sensitive targets [10]].

We then investigated whether lack of MCD might also cause additional differences in Ca^{2+} homeostasis relevant to PAH by comparing the response of intracellular Ca^{2+} to phenylephrine and endothelin-1, both strong pulmonary vasoconstrictors that increase intracellular Ca^{2+} via receptor-mediated release from the endoplasmic reticulum. We showed that the intracellular Ca^{2+} in the $MCD^{-/-}$ and $MCD^{+/+}$ PASMCs at rest (Fig. 2-5F) and in response to phenylephrine or endothelin-1, were not different (Fig. 2-9). Thus, the difference in intracellular Ca^{2+} in response to both acute

(Fig. 2-2C) and chronic hypoxia (Fig. 2-5F), the sensing of which is initiated at the mitochondria, is intrinsic to the mitochondria and not due to a generalized defect in Ca^{2+} homeostasis.

2.3. Inhibition of the metabolic enzyme GSK-3β is critical for the apoptosis-resistance in PAH.

Although intracellular Ca^{2+} promotes NFAT entry into the nucleus, glycogen synthase kinase-3β (GSK-3β) promotes its exit and cause its inhibition [29]. In a glycolytic environment, as in cancer, GSK-3β is inhibited [30] and NFAT is activated [3]. In addition to NFAT, GSK-3β can also regulate ΔΨm. In a glycolytic environment, hexokinase-II (HKII), a critical glycolytic enzyme, is upregulated and can translocate from the cytoplasm to the outer mitochondrial membrane where it binds to and inhibits the voltage-gated anion channel (VDAC), a component of the mitochondrial transition pore (MTP). MTP is a voltage-gated mega-channel through which pro-apoptotic mediators move to the cytoplasm, initiating apoptosis [31]. The binding of HKII to VDAC, leads to an increase in ΔΨm (as anions are trapped within the mitochondria) and suppression of apoptosis. GSK-3β inhibits the binding of HKII to VDAC by phosphorylating the HKII-binding site on VDAC. In cancer, GSK-3β activators prevent the translocation of HKII to the mitochondria, resulting in mitochondrial depolarization and initiation of apoptosis, decreasing cancer growth [30].

We studied $MCD^{-/-}$ and $MCD^{+/+}$ PASMC cultured in normoxic and CH conditions, treating them with GSK-3β inhibitors (SB-216763) and activators (wortmannin and LY290042). In addition, we used antibodies against whole GSK-3β and phosphorylated (inactive) GSK-3β in both isolated intrapulmonary PAs and whole-lung tissue (Fig. 2-10A, 2-10B, 2-11). Compared to normoxic $MCD^{+/+}$, CH-$MCD^{+/+}$ PASMCs showed decreased GSK-3β activity, activated NFATc2 and decreased Kv1.5. GSK-3β

activators prevented these effects of CH. In contrast, CH-MCD$^{-/-}$ PASMCs showed no decrease in GSK-3β activity, NFATc2 remained inactive, and Kv1.5 was unchanged. The GSK-3β inhibitor SB-216763 mimicked CH, causing NFATc2 activation and Kv1.5 downregulation.

As predicted, in CH-MCD$^{+/+}$ PASMCs, but not in all the other groups, HKII was both upregulated and translocated onto the mitochondria (Fig. 2-12A). The effect of HKII translocation on ΔΨm was shown by the fact that GSK-3β activators prevented the increase in ΔΨm in CH-MCD$^{+/+}$ PASMCs, while GSK-3β inhibitors increased ΔΨm in CH-MCD$^{-/-}$ PASMCs (Fig. 2-12B). To show that in these cells HKII translocation increases ΔΨm via VDAC inhibition, we used a cell-permeable competing peptide that binds VDAC, prohibiting its phosphorylation by GSK-3β [30]. As expected, the increase in ΔΨm was prevented by this peptide (Fig. 2-12B). However, the direct VDAC inhibitor 4-diisothiocyano-2,2-disulfonic acid stilbene (DIDS) increased ΔΨm, indicating that the VDAC remained open and functional.

To determine whether this regulation involved Akt, a known inhibitor of GSK-3β [32] that is activated in cancer, we measured Akt activity by immunobloting with antibodies against its phosphorylated (active) site. Akt activity was not different among the groups (Fig. 2-13), suggesting that other, metabolism-based mechanisms may inhibit GSK-3β in CH-PASMC. Our data on acute and chronic hypoxia in MCD$^{-/-}$ PASMC suggest that the mitochondria-based oxygen sensing and its downstream signaling are suppressed. Metabolic signals [mROS [33], the diffusible Krebs' cycle product α-ketoglutarate [34] and GSK-3β [35]] also regulate the hypoxia-inducible factor-1α (HIF-1α). This may explain the fact that, although HIF-1α was activated (nuclear localization) in CH-MCD$^{+/+}$, it remained inactive in CH-MCD$^{-/-}$ PASMC (Fig. 2-14).

Finally, CH-MCD$^{+/+}$ PASMCs exhibit increased resistance to apoptosis, as measured by TUNEL, in response to exposure to 0.1% serum, compared to the CH-MCD$^{-/-}$ PASMC. In addition, the CH-MCD$^{+/+}$ PASMC showed more proliferation (PCNA) than CH-MCD$^{-/-}$ PASMC (Fig. 2-12C). These data directly link the mitochondria-GSK3β-NFAT-Kv axis with the increased PASMC proliferation/apoptosis ratio that characterizes PAH (Fig. 2-12D).

2.4. Metabolic modulators mimic MCD loss and reverse PAH in several models.

The mitochondrial signaling downstream of MCD can be mimicked by clinically used drugs such as the metabolic modulators trimetazidine (TMZ) [36] and DCA [37]. We studied the effects of DCA and TMZ in CH-PAH in vivo and in vitro as well as of the specific MCD inhibitor CBM-300864 in vitro [20] (CBM-300864 is not available for in vivo use). Although DCA and TMZ inhibit different enzymes (PDK and 3-ketoacyl CoA thiolase, respectively) the downstream effects of these drugs are the same, mimicking MCD deletion and decreasing the GLY/GO ratio.

In CH-MCD$^{+/+}$ PASMC, all three drugs normalized $\Delta\Psi$m, mROS, Kv current, plasma membrane potential and intracellular Ca^{2+} in vitro (Figs. 2-15A-B). In vivo, three week therapy in CH-MCD$^{+/+}$ mice (with established PAH) with DCA (30mg/day) or TMZ (420μg/day) at clinically relevant doses (in the drinking water), decreased mean PA pressure, RV hypertrophy, % medial wall thickness in 100-300μm and <100μm PAs as well as reversed the muscularization of small PAs (<50μm); in addition, these drugs improved the animals' functional capacity (treadmill test) without affecting systemic arterial blood pressure or heart rate (Figs. 2-15C, 2-16A, 2-17, 2-18, 2-19). Apoptosis was induced in the wall of the remodeled PAs in vivo, measured by TUNEL, caspase-3 and apoptosis-inducing factor (AIF) activity (nuclear localization) (Figs. 2-16B, 2-20, 2-

21). Also, proliferation was decreased in DCA and TMZ-treated CH-MCD$^{+/+}$ mice PAs (Figs. 2-16B, 2-20).

To show that our findings are relevant to models other than hypoxia-treated mice, we used the monocrotaline-induced PAH in rats (MCT-PAH) and PASMCs cultured from patients with idiopathic PAH and from normal controls (transplant donors). TMZ reversed established rat MCT-PAH (improved mean PA pressure, cardiac output, total pulmonary vascular resistance, PA % medial wall thickness) (Figs. 2-16C-D, 2-22). Both DCA and TMZ normalized the increased intracellular Ca^{2+} in the human PAH PASMC without affecting PASMCs from healthy individuals (Fig. 2-23).

Discussion

We have shown that lack of a key metabolic enzyme, MCD, offers complete resistance to the development of PAH in a mouse model. We have previously provided pharmacologic evidence that increasing the GO/GLY ratio with DCA (a drug that increases the activity of the mitochondrial PDH), suppresses proliferation and promotes apoptosis, reversing PAH in animal models and cancer growth in animal models and humans [3, 4, 14, 15]. Here we demonstrate the critical role of a metabolic gene for the development of PAH in vivo, suggesting a number of potential novel drug targets.

Using both molecular and pharmacologic interventions we have shown that suppression of FAO promotes GO, increasing the GO/GLY ratio in the pulmonary circulation. MCD knockdown and TMZ on the one hand, and DCA on the other hand, share a common downstream mechanism that prevents the switch from the mitochondria-based oxidative phosphorylation (OXPHOS) to the cytoplasm-based GLY (Fig. 2-24). There is emerging evidence that a glycolytic environment is associated with a resistance to apoptosis. Several glycolytic enzymes have direct anti-apoptotic effects [38] and GSK-3β, which is inhibited in a glycolytic environment, has been implicated in proliferative diseases like cancer and the vascular response to injury [30, 39]. The vasculature in PAH

is glycolytic, as shown by the fact that, like cancer, it shows increased uptake of glucose (as imaged by positron emission tomography) in vivo [40], perhaps in an attempt to compensate energetically, since GLY is less efficient than OXPHOS in producing ATP. Like mitochondria in cancer cells, mitochondria in PASMC from several PAH animal and human models or normal PASMC in hypoxia are hyperpolarized [3, 4, 12, 14, 15, 23, 28]. Mitochondrial hyperpolarization is associated with a decreased threshold for the opening of the voltage-gated MTP, through which pro-apoptotic mediators leak to the cytoplasm to induce apoptosis [31]. The mechanism for this hyperpolarization is unclear and complex, but it appears that factors intrinsic (respiration and generation of mROS with concomitant efflux of H^+ ions) and extrinsic (GSK-3β-mediated HKII translocation and inhibition of VDAC) to mitochondria participate. We have now shown that primary suppression of FAO causes secondary increase of the GO/GLY ratio, which in turn reverses the glycolytic environment and the hyperpolarization of mitochondria, thus promoting mitochondria-dependent apoptosis (Fig. 2-24).

The third way that mitochondrial potential can be regulated is by the induction of uncoupling (UCP) proteins. When inserted into mitochondrial membranes, UCPs short-circuit the electron transport chain, dissociating $\Delta\Psi m$ from OXPHOS.

In addition to apoptosis, mitochondria also regulate a number of critical signaling pathways since they produce mROS (and thus regulate redox-sensitive targets including transcription factors like HIF-1α or Kv channels) and being highly negatively charged organelles, can uptake large amounts of Ca^{2+}. Thus alterations in mitochondrial function can have a number of diverse downstream effects. In hypoxic PASMC, the lack of MCD is associated with sustained mROS production (which promotes Kv channel opening and may contribute to HIF-1α inhibition) and decreased intracellular Ca^{2+}, which contributes

to the inhibition of proliferation and NFAT activation. In addition to the promotion of apoptosis, these effects all contribute to the prevention and reversal of PAH (Fig. 2-24).

PAH therapies that target mitochondria may be relatively selective to the pulmonary circulation, since mitochondria are different between the pulmonary and systemic circulations [8]. Our observation that lack of MCD causes a selective suppression of HPV and does affect systemic hemodynamics is promising in terms of the development of relatively selective PAH therapies.

Our work is consistent with several other postulated mechanisms for PAH, clearly a multi-factorial disease. PASMC may respond to metabolic stress by switching to a glycolytic environment. As in cancer, this switch may be energetically suboptimal, but induce a resistance to apoptosis, a top priority during stress. In addition, when GO is inhibited and GLY increases, the suppression of pyruvate's entry into the mitochondria allows it to enter anaplerotic reactions and amino acid biosynthesis, which are critical for proliferating cells. Such metabolic stress may be direct, as hypoxia, or indirect, following exposure to proliferative signals (like EGF[41] or PDGF [42]) or endoplasmic reticulum stress. Examples include the misfolded protein stress response that follows BMPRII mutations in PAH [43] or the viral infections that cause PAH such as HIV [44, 45] or HSV [46].

Our work also supports the emerging evidence that PPAR signaling, a critical regulator of metabolism, is abnormal in PAH [47]. This is despite of the fact that PPAR's direct effects on mitochondria remain unclear and its role in inflammation (also critical for PAH) makes the dissection of its metabolic effects on the vasculature difficult. Lithium has been associated with unexpected PAH in both adults [48] and neonates [49]. Our current work may explain these reports since lithium is a direct GSK-3β inhibitor. NFATc2 is critical for the development of PAH [28]; our work now indicates that early metabolic signals may explain the activation of NFATc2, via their downstream effects on

GSK-3β and intracellular Ca^{2+}. Another important transcription factor activated in PAH is HIF-1α [12, 50]. The suppression of metabolic signals from mitochondria in cells lacking MCD resulted in lack of activation of both NFAT and HIF-1α in hypoxia. This lack of HIF-1α activation in sustained hypoxia is also compatible with the lack of HPV under acute hypoxia when MCD is absent.

Although our study has focused on the proliferative, anti-apoptotic diathesis of PASMC, not endothelial cells, our work is consistent with the recent observations that endothelial cells have a glycolytic phenotype in human PAH [40], suggesting that metabolic remodeling may characterize the whole PA wall during PAH.

A caveat regarding the translational potential of our work is the fact that in the 24 patients that have been described with *MCD*-deficiency in the literature so far, a subgroup developed cardiomyopathy. Nevertheless, in those patients who completely lacked MCD (MCD deletion, similar to $MCD^{-/-}$ mice), no cardiomyopathy was observed. The patients with cardiomyopathy had evidence of MCD mutations (not deletions), which often resulted in sub-cellular protein mis-targeting, potentially causing endoplasmic reticulum stress and secondary cellular effects [51, 52]. Taken together our data suggest that the pulmonary arterial wall in PAH exhibits a metabolic remodeling that supports anti-apoptotic and proliferative diathesis and can be therapeutically targeted with metabolic modulators, some of which are already clinically used for different diseases.

Materials and Methods

All experiments on human tissues and rodents were done with permission from the University of Alberta committees on human ethics and animal policy and welfare, respectively.

Animal models for PAH: In the chronic hypoxic model, eight- to ten-week old $MCD^{+/+}$ and $MCD^{-/-}$ mice were placed into hypoxic chambers (Reming Bioinstruments) and maintained in normobaric hypoxia (10% O_2 and 90% N_2) for three weeks as previously described [15]. In the monocrotaline model, rats were randomized to control (sham saline injection) and 60 mg/kg subcutaneous monocrotaline (MCT) injection (Sigma-Aldrich). Three weeks post normobaric hypoxia or MCT injection, PAH was confirmed by echocardiography (RV free wall thickness and PAAT). CH-$MCD^{+/+}$ mice and MCT-rats were treated with DCA or trimetazidine for 3 additional weeks (given in the drinking water, as described under in vivo drugs).

Targeted mutation of the MCD locus and MCD knockout mice generation and breeding: MCD mutant mice were back-crossed for six generations to a C57BL6 wild-type animal, in order to produce a background >99% similar to the genetic background of a C57BL6 animal. Homozygous pairs allowed congenic lines of knockout and littermate wild-type animals to propagate.

Metabolic studies: Isolated homogenized pulmonary arteries or pulmonary artery smooth muscle cells (PASMC) were grown to confluency in T-175 flasks. To measure GLY rates, tissues were incubated in Krebs'-Henseleit buffer supplemented with 1.2 mM palmitate and 5 mM [5-^{3}H]-glucose and assessed for ^3H_2O. For palmitate oxidation, the Krebs'-Henseleit solution contained 1.2 mM [9,10-^{3}H]-palmitate and 5 mM glucose and assessed for ^3H_2O. For GO, the buffer contained 1.2 mM palmitate and 5 mM [U-^{14}C]-glucose and assessed for $^{14}CO_2$ production. Rates of energy metabolism were found to be

linear to 360 minutes, and therefore metabolic rates were determined over a 180 min period.

In-vivo drugs: CH-MCD$^{+/+}$ mice were then randomly assigned to 3 week DCA or trimetazidine treatment, while MCT induced-PAH rats were randomly assigned to trimetazidine treatment (given in the drinking water). By measuring the amount of water consumed by each mouse and rat we were able to adjust the treatment such that the average daily dose of DCA was 70 mg/kg and trimetazidine was 420 μg/day, similar to clinically used doses.

Treadmill test: A graded sub-maximal exercise tolerance test was performed on a calibrated, motor-driven treadmill in a Plexiglas cage (Treadmill Simplex II, Columbus Instruments) under both normoxic (pO_2 ~130-150 mmHg) and hypoxic (sealed treadmill perfused with 5.02% CO_2 and 2.48% O_2 for a resulting pO_2 ~50-70 mmHg; oxygen levels measured with a blood gas analyzer (Bayer Rapidlab 850). Incremental increases in treadmill belt speed were made: 1 min warm up at 3 m/min, then 1 min at 4 m/min, 2 min at 5 m/min, 2 min at 6 m/min, 6 min at 7 m/min, and finally 8 m/min until the mouse exhibited signs of exhaustion. Exhaustion was defined as the mouse spending >50% of the time or >10 consecutive seconds on the shock grid. Both distance and time for exhaustion were used as end points.

Cell culture: PASMC were freshly isolated from mice and human pulmonary arteries with an enzymatic cocktail containing papain (1 mg/mL), DTT (0.5 mg/mL), collagenase (0.6 mg/mL) and BSA (0.6 mg/mL) (Sigma-Aldrich). Human PASMC were established in accordance with University of Alberta human ethics committee approval from transplant material from a 31-year-old male with idiopathic PAH (iPAH) and 28-year-old male donor (control). Small intrapulmonary arteries were excised and used for PASMC isolation. Cultured cells were maintained in Dulbecco's modified Eagle's medium (DMEM) supplemented with 10% fetal bovine serum (FBS) and 1%

antibiotic/antimycotic (Gibco, Invitrogen) and placed in an incubator set at 37°C in either normoxic conditions (gas perfused incubator with 5.2% CO_2, 21% O_2 and balanced N_2) or hypoxic conditions (gas perfused incubator with 5.2% CO_2, 4% O_2 and balanced N_2). The solutions also contained 10 mmol/L HEPES and the resulting blood gases showed PO_2~40-50 in hypoxic and ~130-140 in normoxic solutions, with the pH and PCO_2 remaining within normal levels in both solutions.

Calcium imaging: PASMC were cultured either in normoxic or hypoxic conditions (see Cell Culture Supplemental Data) to 50% confluence in order to measure the intracellular Ca^{2+} in individual PASMC. The medium was removed and cells were incubated for about 45 minutes in the dark with a solution (pH 7.4 at 25°C) containing 140 mM NaCl, 4.2 mM KCl, 1.2 mM KH_2PO_4, 1.5 mM $MgCl_2$, 1.5 mM $CaCl_2$, 10 mM HEPES and 2 μM fura-2/AM (Molecular probes), a fluorescence Ca^{2+} indicator. The cells were washed before measurements. The excitation wavelengths for Ca^{2+} indicator were 340 nm and 380 nm and the emission was 500 nm. After background was subtracted, the fluorescence ratio (FI340/FI380) was obtained. The maximal ratio was then obtained when adding an ionophore (Ionomycin, 10 μM, Sigma-Aldrich), whereas the minimum was recorded after washing the cells with a solution containing 10 mM EGTA.

Confocal microscopy: Imaging was performed with a Zeiss LSM 510 confocal microscope (Carl Zeiss Canada) as previously described [3, 28]. Apoptag apoptosis detection kit (TUNEL Serologicals) and the proliferating cell nuclear antigen (PCNA) antibody (1/40) (DAKO) were used. Percent of PCNA or TUNEL positive cells were measured blindly in 5 random fields/slide; a minimum of 3 slides/experiment were used and 5 repetition experiments were typically performed (involving tissues from ~3-5 animals). Hexokinase II (1/50) (Santa Cruz Biotechnology), NFAT-c2 (1/100) (Novus Biologicals), Kv1.5 (1/50) (Santa Cruz Biotechnology), GSK3β (1/50) and phosphoylated GSK (1/50) (Cell Signaling), PDK2 (1/100) (SC-14484, Santa Cruz),

HIF-1α (1/100; AbCam) were used. Mitotracker Red, (500 nM) (Molecular Probes, Invitrogen), tetramethyl-rhodamine methyl ester (10nM Molecular Probes, Invitrogen) and MitoSOX (5μM, Molecular Probes, Invitrogen) were used as previously described [3, 28]. The antibody to MCD was previously developed and validated by our group and was used as previously described [17, 19, 20]. FITC- and TRITC-conjugated (DAKO (1/40), or Molecular Probes, Invitrogen (1/100)) secondary antibodies were used [3, 28]. All experiments included secondary antibody-only staining, which in all presented experiments showed no signal, supporting the specificity of the antibodies used. Percent NFATc2-positive cells were measured as for percent PCNA and TUNEL (see above). TMRM and MitoSOX intensity was measured in 5 random fields/slide; a minimum of 3 slides/experiment were used and a minimum of 5 experiments were performed.

Electrophysiology: Standard whole-cell patch-clamping was performed on cultured cells. 4-aminopyridine (5 mM Sigma-Aldrich), TMZ (10 μM), DCA (500 μM Sigma-Aldrich) and CBM301106 (10 μM) was given acutely. Cells were voltage-clamped at a holding potential of -70 mV. Currents were evoked by 200-ms test pulses from -70 to +70 mV with 20 mV steps, filtered at 1 kHz and sampled at 2-4 kHz as previously described [3, 12, 14, 23, 28]. External solution (138.6 mmol/L NaCl, 5.4 mmol/L KCl, 1.8 mmol/L $CaCl_2$, 1.2 mmol/L $MgCl_2$, 0.33 mmol/L NaH_2PO_4, 10 mmol/L HEPES and 11 mmol/L glucose, pH adjusted to 7.4 with NaOH) was bubbled for either normoxic conditions with 3.52% CO_2, 20% O_2 and balanced N_2 for a pO_2 ~150 mmHg at 37°C or hypoxic conditions with 5.02% CO_2, 2.48% O_2 and balanced N_2 for a pO_2 of ~40 mmHg at 37°C. pO_2 and pH were checked every 30 minutes with a blood gas analyzer (Bayer Rapidlab 850). Pipette solution consisted of 134 mmol/L KCl, 1.2 mmol/L KH_2PO_4, 1.0 mmol/L $MgCl_2$, 5.0 mmol/L HEPES, 5.0 mmol/L Na_2ATP and 5.0 mmol/L EGTA and was pH adjusted to 7.30 with KOH.

Echocariography and right heart catheterization: RV free wall thickness and pulmonary artery acceleration time were measured as previously described [14, 23]. Right heart catheterization including cardiac output measurement and recording of mean PA pressure with a Millar catheter was performed as described [14, 23].

Immunoblotting: Tissues and cells were collected and immunoblotting was performed as previously described [3, 12, 14, 23, 28]. Pooled samples of 4 T-25 dishes or 3-5 resistance pulmonary arteries or lungs (25 μg protein in pooled sample/lane) were used. The films were digitized and quantified using 1D Image Analysis Software (Kodak). Expression was normalized to Ponceau-S and actin to correct for loading differences. Antibodies: Kv1.5 (1:500, Sigma), caspase 3 (1:1000, Upstate) GSK3β and P-GSK3β (1:1000, Cell Signaling). The MCD antibody was previously validated by our group and was used as previously described [17, 19, 20].

Medial wall thickness: % Medial wall thickness was measured at the two ends of the shortest external diameter of the distal pulmonary arteries and the average was taken ([2 x wall thickness/external diameter] x 100).

Muscularization studies: Whole lung tissues were stained for smooth muscle cells [SMC; smooth muscle actin (SMA)] and endothelial cells [von-Willibrand factor (vWF)]. Complete enclosure of the distal pulmonary artery with SMA was classified as fully-muscularized arteries. Partial enclosure of the distal pulmonary artery with SMA was classified as partially-muscularized arteries.

Vascular ring studies in tissue baths: Fifth generation PA's were isolated and placed into a tissue bath consisting of Krebs's solution bubbled with 3.52% CO_2, 20% O_2 and balanced N_2 for a pO_2 ~150 mmHg at 37°C, pH was adjusted between 7.35 and 7.45 with HCl. Optimal resting tone was determined to be 200mg. PAs were pre-incubated with meclofenamic acid (10^{-5} M Sigma-Aldrich) and L-N^G-Nitroarginine methyl ester (L-NAME, 10^{-4} M Sigma-Aldrich) before constriction to either phenylephrine (10^{-5} M

Sigma-Aldrich) or hypoxia (Krebs's solution bubbled with 5.02% CO_2 and 2.48% O_2 to a pO_2 of 40-45 mmHg, pH 7.35-7.45), which was applied for one hour and measured as previously described[8]. No pre-constriction protocol was used in order to elicit hypoxic constrictions.

Drugs and peptides: Cultured cells (primary culture when stated or less than passage 5) were pre-incubated with wortmannin (5 nM, Sigma-Aldrich), SB216763 (10 μM Sigma-Aldrich), LY294002 (10 μM) (Calbiochem) for 48 hours before being fixed and stained for immunohistochemistry or stained with TMRM. The hexokinase-VDAC competitive peptide (100 μM) (Calbiochem) and its control peptide antennapedia (100 μM) (ED Biosciences) was used as described [28].

Statistics: Values are expressed as the mean±SEM. Inter-group differences in the in vivo experiments were assessed by Kruskal-Wallis; while in vitro data were analyzed with one-way ANOVA. Post hoc analysis with Fisher's Exact Test was performed (Statview 4.02, SAS Institute). $P<0.05$ was considered significant.

Figures

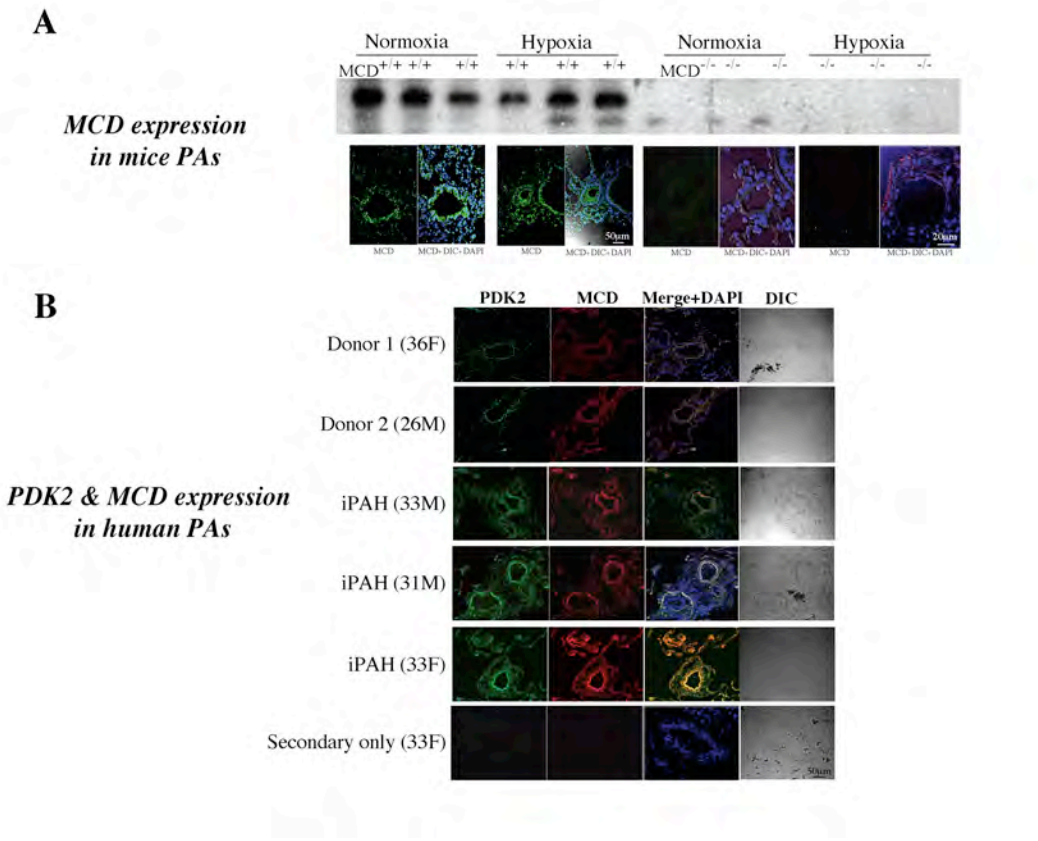

Fig. 2-1. MCD and PDK are present in mice and human PAs

(A) Contrary to wild-type mice, $MCD^{-/-}$ mice do not express MCD in their lungs (western blot) or pulmonary vasculature (immunohistochemistry). In addition, exposure to 3 weeks of chronic hypoxia did not affect MCD expression in both $MCD^{+/+}$ and $MCD^{-/-}$ animals. The absence of MCD was also confirmed in the heart, muscle and brain, data not shown and as previously published [19]. **(B)** Both transplant donor and idiopathic PAH patient lungs express PDK2 (green staining) and MCD (red staining) in the PAs (immunohistochemistry). Age and sex of the patients are shown in parenthesis. All three iPAH patients were on epoprostenol infusions, and either endothelin receptor blockers (bosentan) or sildenafil. The tissues were obtained and studied with approval from the University of Alberta human ethics committee.

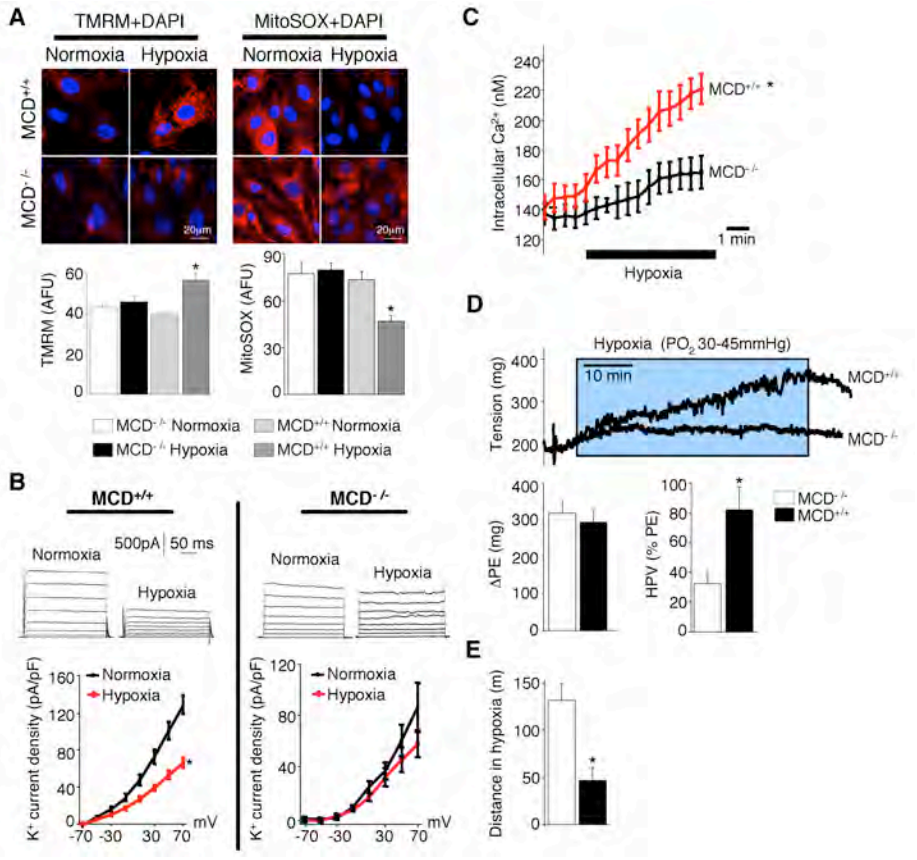

Fig. 2-2. MCD$^{-/-}$ mice lack HPV

(A) MCD$^{-/-}$ mice PASMC have similar ΔΨm (measured by TMRM) and mROS production (measured by MitoSOX) in acute moderate hypoxia (PO_2 30-40 mmHg) and normoxia; whereas MCD$^{+/+}$ PASMC exposed to acute hypoxia have significantly increased ΔΨm and decreased mROS (n=50; **P*<0.05). **(B)** MCD$^{-/-}$ PASMC have similar K^+ current (measured by whole-cell patch clamping) in acute hypoxia and normoxia; whereas MCD$^{+/+}$ mice PASMC exposed to acute hypoxia have decreased K^+ current (n=7-10; **P*<0.05 for the difference across all voltages, measured by ANOVA). **(C)** MCD$^{-/-}$ PASMC show a minimal increase, while MCD$^{+/+}$ PASMC show a significant rise in intracellular Ca^{2+} (measured by Fura 2AM) when exposed to acute hypoxia (n=10; **P*<0.05 for the difference across all time points, measured by ANOVA). **(D)** MCD$^{-/-}$ mice intact resistance PA rings constrict significantly less to acute moderate hypoxia than MCD$^{+/+}$ mice in the presence of L-NAME 10^{-4} M and meclofenamic acid 10^{-5}M (to inhibit nitric oxide and prostacyclin) without pre-constriction; a representative trace is shown at the top. HPV was normalized to the increase in tension induced by 10^{-5} M phenylephrine (ΔPE), which was similar between the two groups (n=6, **P*<0.05). **(E)** MCD$^{-/-}$ mice had superior exercise tolerance compared to MCD$^{+/+}$ mice when exposed to acute ambient hypoxia in an air-sealed treadmill (n=10, **P*<0.05).

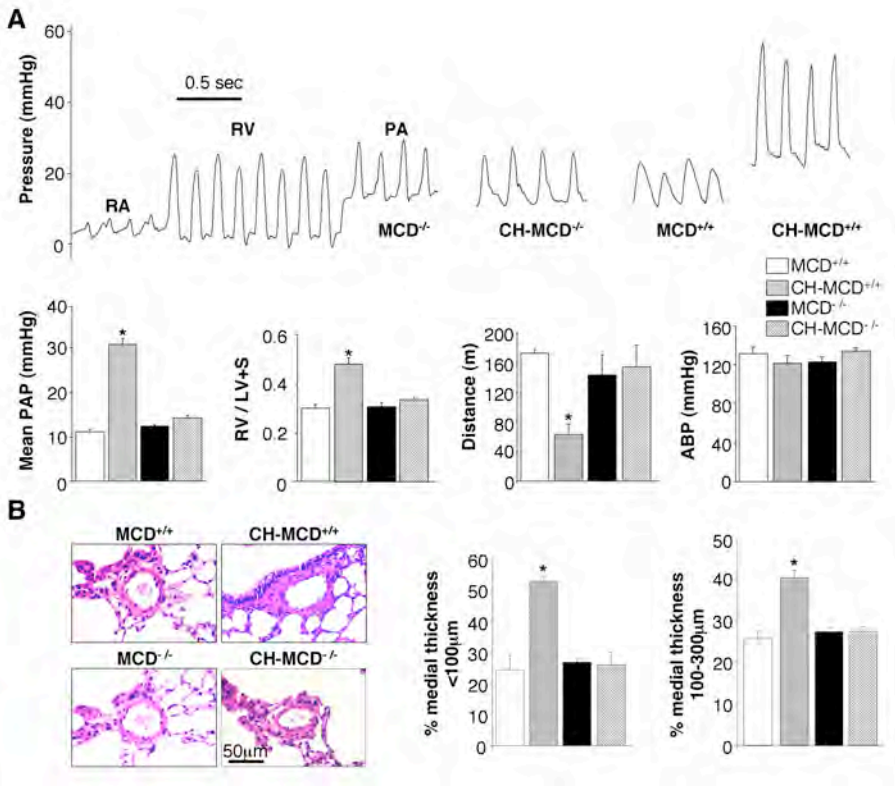

Fig. 2-3. MCD$^{-/-}$ mice are resistant to CH-PAH

(A) MCD$^{-/-}$ mice exposed to moderate, chronic normobaric hypoxia (CH) were resistant to the development of PAH while MCD$^{+/+}$ mice developed PAH as shown by significantly increased mean PA pressure (PAP), increased RV mass (RV/LV+septum weight ratio) and decreased exercise tolerance (distance run in standard rodent treadmill), while arterial blood pressure (ABP) was not altered. Representative traces obtained by using high fidelity Millar catheters during right heart catheterization are shown at the top (n=9-10 mice/group; **P*<0.05 vs normoxic controls). RA: right atrium. **(B)** CH-MCD$^{+/+}$ mice, but not CH-MCD$^{-/-}$ mice, had increased percent medial thickness in small (<100μm) and medium (100-300μm) sized pulmonary arteries (n=9-10 mice/group; **P*<0.05 vs normoxic controls).

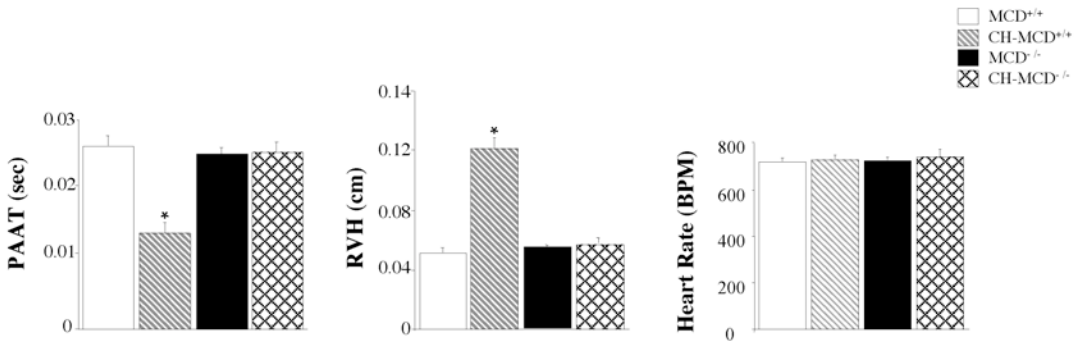

Fig. 2-4. CH-MCD$^{-/-}$ mice do not develop PAH

MCD$^{+/+}$ but not MCD$^{-/-}$ mice exposed to moderate chronic normobaric hypoxia (CH) developed PAH as shown by significantly decreased pulmonary artery acceleration time (PAAT, measured non-invasively with cardiac ECHO in non-anesthetized mice) and increased right ventricular free wall thickness (measured by M-mode echo) compared to normoxic control (n=9-10 mice/group; *P<0.05). Heart rate values [beats per minute (BPM)] were not different between any of the groups (n=5 mice/group).

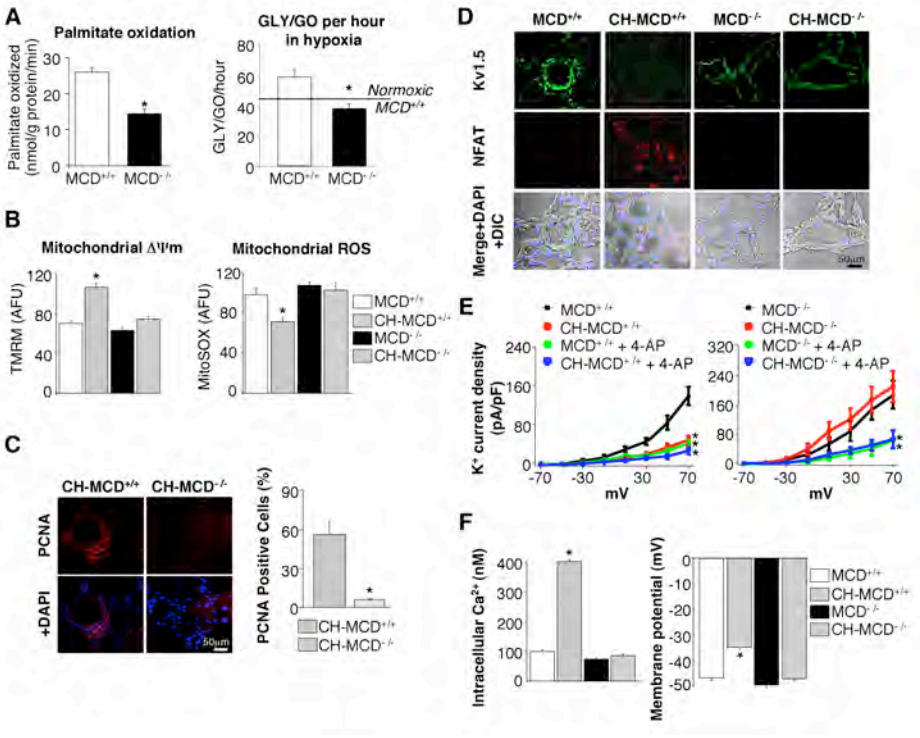

Fig. 2-5. MCD$^{-/-}$ mice do not undergo metabolic changes under hypoxia

(A) Baseline palmitate oxidation is significantly decreased in MCD$^{-/-}$ compared to MCD$^{+/+}$ PAs. GLY/GO is significantly increased in hypoxic compared to normoxic MCD$^{+/+}$ tissues, a metabolic switch that does not take place in MCD$^{-/-}$ tissues (n=5/group, **P*<0.05). **(B)** PAs freshly excised from CH-MCD$^{+/+}$ mice had significantly increased ΔΨm (TMRM) and decreased mROS production (MitoSOX), compared to those from CH-MCD$^{-/-}$ mice (n=50-60 PAs; 5 mice/group; **P*<0.05 vs normoxic controls). **(C)** Immunohistochemistry and confocal microscopy shows increased proliferation (PCNA) in PAs of CH-MCD$^{+/+}$ compared to CH-MCD$^{-/-}$ mice (n=50-60 PAs; 5 mice/group; **P*<0.05). **(D)** CH-MCD$^{+/+}$ PAs have decreased Kv1.5 and increased activation of NFATc2 (co-localized with DAPI as shown on the merged panels) compared to normoxic MCD$^{+/+}$, normoxic MCD$^{-/-}$ and CH-MCD$^{-/-}$ mice (representative images from 5 mice/group are shown). **(E)** PASMC freshly excised from CH-MCD$^{+/+}$ mice have decreased K^+ current density compared to normoxic MCD$^{+/+}$, normoxic MCD$^{-/-}$ and CH-MCD$^{-/-}$ PASMCs. The normoxic MCD$^{+/+}$ PASMC are sensitive to 4-aminopyridine (4-AP), showing a significant decrease in current density. The residual current is similar to that from CH-MCD$^{+/+}$, which is not inhibited by 4-AP. In contrast, normoxic and CH-MCD$^{-/-}$ PASMC have similar current density and both respond similarly to 4-AP (n=8-10 cells/group; **P*<0.05 vs normoxic and pre-4-AP control). **(F)** CH-MCD$^{+/+}$ PASMC have significantly higher intracellular Ca^{2+} (measured with Fura2-AM) than normoxic MCD$^{+/+}$, MCD$^{-/-}$ and CH-MCD$^{-/-}$ PASMC (n=40-50 cells from 5 mice/group; **P*<0.05). CH-MCD$^{+/+}$ mice PASMC have decreased plasma-membrane resting membrane potential (measured by whole-cell patch clamping) and intracellular Ca^{2+} (n=8-10; **P*<0.05).

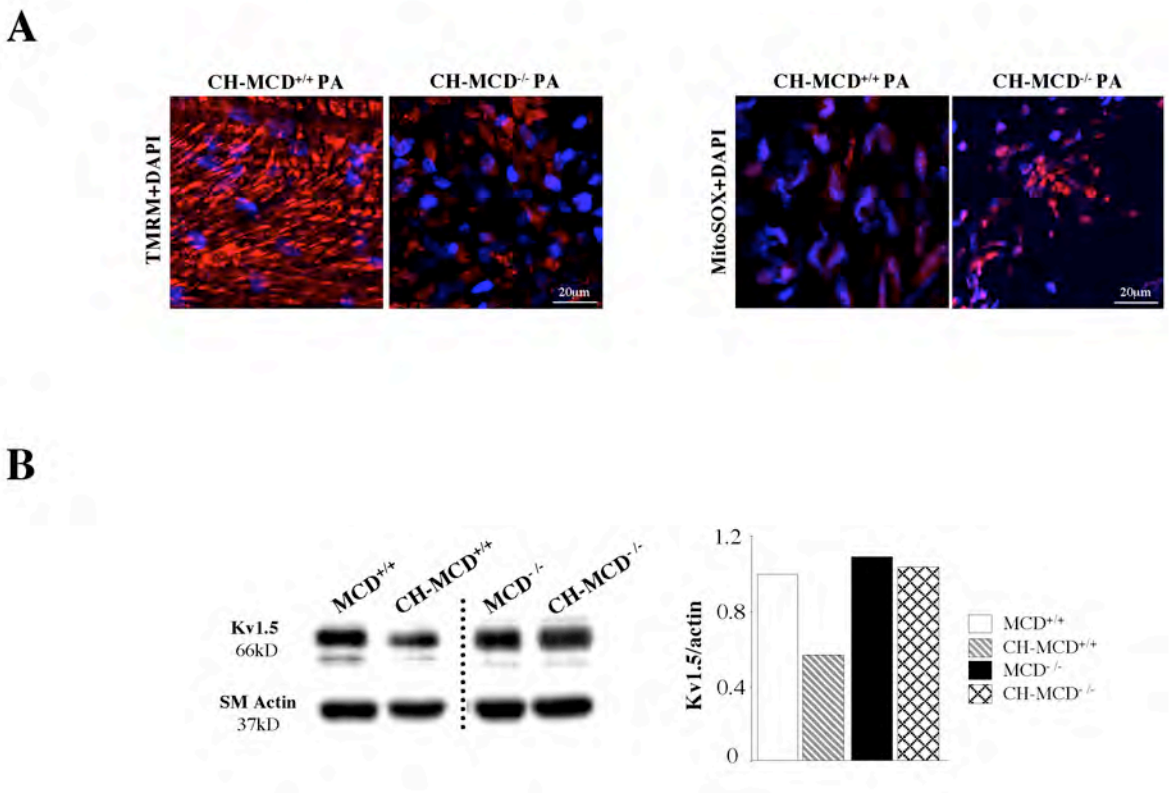

Fig. 2-6. CH-MCD$^{-/-}$ mice resistance PAs do not show the changes in mitochondrial function and Kv1.5 seen in the CH-MCD$^{+/+}$PAs

(A) Representative confocal microscopy at high magnification (x100) of freshly isolated PAs freshly excised from CH-MCD$^{+/+}$ mice showing increased ΔΨm (TMRM) and decreased mROS production (MitoSOX) in vascular wall cells, compared to those from CH-MCD$^{-/-}$ mice. **(B)** CH-MCD$^{+/+}$ mice resistance PAs have decreased Kv1.5 expression compared to normoxic MCD$^{+/+}$, normoxic MCD$^{-/-}$ and CH-MCD$^{-/-}$ as shown by immunoblots; *pooled* PAs from 5 mice in each lane; the ratio of the signal to smooth muscle actin is shown to the right.

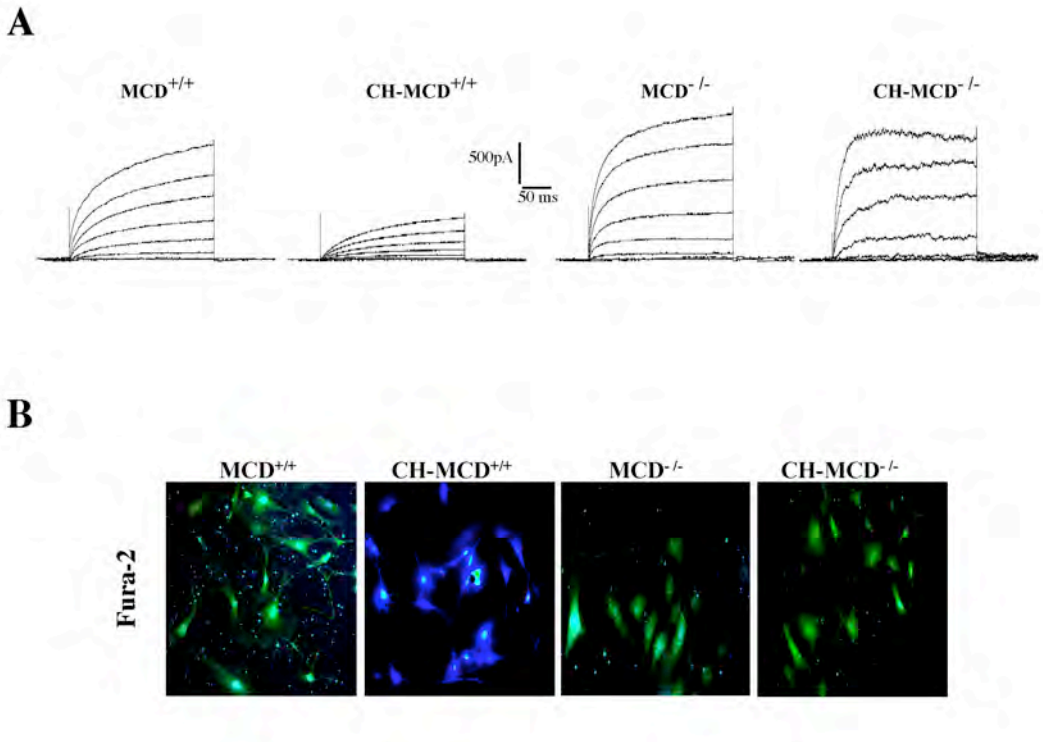

Fig. 2-7. CH-MCD$^{-/-}$ mice PASMC do not show the changes in K^+ current and intracellular Ca^{2+} seen in the CH-MCD$^{+/+}$PASMC

(A) Representative traces of K^+ current shows that PASMC from CH-MCD$^{+/+}$ mice have decreased K^+ current compared to normoxic MCD$^{+/+}$, normoxic MCD$^{-/-}$ and CH-MCD$^{-/-}$ PASMCs. **(B)** Representative images showing cytosolic calcium concentration as measured by Fura2-AM. CH-MCD$^{+/+}$ PASMC have significantly higher intracellular Ca^{2+} than normoxic MCD$^{+/+}$, MCD$^{-/-}$ and CH-MCD$^{-/-}$ PASMC.

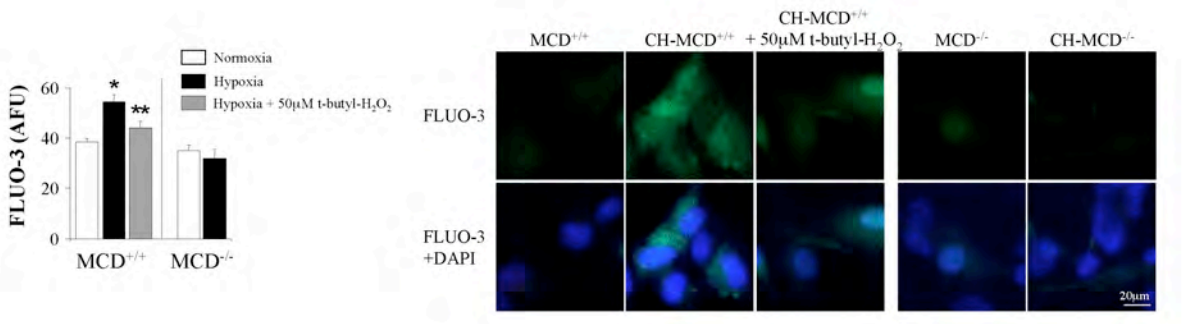

Fig. 2-8. Exogenous H_2O_2 inhibits the hypoxia-induced increase in intracellular Ca^{2+} in PASMC

Intracellular Ca^{2+} was measured with FLUO-3. CH-MCD$^{+/+}$ PASMCs have significantly increased intracellular Ca^{2+} levels compared to normoxic controls. Treatment of CH-MCD$^{+/+}$ PASMCs with exogenous H_2O_2 (50μm, t-butyl- H_2O_2) decreases intracellular Ca^{2+} levels. CH-MCD$^{-/-}$ mice PASMCs have similar intracellular Ca^{2+} levels to their normoxic controls (n=50 cells per group; **P*<0.05 vs. normoxic control, ***P*<0.05 vs. hypoxia-treated cells).

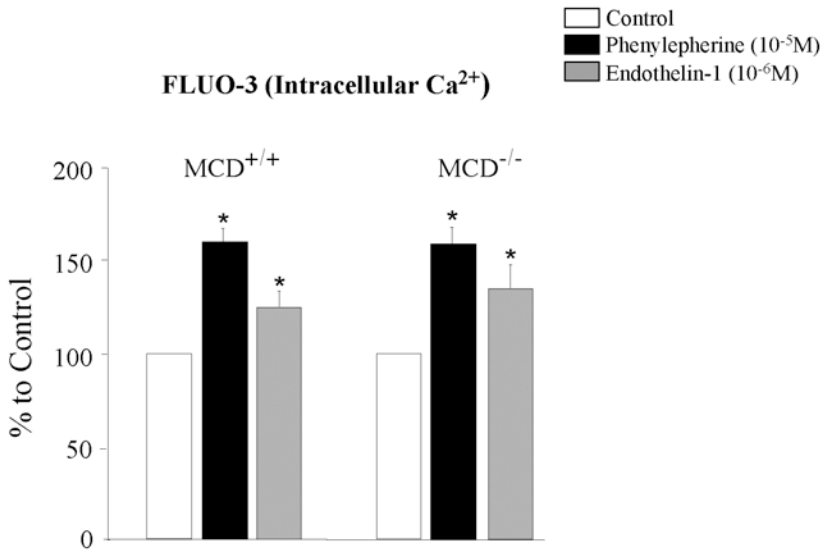

Fig. 2-9. $MCD^{+/+}$ and $MCD^{-/-}$ mice PASMC show a similar intracellular Ca^{2+} response to phenylephrine and endothelin-1

$MCD^{+/+}$ and $MCD^{-/-}$ mice PASMC have similar increases in intracellular Ca^{2+} when treated with phenylepherine (10^{-5}M) or endothelin-1 (10^{-6}M) (n=50 cells from 3 mice/group; **P*<0.05).

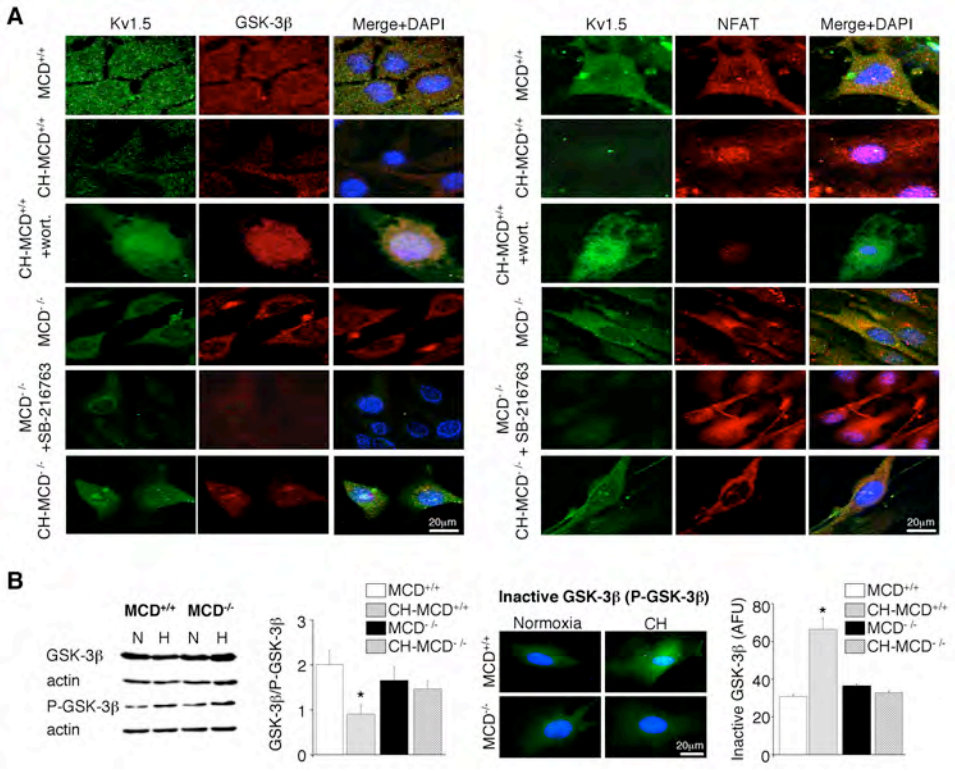

Fig. 2-10. Metabolic regulation of the GSK-3β-NFATc2-Kv1.5 axis in PASMC

(A) Confocal imaging and triple-staining of CH-MCD$^{+/+}$ PASMC shows that whole (active) GSK-3β and Kv1.5 are decreased (left panel) while NFATc2 activation (nuclear) is increased (right panel). When CH-MCD$^{+/+}$ PASMC are treated with the GSK-3β activator wortmannin (5nM), Kv1.5 and GSK-3β are increased and NFATc2 activation is decreased. Normoxic MCD$^{+/+}$, normoxic MCD$^{-/-}$ and CH-MCD$^{-/-}$ PASMC all similarly produce Kv1.5, GSK-3β and inactive NFATc2. When normoxic MCD$^{-/-}$ PASMC are treated with a GSK-3β inhibitor (SB216763, 10μM), Kv1.5 and GSK-3β are decreased and NFATc2 activation is increased, mimicking CH in MCD$^{+/+}$ mice. **(B)** Immunoblots of isolated PASMC from resistance PAs in primary culture with antibodies against whole active GSK-3β as well as inactive (phosphorylated) GSK-3β antibodies. PASMC immunocytochemistry with the same antibodies is shown on the right. Both methods reveal an overall decrease in GSK-3β activity (active/inactive ratio) by CH in MCD$^{+/+}$, but not MCD$^{-/-}$ tissues (*P<0.05 vs. normoxic control).

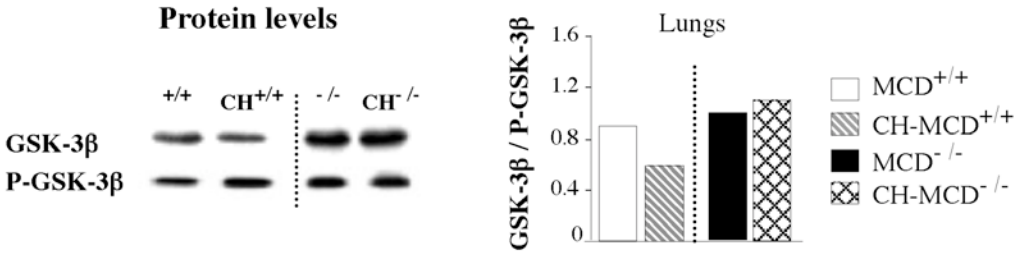

Fig. 2-11. GSK-3β activity is decreased in the lungs of CH-MCD$^{+/+}$ but not CH-MCD$^{-/-}$ mice

Immunoblots of whole lung (rich in pulmonary microvessels) with antibodies against whole active GSK-3β as well as inactive (phosphorylated) GSK-3β antibodies are shown.

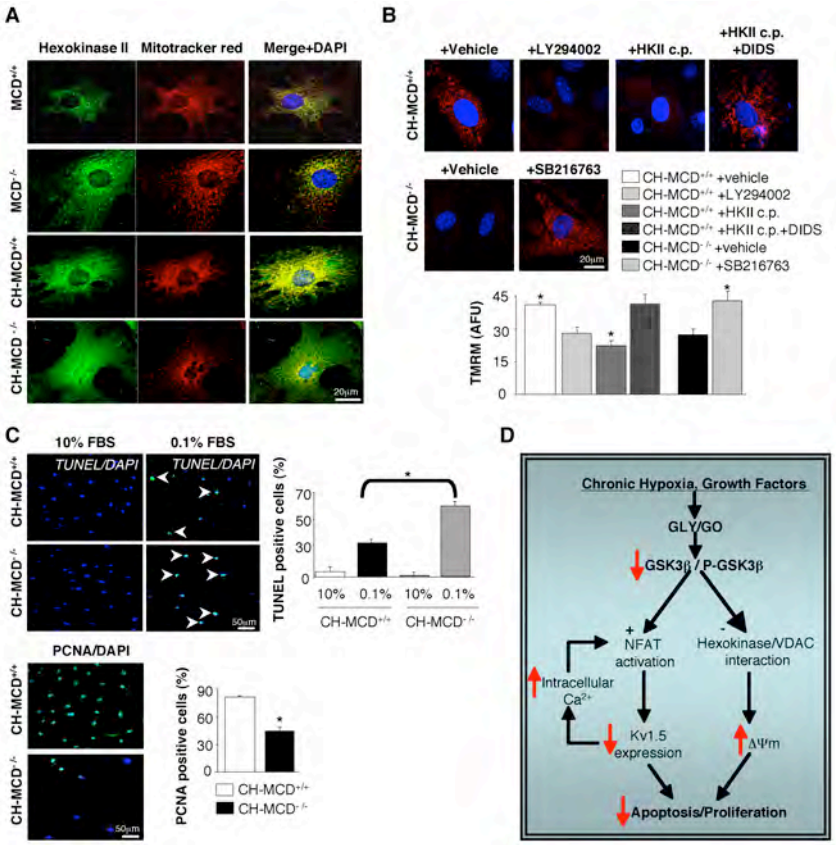

Fig. 2-12. Metabolic regulation of the GSK-3β-hexokinase axis and apoptosis resistance in PASMC

(A) Confocal imaging of normoxic MCD$^{+/+}$ and MCD$^{-/-}$ along with CH-MCD$^{-/-}$ PASMC showed a diffuse cytoplasmic staining of HKII, while CH-MCD$^{+/+}$ PASMC showed a mitochondrial pattern for HKII (yellow staining when merged with the mitochondrial dye mitotracker red). **(B)** CH-MCD$^{+/+}$ PASMC treated for 48hrs with a cell-permeable competitive peptide (c.p.) inhibiting the interaction between HKII and VDAC (100 μM) significantly decreased the ΔΨm (n=50 cells from 3 mice/group; **P*<0.05), and addition of the VDAC inhibitor DIDS (0.5 mM) returned the ΔΨm to the pretreatment CH-MCD$^{+/+}$ PASMC values. A GSK-3β activator (LY290042, 10μM) decreased ΔΨm in CH-MCD$^{+/+}$ PASMC while a GSK-3β inhibitor (SB216763, 10μM) increased ΔΨm in CH-MCD$^{-/-}$ PASMC (**P*<0.05 vs. vehicle). **(C)** CH-MCD$^{+/+}$ PASMC exposed to serum deprivation (0.1% FBS) show significantly decreased apoptosis (TUNEL-positive cells) compared to CH-MCD$^{-/-}$ PASMC. CH-MCD$^{+/+}$ PASMCs are more proliferative (PCNA-positive cells) compared to CH-MCD$^{-/-}$ PASMC (n=80 cells from 3 mice/group, **P*<0.05). **(D)** Proposed mechanism by which either metabolic (hypoxia) or molecular signals lead to an anti-apoptotic and pro-proliferative environment, which results in vascular remodeling and PAH. The central role of GSK-3β is shown, explaining the NFATc2 activation, Kv1.5 downregulation and mitochondrial hyperpolarization.

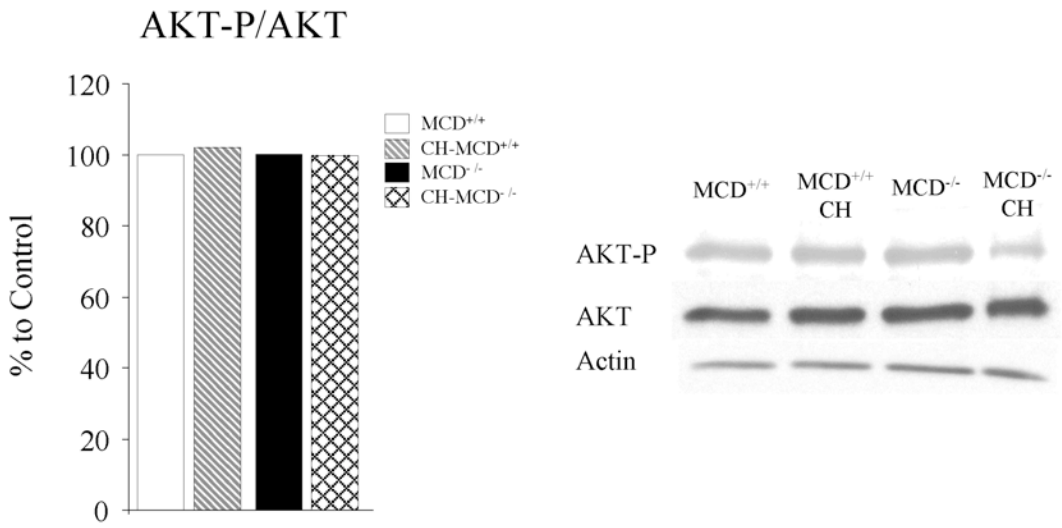

Fig. 2-13. PASMC Akt activity is similar between CH-MCD$^{+/+}$ and CH-MCD$^{-/-}$ mice

Immunoblot of PASMC with antibodies against active Akt (phosphorylated at serine 473) as well as inactive (non-phosphorylated) AKT are shown. Ratios of AKT-P/AKT (i.e. Akt activity) are similar between the MCD$^{+/+}$ and MCD$^{-/-}$ PASMC exposed to 48 hours of hypoxia compared to their normoxic controls.

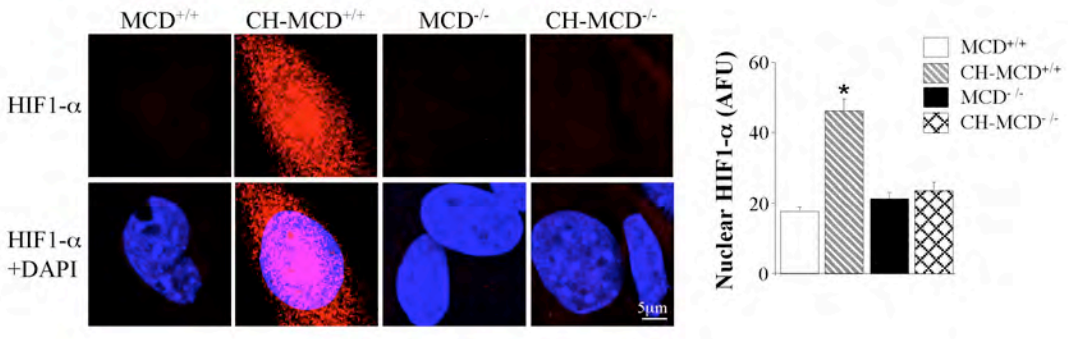

Fig. 2-14. HIF-1α is not activated in CH-MCD$^{-/-}$ PASMC

Freshly isolated PASMC from CH-MCD$^{+/+}$ mice have significantly increased activation of HIF-1α (nuclear localization) compared to normoxic controls. This increase in HIF-1α activation was not observed in CH-MCD$^{-/-}$ PASMCs (plated cells were studied in 3 experiments with 3 plates/experiment, n=50 cells, **P*<0.01).

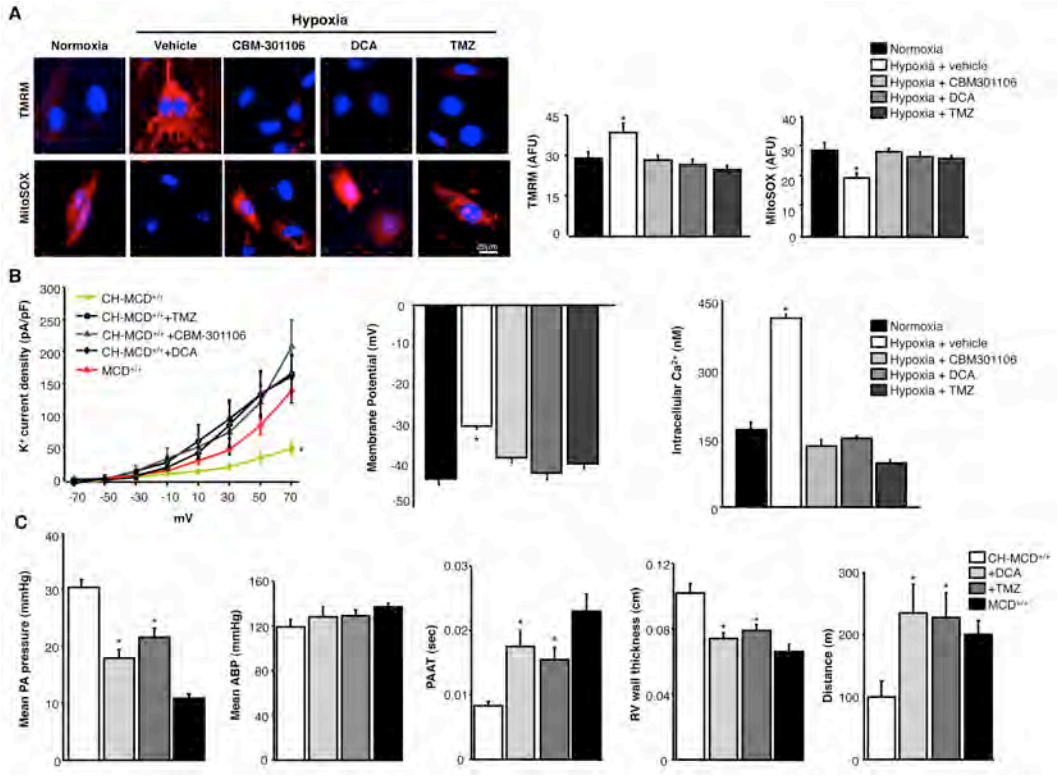

Fig. 2-15. Clinically available metabolic modulators mimic MCD loss and reverse CH-PAH

(A) CH-MCD$^{+/+}$ PASMC treated with dichloroacetate (DCA, 500μM), trimetazidine (TMZ, 10μM) and CBM301106 (10μM) [19]) returned ΔΨm (TMRM) and mROS production (MitoSOX) to values comparable to normoxic MCD$^{+/+}$ PASMC (n=50 from 3 mice/group; **P*<0.05). **(B)** CH-MCD$^{+/+}$ PASMC treated with DCA, TMZ and CBM301106 had similar K^+ current density (n=8-10), plasma membrane potential and cytosolic Ca^{2+} concentration, to the normoxic untreated control group (n=50 from 3 mice/group; **P*<0.05). **(C)** Vehicle (water)-treated CH-MCD$^{+/+}$ mice had significantly increased mean PA pressure, decreased PAAT, increased RV wall thickness, decreased exercise tolerance and similar systemic blood pressure compared to CH-MCD$^{+/+}$ mice treated for 3 weeks with either DCA (70mg/kg/day) or TMZ (420μg/day) or normoxic MCD$^{+/+}$ mice (n=8, **P*<0.05).

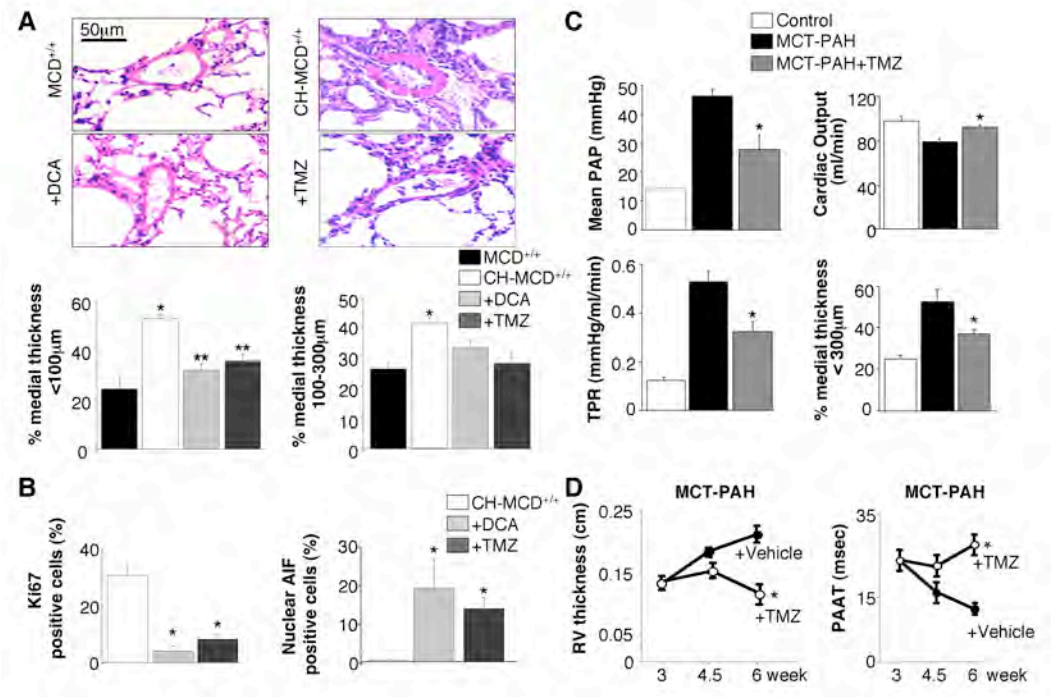

Fig. 2-16. DCA and TMZ reverse CH-PAH and monocrotaline-induced PAH

(A) Histology sections stained with hematoxylin and eosin showed that DCA and TMZ-treated mice had decreased % medial wall thickness of small (<100μm) and medium sized (100-300μm) PAs compared to vehicle-treated CH-MCD$^{+/+}$ mice (n=30-40 PAs, 5 mice/group, **P*<0.05 vs. MCD$^{+/+}$, ***P*<0.05 vs. CH-MCD$^{+/+}$). **(B)** Proliferation, as measured by Ki67, was significantly decreased in DCA and TMZ-treated CH-MCD$^{+/+}$ mice resistance PAs. Apoptosis measured by nuclear translocation of AIF was increased in DCA and TMZ-treated CH-MCD$^{+/+}$ mice resistance PAs (positive cells per PA are shown, n~50 arteries from 5 mice/groups, **P*<0.05). **(C)** Treatment for 3 weeks after monocrotaline (MCT) PAH was established in Sragues-Dawley rats (week 3 to 6) with TMZ resulted in decreased mean PA pressure, total pulmonary resistance (mean PA pressure / cardiac output) and % medial thickness (n=6; **P*<0.05). **(D)** TMZ treatment in MCT-PAH resulted in decreased RV wall thickness and increased PAAT compared to vehicle-treated control MCT-PAH rats (n=6; **P*<0.05).

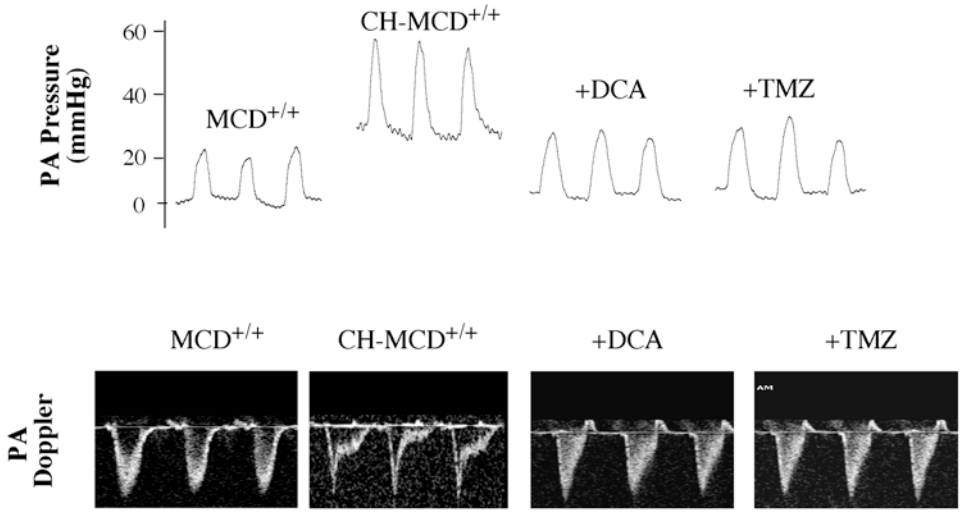

Fig. 2-17. Metabolic modulators reverse PAH in CH-MCD$^{+/+}$ mice

Representative PA pressure tracings (top) of MCD$^{+/+}$, vehicle (water)-treated CH-MCD$^{+/+}$ showing increased mean PA pressure compared to CH-MCD$^{+/+}$ mice treated for 3 weeks with either DCA (70mg/kg/day) or TMZ (420µg/day. Representative pulmonary artery pulsed wave Doppler traces (below) of MCD$^{+/+}$, CH- MCD$^{+/+}$, and CH- MCD$^{+/+}$ treated with DCA (70mg/kg/day) or TMZ (420µg/day); DCA and MCD treatment caused a significant decrease in the pulmonary artery acceleration time (the time form the beginning of the Doppler signal deflection to the peak of the deflection). In humans and rodents PAAT correlates negatively with mean PA pressure (the shorter the PAAT the higher the PA pressure).

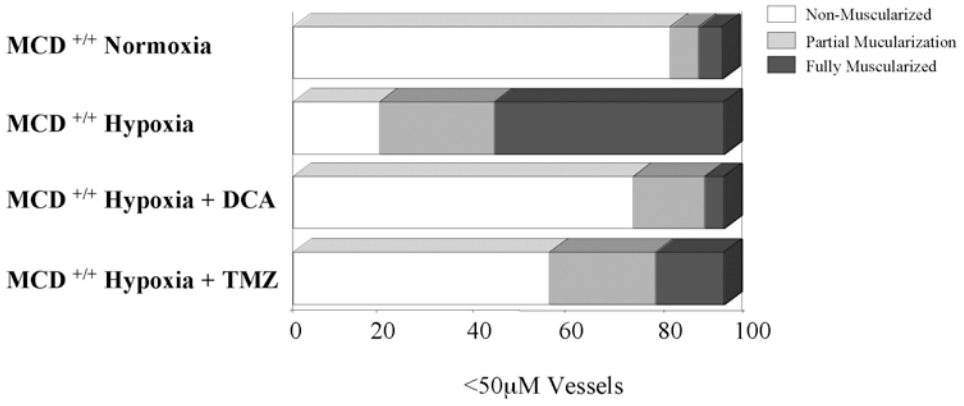

Fig. 2-18. Metabolic modulators reverse small PA muscularization in CH-MCD$^{+/+}$ mice

DCA and TMZ treatment decreased muscularization (see methods) in small PAs (<50μm) compared to placebo-treated controls. % of PAs per field from 5 mice/group are shown.

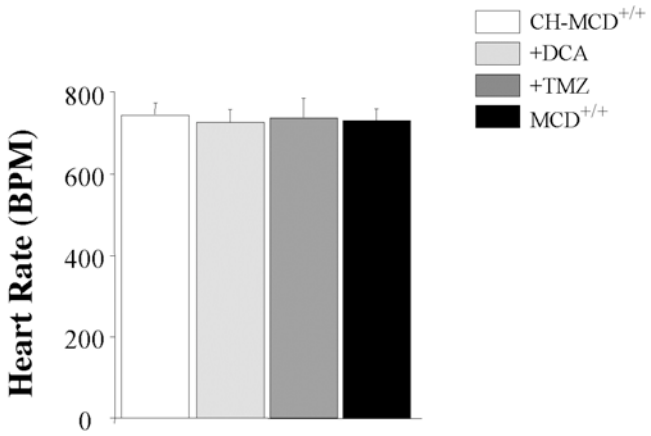

Fig. 2-19. Metabolic modulators do not alter heart rate in CH-MCD$^{+/+}$mice

Heart rate [beats per minute (BPM)] was similar between CH-MCD$^{+/+}$, CH-MCD$^{+/+}$ mice treated for 3 weeks with either DCA and TMZ (420μg/day) and normoxic MCD$^{+/+}$ mice (n=5 mice per group).

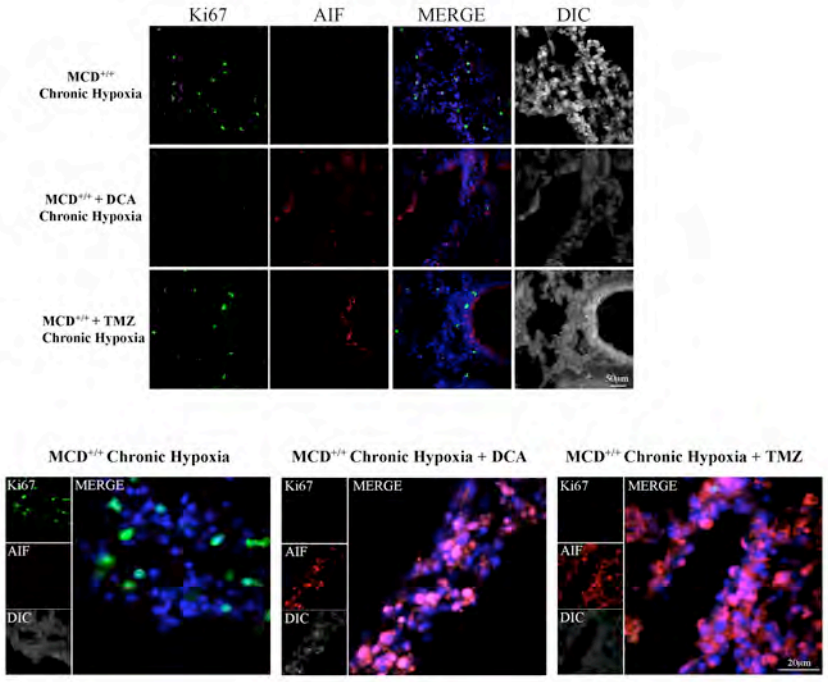

Fig. 2-20. Metabolic modulators decrease proliferation and increase apoptosis in the CH-MCD$^{+/+}$ resistance PAs

Representative images showing increased proliferation as measured by Ki67 (green, low magnification (Top), high magnification (Bottom)) in CH-MCD$^{+/+}$ mice resistance PAs. Apoptosis was measured by nuclear translocation of AIF. Nuclear AIF was increased in DCA and TMZ-treated CH-MCD$^{+/+}$ mice distal PAs (red).

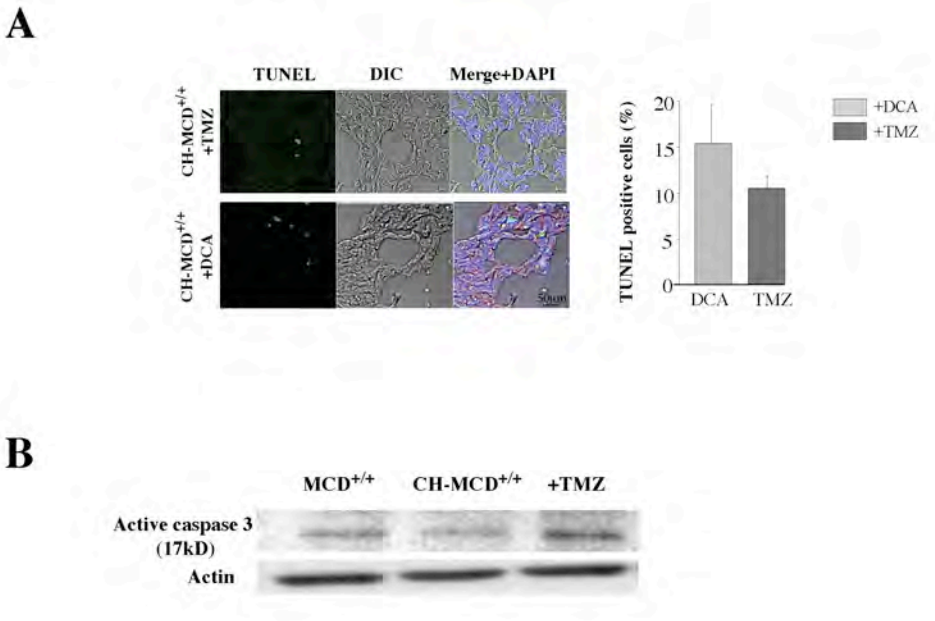

Fig. 2-21. Metabolic modulators increase apoptosis in the CH-MCD$^{+/+}$ resistance PAs

Immunohistochemistry **(A)** and immunoblots **(B)** showed that DCA and TMZ therapy induced apoptosis in the PA vascular wall (% positive TUNEL cells (top) and increased caspase 3 activity (bottom) in excised pulmonary arteries) (n~50 cells; in the immunoblot there are pooled resistance PAs from 3 mice per lane per group).

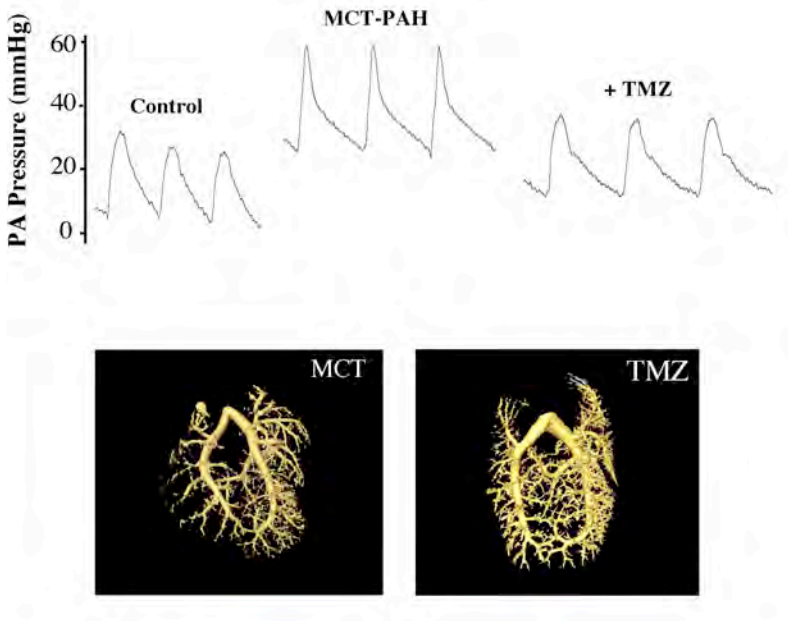

Fig. 2-22. TMZ reverses rat MCT-PAH

Representative PA pressure tracings (top) of control Sprague Dawley (SD) rats, monocrotaline (MCT) induced-PAH SD rats and trimetazidine (TMZ)-treated MCT-PAH SD rats. Barium infused micro-CT angiogram (below) shows increased pulmonary vascular perfusion in a TMZ treated rat compared to an untreated group.

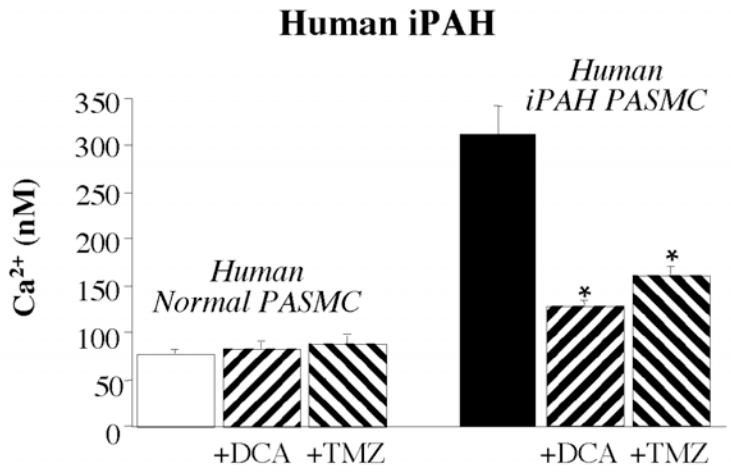

Fig. 2-23. Metabolic modulators decrease intracellular Ca^{2+} in human PAH PASMC in culture

DCA (500μM) and TMZ (10μM) treatment did not change the intracellular Ca^{2+} in normal human PASMC but significantly decreased and normalized the intracellular Ca^{2+} in idiopathic PAH PASMC (n=40; *P<0.05).

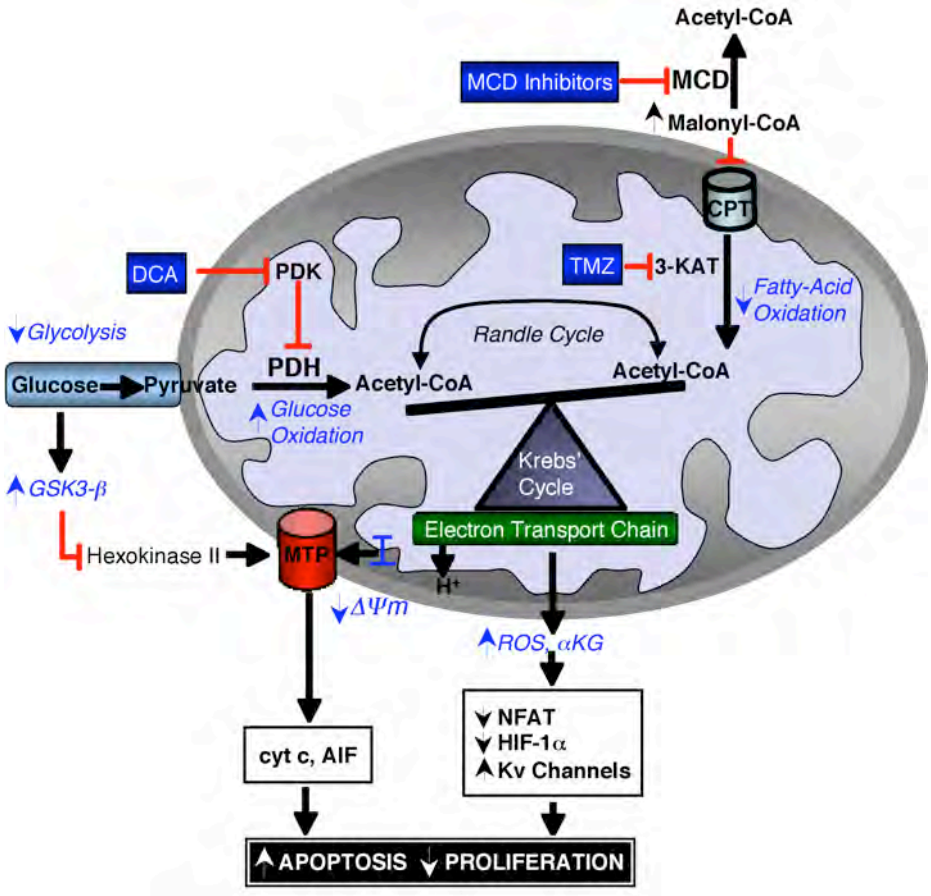

Fig.2-24. Proposed mechanism for the effects of metabolic modulators in PAH

Molecular or pharmacologic MCD inhibition, shares with clinically-used metabolic modulators (like DCA and TMZ) the downstream effects on mitochondria signaling that lead to reversal of the proliferative and anti-apoptotic diathesis in PAH (see discussion). 3-KAT; 3-ketoacyl-CoA-thiolase.

References

1. Michelakis ED, Wilkins MR, Rabinovitch M (2008) Emerging concepts and translational priorities in pulmonary arterial hypertension. Circulation 118: 1486-1495

2. Archer SL, Weir EK, Wilkins MR (2010) Basic science of pulmonary arterial hypertension for clinicians: new concepts and experimental therapies. Circulation 121: 2045-2066

3. Bonnet S, Archer SL, Allalunis-Turner J, Haromy A, Beaulieu C, Thompson R, Lee CT, Lopaschuk GD, Puttagunta L, Bonnet S, Harry G, Hashimoto K, Porter CJ, Andrade MA, Thebaud B, Michelakis ED (2007) A mitochondria-K+ channel axis is suppressed in cancer and its normalization promotes apoptosis and inhibits cancer growth. Cancer Cell 11: 37-51

4. Michelakis ED, Sutendra G, Dromparis P, Webster L, Haromy A, Niven E, Maguire C, Gammer TL, Mackey J, Fulton D, Abdulkarim B, McMurtry SM, Petruk KC (2010) Metabolic modulation of glioblastoma with dichloroacetate. Science Translational Medicine 2: 31ra34

5. Pan JG, Mak TW (2007) Metabolic targeting as an anticancer strategy: dawn of a new era? Sci STKE 2007: pe14

6. Vander Heiden MG, Cantley LC, Thompson CB (2009) Understanding the Warburg effect: the metabolic requirements of cell proliferation. Science 324: 1029-1033

7. Michelakis ED (2008) Mitochondrial medicine: a new era in medicine opens new windows and brings new challenges. Circulation 117: 2431-2434

8. Michelakis ED, Hampl V, Nsair A, Wu X, Harry G, Haromy A, Gurtu R, Archer SL (2002) Diversity in mitochondrial function explains differences in vascular oxygen sensing. Circ Res 90: 1307-1315.

9. Michelakis ED, Weir EK (2008) The metabolic basis of vascular oxygen sensing: diversity, compartmentalization, and lessons from cancer. Am J Physiol Heart Circ Physiol 295: H928-H930

10. Weir EK, Lopez-Barneo J, Buckler KJ, Archer SL (2005) Acute oxygen-sensing mechanisms. N Engl J Med 353: 2042-2055

11. Stacpoole PW (1989) The pharmacology of dichloroacetate. Metabolism 38: 1124-1144

12. Bonnet S, Michelakis ED, Porter CJ, Andrade-Navarro MA, Thebaud B, Bonnet S, Haromy A, Harry G, Moudgil R, McMurtry MS, Weir EK, Archer SL (2006) An abnormal mitochondrial-hypoxia inducible factor-1alpha-Kv channel pathway disrupts oxygen sensing and triggers pulmonary arterial hypertension in fawn hooded rats: similarities to human pulmonary arterial hypertension. Circulation 113: 2630-2641

13. Guignabert C, Tu L, Izikki M, Dewachter L, Zadigue P, Humbert M, Adnot S, Fadel E, Eddahibi S (2009) Dichloroacetate treatment partially regresses established pulmonary hypertension in mice with SM22alpha-targeted overexpression of the serotonin transporter. FASEB J 23: 4135-4147

14. McMurtry MS, Bonnet S, Wu X, Dyck JR, Haromy A, Hashimoto K, Michelakis ED (2004) Dichloroacetate prevents and reverses pulmonary hypertension by inducing pulmonary artery smooth muscle cell apoptosis. Circ Res 95: 830-840

15. Michelakis ED, McMurtry MS, Wu XC, Dyck JR, Moudgil R, Hopkins TA, Lopaschuk GD, Puttagunta L, Waite R, Archer SL (2002) Dichloroacetate, a metabolic modulator, prevents and reverses chronic hypoxic pulmonary hypertension in rats: role of increased expression and activity of voltage-gated potassium channels. Circulation 105: 244-250

16. Randle PJ (1998) Regulatory interactions between lipids and carbohydrates: the glucose fatty acid cycle after 35 years. Diabetes Metab Rev 14: 263-283

17. Dyck JR, Barr AJ, Barr RL, Kolattukudy PE, Lopaschuk GD (1998) Characterization of cardiac malonyl-CoA decarboxylase and its putative role in regulating fatty acid oxidation. Am J Physiol 275: H2122-2129

18. Ussher JR, Lopaschuk GD (2008) The malonyl CoA axis as a potential target for treating ischaemic heart disease. Cardiovasc Res 79: 259-268

19. Dyck JR, Hopkins TA, Bonnet S, Michelakis ED, Young ME, Watanabe M, Kawase Y, Jishage K, Lopaschuk GD (2006) Absence of malonyl coenzyme A decarboxylase in mice increases cardiac glucose oxidation and protects the heart from ischemic injury. Circulation 114: 1721-1728

20. Dyck JR, Cheng JF, Stanley WC, Barr R, Chandler MP, Brown S, Wallace D, Arrhenius T, Harmon C, Yang G, Nadzan AM, Lopaschuk GD (2004) Malonyl coenzyme a decarboxylase inhibition protects the ischemic heart by inhibiting fatty acid oxidation and stimulating glucose oxidation. Circ Res 94: e78-84

21. Maggiorini M (2003) Cardio-pulmonary interactions at high altitude. Pulmonary hypertension as a common denominator. Adv Exp Med Biol 543: 177-189

22. Stenmark KR, Meyrick B, Galie N, Mooi WJ, McMurtry IF (2009) Animal models of pulmonary arterial hypertension: the hope for etiological discovery and pharmacological cure. Am J Physiol Lung Cell Mol Physiol 297: L1013-1032

23. McMurtry MS, Archer SL, Altieri DC, Bonnet S, Haromy A, Harry G, Bonnet S, Puttagunta L, Michelakis ED (2005) Gene therapy targeting survivin selectively induces pulmonary vascular apoptosis and reverses pulmonary arterial hypertension. J Clin Invest 115: 1479-1491

24. Yuan XJ, Wang J, Juhaszova M, Gaine SP, Rubin LJ (1998) Attenuated K+ channel gene transcription in primary pulmonary hypertension. Lancet 351: 726-727

25. Archer SL, Souil E, Dinh-Xuan AT, Schremmer B, Mercier JC, El Yaagoubi A, Nguyen-Huu L, Reeve HL, Hampl V (1998) Molecular identification of the role of

voltage-gated K+ channels, Kv1.5 and Kv2.1, in hypoxic pulmonary vasoconstriction and control of resting membrane potential in rat pulmonary artery myocytes. J Clin Invest 101: 2319-2330

26. Platoshyn O, Golovina VA, Bailey CL, Limsuwan A, Krick S, Juhaszova M, Seiden JE, Rubin LJ, Yuan JX (2000) Sustained membrane depolarization and pulmonary artery smooth muscle cell proliferation. Am J Physiol Cell Physiol 279: C1540-1549

27. Remillard CV, Yuan JX (2004) Activation of K+ channels: an essential pathway in programmed cell death. Am J Physiol Lung Cell Mol Physiol 286: L49-67

28. Bonnet S, Rochefort G, Sutendra G, Archer SL, Haromy A, Webster L, Hashimoto K, Bonnet SN, Michelakis ED (2007) The nuclear factor of activated T cells in pulmonary arterial hypertension can be therapeutically targeted. Proc Natl Acad Sci U S A 104: 11418-11423

29. Macian F (2005) NFAT proteins: key regulators of T-cell development and function. Nat Rev Immunol 5: 472-484

30. Pastorino JG, Hoek JB, Shulga N (2005) Activation of glycogen synthase kinase 3beta disrupts the binding of hexokinase II to mitochondria by phosphorylating voltage-dependent anion channel and potentiates chemotherapy-induced cytotoxicity. Cancer Res 65: 10545-10554

31. Zamzami N, Kroemer G (2001) The mitochondrion in apoptosis: how Pandora's box opens. Nat Rev Mol Cell Biol 2: 67-71

32. Cohen P, Goedert M (2004) GSK3 inhibitors: development and therapeutic potential. Nat Rev Drug Discov 3: 479-487

33. Denko NC (2008) Hypoxia, HIF1 and glucose metabolism in the solid tumour. Nat Rev Cancer 8: 705-713

34. MacKenzie ED, Selak MA, Tennant DA, Payne LJ, Crosby S, Frederiksen CM, Watson DG, Gottlieb E (2007) Cell-permeating alpha-ketoglutarate derivatives alleviate pseudohypoxia in succinate dehydrogenase-deficient cells. Mol Cell Biol 27: 3282-3289

35. Mottet D, Dumont V, Deccache Y, Demazy C, Ninane N, Raes M, Michiels C (2003) Regulation of hypoxia-inducible factor-1alpha protein level during hypoxic conditions by the phosphatidylinositol 3-kinase/Akt/glycogen synthase kinase 3beta pathway in HepG2 cells. J Biol Chem 278: 31277-31285

36. Fragasso G, Piatti Md PM, Monti L, Palloshi A, Setola E, Puccetti P, Calori G, Lopaschuk GD, Margonato A (2003) Short- and long-term beneficial effects of trimetazidine in patients with diabetes and ischemic cardiomyopathy. Am Heart J 146: E18

37. Stacpoole PW, Nagaraja NV, Hutson AD (2003) Efficacy of dichloroacetate as a lactate-lowering drug. J Clin Pharmacol 43: 683-691

38. Kim JW, Dang CV (2005) Multifaceted roles of glycolytic enzymes. Trends Biochem Sci 30: 142-150

39. Bonnet S, Paulin R, Sutendra G, Dromparis P, Roy M, Watson KO, Nagendran J, Haromy A, Dyck JR, Michelakis ED (2009) Dehydroepiandrosterone reverses systemic vascular remodeling through the inhibition of the Akt/GSK3-{beta}/NFAT axis. Circulation 120: 1231-1240

40. Xu W, Koeck T, Lara AR, Neumann D, DiFilippo FP, Koo M, Janocha AJ, Masri FA, Arroliga AC, Jennings C, Dweik RA, Tuder RM, Stuehr DJ, Erzurum SC (2007) Alterations of cellular bioenergetics in pulmonary artery endothelial cells. Proc Natl Acad Sci U S A 104: 1342-1347

41. Merklinger SL, Jones PL, Martinez EC, Rabinovitch M (2005) Epidermal growth factor receptor blockade mediates smooth muscle cell apoptosis and improves survival in rats with pulmonary hypertension. Circulation 112: 423-431

42. Schermuly RT, Dony E, Ghofrani HA, Pullamsetti S, Savai R, Roth M, Sydykov A, Lai YJ, Weissmann N, Seeger W, Grimminger F (2005) Reversal of experimental pulmonary hypertension by PDGF inhibition. J Clin Invest 115: 2811-2821

43. Sobolewski A, Rudarakanchana N, Upton PD, Yang J, Crilley TK, Trembath RC, Morrell NW (2008) Failure of bone morphogenetic protein receptor trafficking in pulmonary arterial hypertension: potential for rescue. Hum Mol Genet 17: 3180-3190

44. Sitbon O, Lascoux-Combe C, Delfraissy JF, Yeni PG, Raffi F, De Zuttere D, Gressin V, Clerson P, Sereni D, Simonneau G (2008) Prevalence of HIV-related pulmonary arterial hypertension in the current antiretroviral therapy era. Am J Respir Crit Care Med 177: 108-113

45. Sehgal PB, Mukhopadhyay S, Patel K, Xu F, Almodovar S, Tuder RM, Flores SC (2009) Golgi dysfunction is a common feature in idiopathic human pulmonary hypertension and vascular lesions in SHIV-nef-infected macaques. Am J Physiol Lung Cell Mol Physiol 297: L729-737

46. Cool CD, Rai PR, Yeager ME, Hernandez-Saavedra D, Serls AE, Bull TM, Geraci MW, Brown KK, Routes JM, Tuder RM, Voelkel NF (2003) Expression of human herpesvirus 8 in primary pulmonary hypertension. N Engl J Med 349: 1113-1122

47. Hansmann G, Zamanian RT (2009) PPARgamma activation: a potential treatment for pulmonary hypertension. Sci Transl Med 1: 12ps14

48. Ceylan ME, Alpsan MH (2007) Pulmonary hypertension during lithium therapy: clinical case study. Psychopharmacol Bull 40: 110-112

49. Filtenborg JA (1982) Persistent pulmonary hypertension after lithium intoxication in the newborn. Eur J Pediatr 138: 321-323

50. Tuder RM, Chacon M, Alger L, Wang J, Taraseviciene-Stewart L, Kasahara Y, Cool CD, Bishop AE, Geraci M, Semenza GL, Yacoub M, Polak JM, Voelkel NF (2001)

Expression of angiogenesis-related molecules in plexiform lesions in severe pulmonary hypertension: evidence for a process of disordered angiogenesis. J Pathol 195: 367-374

51. Salomons GS, Jakobs C, Pope LL, Errami A, Potter M, Nowaczyk M, Olpin S, Manning N, Raiman JA, Slade T, Champion MP, Peck D, Gavrilov D, Hillman R, Hoganson GE, Donaldson K, Shield JP, Ketteridge D, Wasserstein M, Gibson KM (2007) Clinical, enzymatic and molecular characterization of nine new patients with malonyl-coenzyme A decarboxylase deficiency. J Inherit Metab Dis 30: 23-28

52. Wightman PJ, Santer R, Ribes A, Dougherty F, McGill N, Thorburn DR, FitzPatrick DR (2003) MLYCD mutation analysis: evidence for protein mistargeting as a cause of MLYCD deficiency. Hum Mutat 22: 288-300

A version of this chapter has been accepted for publication. Sutendra G, Bonnet S, Rochefort G, Cutbert K, Lopaschuck G, Dyck J and Michelakis ED. Fatty acid oxidation and malonyl-CoA decarboxylase in the vascular remodeling of pulmonary hypertension. Sci. Transl. Med. 2010. August; 2, 44ra58.

Chapter Three

The Role of Nogo and the Mitochondria-Endoplasmic Reticulum unit in Pulmonary Hypertension

Abstract

Pulmonary arterial hypertension (PAH) is caused by excessive proliferation of vascular cells, occluding the lumen of pulmonary arteries (PA) and leading to right ventricular failure. The cause of the vascular remodeling in PAH remains unknown and despite existing therapies its prognosis remains poor. Mitochondria, which form a functional unit with the endoplasmic reticulum (ER), are abnormal in PAH PA smooth muscle cells (SMCs), leading to a suppression of mitochondria-dependent apoptosis and contributing to the vascular remodeling. We hypothesized that early endoplasmic reticulum (ER) stress, which is associated with many clinical triggers of PAH including hypoxia, bone morphogenetic protein receptor-II mutations and HIV/HSV infections, may explain the mitochondrial abnormalities and have a causal role in PAH. We showed that Nogo-B, a regulator of ER structure, was induced in hypoxic PA but not systemic SMCs, by activation of the ER stress-sensitive transcription factor ATF6. Nogo-B induction caused an increased distance between the ER and mitochondria and decreased ER to mitochondria phospholipid transfer and intra-mitochondrial calcium. This was associated with inhibition of calcium-sensitive mitochondrial enzymes, increased mitochondrial membrane potential, decreased mitochondrial reactive oxygen species and decreased mitochondria-dependent apoptosis. Lack of Nogo-B in PASMCs from *Nogo-A/B*$^{-/-}$ mice prevented these hypoxia-induced changes *in vitro* and similarly *in vivo*, resulting in complete resistance to PAH. Hypoxic heterozygous mice developed less pronounced hemodynamic and molecular changes compared to wild-type controls, exhibiting a gene dose-dependent effect. Nogo-B in the serum and pulmonary arteries of PAH patients was also increased. Therefore, triggers of PAH may induce Nogo-B, which disrupts the ER-mitochondria unit and suppresses apoptosis. The disruption of the ER-mitochondria unit may be relevant to other diseases where Nogo is implicated, like cancer or neurodegeneration.

Introduction

Pulmonary Arterial Hypertension (PAH) is a disease of the pulmonary circulation caused by an excessive proliferation of vascular cells eventually leading to obliteration of the lumen in resistance pulmonary arteries (PA), while sparing systemic vessels [1]. Although its idiopathic and familial forms are rare, PAH is associated with several more common diseases like collagen vascular diseases, congenital heart disease or AIDS, among others [1]. The median survival of untreated patients is less than 3 years after the time of diagnosis [1]. The existing therapies have all been originally developed as vasodilators for systemic vascular diseases and not as anti-proliferative or pro-apoptotic therapies aiming to reverse established pulmonary vascular remodeling. Thus, it is not surprising that although they improve some symptoms, they do not reverse the disease or prolong survival [2, 3].

Several environmental and genetic triggers in PAH have been proposed, including alveolar hypoxia, loss-of-function mutations of bone morphogenetic protein receptor II (BMPRII) or viral infections with herpes simplex virus (HSV) or human immunodeficiency virus (HIV) [4]. Diverse signaling abnormalities accompany the disease, pointing to comprehensive therapeutic approaches [4]. As in cancer, a glycolytic metabolic phenotype appears to be a common downstream feature of several genetic and signaling abnormalities in PAH [5]. For example, in cancer, loss of p53 or activation of AKT or cmyc, results in suppression of mitochondria-based glucose oxidation (GO), with a resultant shift to the cytoplasm-based glycolysis [6]. This shift has been associated with a resistance to mitochondria-dependent apoptosis and provides a potential explanation for the Warburg effect in cancer, in which there is a shift in the energy production from GO toward glycolysis, even in the absence of hypoxia [7]. There is a similar shift in PAH, and metabolic modulators or genetic interventions that reverse the suppression of GO also reverse the disease in animal models of PAH as they do in cancer [7-10]. In both

cancer and PAH however, the primary cause of this metabolic switch remains unknown [5, 11].

Endoplasmic reticulum (ER) stress is a fundamental cellular response that may be a common feature of several triggers of PAH. For example, hypoxia [4], viral infections [12], the unfolded protein response that follows BMPRII mutations (which occur in 75% of familial and less than 20% of sporadic PAH cases [1]) and inflammation [4] or Notch induction [13] are all associated with variable degrees of ER stress [14-17]. In addition, abnormal ER structure, suggestive of ER stress, has been shown in electron microscopy studies of PAH tissues more than 30 years ago [18], but its potential role in PAH pathogenesis remains unknown. The lung and its resistance PAs, which lie adjacent to the alveoli, are highly exposed to stress signals, as one of the body's major contact points with the environment. The resistance PAs (normally exposed to a pO_2 of more than 100mmHg) are also exposed to much more oxidative stress than systemic resistance arteries (exposed to pO_2 of about 50mmHg) [19, 20], suggesting that the regulation of and threshold for ER stress may be unique in the pulmonary vasculature. We hypothesized that ER stress may participate in pulmonary circulation-specific metabolic and mitochondrial remodeling in PAH.

Nogo is a member of the reticulon family of proteins and is critical in regulating the tubular structure of the ER [21]. Nogo exists in three isoforms, A, B and C, with Nogo-A expressed in the central nervous system, Nogo-B expressed ubiquitously and Nogo-C expressed in both neurons and skeletal muscle [22-24]. Nogo-B was decreased in mice femoral arteries following wire injury and was shown to inhibit smooth muscle cell (SMC) migration but promote endothelial cell migration [25]. Mice lacking Nogo-A/B developed exaggerated neointimal remodeling, which was rescued with adenoviral-mediated gene transfer of Nogo-B [25]. Furthermore, Nogo-A was increased in hypoxic areas of the brain in rat models of cerebral ischemia by an unknown mechanism [26].

Nogo-A is thought to promote neuronal survival by suppressing apoptosis during sustained ER stress, but its intracellular mechanisms remain unknown [24]. Animals lacking both Nogo-A and Nogo-B have a relatively normal phenotype suggesting compensation and functional overlap among Nogo isoforms [25, 27]. Because Nogo is implicated in vascular remodeling and in tissue response to hypoxia, we speculated that Nogo-B might play role in PAH. While Nogo-A is absent from blood vessels and the lung, Nogo-B is present in both [25, 27].

The close physical proximity of the ER and mitochondria networks in cells allows for the efficient exchange of mediators between the two organelles [28]. Calcium from the ER, the largest Ca^{2+} store in the cell, can enter the mitochondria and activate critical Ca^{2+}-dependent mitochondrial enzymes [29, 30] such as pyruvate dehydrogenase (PDH), an enzyme that regulates the influx of pyruvate into the mitochondria and promotes GO. The entry of the positively charged Ca^{2+} also promotes mitochondrial depolarization and apoptosis. This is because the opening of the mitochondrial transition pore, through which pro-apoptotic mediators can efflux initiating mitochondria-dependent apoptosis, is voltage-gated and promoted by depolarization [31]. Because of the mitochondrial Ca^{2+}-uniporter's low affinity for Ca^{2+}, its influx depends on Ca^{2+} microdomains, allowing mitochondrial entry down a concentration gradient [32]. Such gradients are facilitated by the close proximity of the Ca^{2+}-rich ER to the mitochondria networks [29, 30]. Such proximity also allows ATP from the mitochondria to efficiently reach the ER, its largest consumer. In addition to the close proximity, the two organelles are linked by tethers [28, 33] and specialized contact points (mitochondria-associated membranes, MAM), facilitating exchange of phospholipids [34], thus forming a functional mitochondria-ER unit.

Both suppressed PDH activity and hyperpolarized mitochondria in PASMC are associated with the pathogenesis of PAH [5, 9, 10]. Thus, a potential disruption of the

mitochondria-ER unit may explain these important abnormalities. Because Nogo regulates the structure of the ER it is possible that induction of Nogo-B may disrupt the mitochondria-ER unit. Here we test the effects of hypoxia and ER stress on PASMC Nogo-B induction, on the mitochondria-ER unit and on the pathogenesis of PAH.

Results

3.1. Nogo-B expression is increased in human PAH

We examined the levels of Nogo-B in the PAs of age-sex matched patients with (*n*=5) and without PAH (*n*=3) who underwent transplant surgery at our center. Using immunohistochemistry with multiphoton confocal microscopy, we found that Nogo-B levels were increased in the vascular wall of PAH compared to control patient tissues (Fig. 3-1A, 3-2).

In order to explore Nogo as a potential biomarker in PAH, we measured serum Nogo-A/B levels in PAH patients (*n*=41), in age and sex-matched healthy subjects (*n*=18) and in patients with secondary pulmonary hypertension due to thromboembolic disease (*n*=6), a condition in which pulmonary hypertension is caused by a mechanical obstruction (embolized thrombus) and not by primary abnormalities intrinsic to the PAs. Nogo-A/B was increased in the serum of PAH patients compared to the control groups (Fig. 3-1B, 3-3). Nogo-A/B serum levels were highest in patients with the most advanced disease (World Health Organization functional class III and IV) (Fig. 3-3).

We then measured Nogo-B mRNA and protein in primary cultures of normal and PAH human PASMCs, isolated from intrapulmonary resistance pulmonary arteries (<300μm) immediately after lung tissue extraction in the operating room. Both Nogo-B protein and mRNA levels were also upregulated in PAH PASMCs *in vitro* (Fig. 3-1C and 3-1D).

Because Nogo-B levels are decreased in a mouse model of systemic vascular remodeling after injury [25], we also measured Nogo-B in carotid artery SMCs

(CASMCs), isolated from two transplant donors (Fig. 3-1D). To test for differences in the regulation of Nogo-B between the pulmonary and systemic circulations, we exposed normal human PASMCs and CASMCs to two inducers of ER stress, hypoxia and thapsigargin [14, 35]. Nogo-B expression was induced in physiologic hypoxia, [pO_2~40mmHg (versus a normal value of 120mmHg), while the pH and pCO_2 remain normal] in normal PASMCs at levels similar to the PAH PASMCs, but was not induced in CASMCs. Nogo-B expression was not further increased in hypoxic PAH PASMCs compared to normoxic PAH PASMCs (Fig. 3-1D). To prove that ER stress was indeed occurring in hypoxic and PAH PASMCs, we studied GRP-78, an ER stress marker [36]. Similar to Nogo-B, GRP-78 was increased in PAH and hypoxic normal PASMCs compared to normal PASMCs. Hypoxia did not further increase GRP-78 levels in PAH PASMCs (Fig. 3-4). Thapsigargin induced Nogo-B in both PASMCs and CASMCs (Fig. 3-1D).

There are three major ER stress sensors [ATF6, PERK and IRE1 [14]]. Of these, the transcription factor ATF6 is associated with a pro-survival response, is redox-sensitive [35, 37] (and thus is perhaps more responsive to the reducing signals of hypoxia than the other two ER stress sensors) and increases Nogo expression [36]. The protease inhibitor AEBSF, which inhibits the cleavage and activation of ATF6 in the Golgi apparatus [38], and an ATF6 siRNA (but not its scrambled RNA control) prevented the Nogo-B induction in PASMCs subject to ER stress and normalized Nogo-B expression in PAH PASMCs, but not in CASMCs (Fig. 3-1D**)**.

These results were confirmed by immunocytochemistry (Fig. 3-1E**)**. Nuclear levels of ATF6 were increased in hypoxic and PAH PASMCs, indicative of increased activity; in the same cells, we observed increased Nogo-B protein levels. In addition, compared to normoxic PAH PASMCs, ATF6 activation was not further increased by hypoxia (Fig. 3-4). ATF6 inhibition with AEBSF decreased the levels of nuclear ATF6

and Nogo-B in hypoxia (Fig. 3-1E). In contrast, hypoxia did not increase nuclear ATF6 or Nogo-B levels in CASMC (Fig. 3-1E**)**. To confirm the specificity of ATF6 activation in PASMCs, we used a dual luciferase reporter and showed that in identically treated human PASMCs and CASMCs, ATF6 activity was increased by hypoxia only in the PASMCs (Fig. 3-5).

3.2. A gene dose-dependent effect of Nogo-B in PAH

To study the hemodynamic impact and the selectivity of the induction of Nogo-B in the pulmonary circulation, we studied mice with either homozygous (-/-) or heterozygous (+/-) deletion of Nogo-A/B isoforms. Since Nogo-A does not exist in the lungs, Nogo-B is the likely form of Nogo in the lungs of these mice [27]. These mice have a normal phenotype in basal conditions [25, 27], but we hypothesized that lack of Nogo-B would make *Nogo*$^{-/-}$ mice resistant to 3 weeks of chronic normobaric hypoxia-induced PAH (CH-PAH). As in human PAH, Nogo-B levels were increased in the PAs of both CH-wild-type littermates (*Nogo*$^{+/+}$) and CH-heterozygote (*Nogo*$^{+/-}$) mice compared to their normoxic controls (Fig. 3-6A). Immunoblots (Fig. 3-6B) and qRT-PCR (Fig. 3-7) showed a gene dose-dependent increase in Nogo-B protein and mRNA levels between *Nogo*$^{-/-}$, *Nogo*$^{+/-}$ and *Nogo*$^{+/+}$ in CH-PAH PAs.

The CH-*Nogo*$^{-/-}$ mice had normal mean pulmonary artery pressure (mPAP) measured invasively (Fig. 3-6C), no right ventricular hypertrophy (RVH) (Fig. 3-6C) and normal pulmonary artery acceleration time (PAAT), measured with echocardiography (Fig. 3-8A). As expected, the CH-*Nogo*$^{+/+}$ mice developed PAH, with increased mPAP, significant RVH (Fig. 3-6C) and decreased PAAT (Fig. 3-8A**)**. The CH-*Nogo*$^{+/-}$ mice developed PAH to a lesser extent than the CH-*Nogo*$^{+/+}$ mice, suggesting a Nogo-B gene dose-dependent effect on PAH pathogenesis (Fig. 3-6C). To study the functional effects of PAH *in vivo*, all three groups of mice were exercised on a treadmill. CH-*Nogo*$^{+/+}$ and CH-*Nogo*$^{+/-}$, but not CH-*Nogo*$^{-/-}$ mice, had decreased functional capacity compared to

normoxic controls (Fig. 3-6C). All groups had similar systemic blood pressure and heart rate (Fig. 3-6C, 3-8B).

As in human cells, *Nogo*$^{+/+}$ PASMCs isolated from mice resistance PAs showed increased levels of nuclear ATF6 and Nogo-B in response to hypoxia in an AEBSF-sensitive manner (Fig. 3-9A). Nuclear ATF6 was significantly increased in hypoxic *Nogo*$^{-/-}$ PASMCs, suggesting that hypoxia induced ER stress in these cells as well (Fig. 3-9A). In contrast, *Nogo*$^{+/+}$ CASMCs did not exhibit any changes in nuclear ATF6 or Nogo-B levels in response to hypoxia (Fig. 3-9A).

Both *Nogo*$^{+/+}$ and *Nogo*$^{-/-}$ PASMCs, but not CASMCs, showed a similar increase in GRP-78 in response to hypoxia (Fig. 3-9B, 3-10). In order to study hypoxic stress in systemic arteries similar in size to resistance PAs we also studied renal artery SMCs (RASMCs) isolated from *Nogo*$^{+/+}$ resistance renal arteries (<300μm). Similar to CASMCs, hypoxia did not increase GRP-78 or Nogo-B mRNA expression in RASMCs (Fig. 3-9B). This suggests that the resistance pulmonary circulation may have a lower threshold for hypoxia-induced ER stress, specifically ER stress signaling driven by ATF6, demonstrating a pulmonary circulation-specific induction of Nogo-B in response to hypoxia.

3.3. Nogo-B disrupts the mitochondria-ER unit

To study the integrity of the mitochondria-ER unit in hypoxia, we used both structural and functional criteria. Using electron microscopy, we found that the minimal distance between the mitochondria and ER was increased by hypoxia in PASMCs from *Nogo*$^{+/+}$, but not *Nogo*$^{-/-}$ mice, compared to normoxic controls (Fig. 3-9C, 3-11). Using immuno-gold labeling, we found that the most of Nogo-B was present in the ER (Fig. 3-12A), although small amounts were also located within the plasma membrane (Fig. 3-12B). Thus, the upregulation of Nogo-B under hypoxia-induced ER stress, by altering ER

structure, can disrupt the mitochondria-ER unit; the absence of Nogo-B allowed for the persistence of a structurally intact unit.

To determine whether these structural changes caused a functional disruption of the mitochondria-ER unit, we used a phospholipid biosynthesis assay. Phosphatidylserine (PtdSer) is a phospholipid that is synthesized in the ER by PtdSer synthase (PSS) and is subsequently transferred to the outer aspect of the mitochondrial inner-membrane where it is decarboxylated by phosphatidylethanolamine (PtdEtn) decarboxylase (PSD) to PtdEtn (Fig. 3-9D). Because this reaction does not occur elsewhere in the cell, PtdSer decarboxylation is an index of mitochondria-ER unit integrity [34]. PASMCs were incubated with [^{3}H]serine and [^{3}H]PtdEtn was measured. Although no significant differences were seen in any of the groups in the baseline synthesis of PtdSer (Fig. 3-13), [^{3}H]PtdEtn production was lower in CH-*Nogo*$^{+/+}$, but not in CH-*Nogo*$^{-/-}$, PASMCs compared to normoxic controls (Fig. 3-9D). Less [^{3}H]PtdEtn was also synthesized in human PAH PASMCs compared to normal PASMCs (Fig. 3-9D).

An immediate consequence of the mitochondria-ER unit disruption is a decrease in intra-mitochondrial calcium ($[Ca^{2+}]_m$) [29, 30]. We measured $[Ca^{2+}]_m$ with two separate techniques. In the first, we used the chameleon plasmid for mitochondrial FRET-Ca^{2+} and confocal imaging, as previously described [39]. *Nogo*$^{+/+}$, but not *Nogo*$^{-/-}$, PASMCs exposed to hypoxia showed a decreased YFP/CFP signal, indicating a decrease in $[Ca^{2+}]_m$ (Fig. 3-14A). These results were replicated by using Rhod-2AM, a Ca^{2+} fluorophore with specificity for the mitochondria, as shown by its co-localization with the mitochondria marker mito-green (Fig. 3-15).

A decrease in $[Ca^{2+}]_m$ would decrease critical mitochondrial enzyme activity known to be calcium-dependent, i.e. pyruvate dehydrogenase (PDH) and isocitrate dehydrogenase (IDH) [29, 32]. We directly measured PASMC PDH activity and showed that hypoxia caused a significant decrease in *Nogo*$^{+/+}$, but not in *Nogo*$^{-/-}$ PDH activity

(Fig. 3-14B). We then measured α-ketoglutarate (α-KG), a product of IDH and an important mediator of hypoxia inducing factor (HIF) signaling [40]. Hypoxia decreased α-KG levels in *Nogo*$^{+/+}$, but not *Nogo*$^{-/-}$, PASMCs (Fig. 3-14C). The decrease in PDH and IDH activity would suppress GO and overall mitochondrial respiration, a well-known effect of hypoxia on intact cells. Indeed, respiration in the *Nogo*$^{+/+}$ PASMCs, previously exposed to hypoxia, was much less than in their normoxic controls (Fig. 3-14D). There was no detectable difference in respiration between normoxic and previously exposed hypoxic *Nogo*$^{-/-}$ PASMCs (Fig. 3-14D). These data suggest that the induction of Nogo-B causes the metabolic/mitochondrial remodeling and downstream signaling effects previously described in animal and human tissue models of PAH, including CH-PAH (as well as in cancer) [7-10].

3.4. Nogo-deficient PASMCs are resistant to the hypoxia-induced changes in mitochondria-NFAT-HIF-Kv channel axis

We have previously described mitochondrial hyperpolarization and decreased mitochondria-derived reactive oxygen species (mROS) in proliferative, anti-apoptotic PAH PASMCs [9, 10, 41, 42]. These changes are critical for PAH since pharmacologic (dichloroacetate) or molecular reversal of the decrease in PDH activity normalizes this mitochondrial remodeling and reverses PAH in several rodent models [9, 10]. However, the initial signals that cause this mitochondrial remodeling and how the many diverse triggers of PAH all relate to this, remain unknown. We measured mitochondrial potential (ΔΨm) and mROS in normoxic and hypoxic PASMCs. While hypoxia, as expected, increases ΔΨm and decreases mROS in *Nogo*$^{+/+}$ PASMCs, these effects are absent in the *Nogo*$^{-/-}$ PASMCs (Fig. 3-16A, 3-17). Furthermore, *Nogo*$^{+/-}$ PASMCs have levels of ΔΨm and mROS between *Nogo*$^{-/-}$ and *Nogo*$^{+/+}$ PASMCs, in keeping with the Nogo-B gene dose-dependent effect that we described in the severity of mice CH-PAH (Fig. 3-6C).

In human tissues and rodent PAH models there is both decreased opening and down-regulation of redox-sensitive voltage-gated K^+ channels, such as Kv1.5 [10, 41-43]. Using whole-cell patch clamping, we showed that the 4-aminopyridine (4-AP) sensitive K^+ current (i.e. Kv current) is suppressed in the hypoxic *Nogo*$^{+/+}$, but not *Nogo*$^{-/-}$ PASMCs (Fig. 3-16B, 3-18). Inhibition of Kv channels causes plasma membrane depolarization and opening of the voltage-gated Ca^{2+} channels, with a resulting increase in PASMC $[Ca^{2+}]_i$, normally the basis of hypoxic pulmonary vasoconstriction [44]. Although *Nogo*$^{+/+}$, *Nogo*$^{+/-}$ and *Nogo*$^{-/-}$ PASMCs all had similar levels of $[Ca^{2+}]_i$ at baseline, hypoxia increased $[Ca^{2+}]_i$ in *Nogo*$^{+/+}$, but not *Nogo*$^{-/-}$ PASMCs. Hypoxic *Nogo*$^{+/-}$ PASMCs had $[Ca^{2+}]_i$ levels between *Nogo*$^{+/+}$ and *Nogo*$^{-/-}$ PASMCs, in keeping with the gene dose dependent effects of hypoxia on mROS production (Fig. 3-16C, 3-19). These differences in $[Ca^{2+}]_i$ regulation among the three cell types were intrinsic to a mechanism involving the mitochondria [mitochondria are important oxygen sensors that initiate the hypoxic pulmonary vasoconstriction signaling in normal PASMC [44]] since phenylephrine, which causes direct release of Ca^{2+} from the ER, caused a similar increase in $[Ca^{2+}]_i$ (Fig. 3-16C, 3-19). These results suggest that the ER remains functionally normal in normoxic cells lacking Nogo-B, consistent with the overall normal cardiovascular phenotype of *Nogo*$^{-/-}$ mice.

Nuclear factor of activated T-cells (NFATc2), which decreases Kv1.5 expression and is activated in PAH PASMCs by a glycolysis-driven inhibition of glycogen synthase kinase-3β (GSK-3β) and an increase in $[Ca^{2+}]_i$ [9, 42], was activated in CH-*Nogo*$^{+/+}$ PASMCs both *in vitro* and *in vivo* (Fig. 3-20). Accordingly, in cells in which NFATc2 was activated there was a down-regulation of Kv1.5. In contrast, NFATc2 was not activated and Kv1.5 was not down-regulated in *Nogo*$^{-/-}$ PASMCs, *in vitro* or *in vivo* (Fig. 3-20). Similarly, HIF-1α which is also activated in PAH and decreases Kv1.5 expression [41], was activated in CH-*Nogo*$^{+/+}$ PASMCs, in a manner sensitive to the ATF6 inhibitor

AEBSF. In CH-*Nogo*$^{-/-}$ PASMCs there was no significant HIF-1α activation (Fig. 3-16D). This is in keeping with the sustained mROS and α-KG production, both regulators of HIF-1α stabilization, in CH-*Nogo*$^{-/-}$ PASMCs. This suggests that a mitochondrial signal is critical for the activation of HIF-1α in these conditions, while the direct effects of hypoxia on hydroxylation and HIF-1α stability may not be enough to activate HIF-1α in these cells.

Our previous work has provided strong evidence that the above described changes in ΔΨm and the associated suppression of mitochondria-dependent apoptosis, as well as its secondary effects on transcription factors like NFATc2 and HIF, critical kinases like GSK-3β, $[Ca^{2+}]_i$ and Kv channels, largely explain the anti-apoptotic and pro-proliferative environment in the PA wall in PAH [9]. Accordingly, among the *Nogo*$^{+/+}$, *Nogo*$^{+/-}$ and *Nogo*$^{-/-}$ PASMCs both proliferation and apoptosis resistance correlated positively with Nogo-B protein levels (Fig. 3-21A, 3-21B, 3-21C and 3-22). Once again, there was a gene dose-dependent effect both on the expression of proliferating cell nuclear antigen (PCNA) under hypoxia and on the %TUNEL-positive cells under pro-apoptotic, starvation conditions (0.1% serum) *in vitro* (Fig. 3-21A, 3-21B and 3-22). This explains the lack of PA remodeling (% media thickness), a hallmark of PAH in the *Nogo*$^{-/-}$ mice *in vivo* (Fig. 3-21D, 3-23).

3.5. Exogenous expression of Nogo-B disrupts the mitochondria-ER unit and induces a PAH phenotype in normal PASMC, mimicking hypoxia

To study the direct effects of Nogo-B, the only isoform present in the lungs, on the mitochondria-ER unit and determine whether exogenous Nogo-B mimics its endogenous induction and the effects of hypoxia, we infected normoxic PASMCs with an adenovirus carrying the *Nogo-B* gene. As a control we used an adenovirus that carried the green-fluorescent protein (*GFP*) gene at the same multiplicity of infection. Infection with

the *Nogo-B*, but not the *GFP* virus, increased Nogo-B protein levels, caused mitochondrial hyperpolarization, decreased mROS and decreased Kv1.5 protein levels (Fig. 3-24). This suggests that the hypoxia-induced changes in mitochondria and Kv channels are downstream of Nogo-B induction.

Discussion

We report that Nogo-B expression is increased in PAH in humans and in a mouse model of PAH and is critical for the development of this deadly proliferative vascular disease. In addition to the well-established receptor-mediated signaling of Nogo isoforms, particularly in axonal regeneration in the central nervous system, we propose that Nogo-B has direct intracellular effects on the mitochondria-ER unit. We determined that there was a Nogo-B gene dose-dependent effect for the severity of CH-PAH in mice *in vivo*, i.e. the higher the expression of Nogo-B, the more severe the hemodynamic as well as the molecular changes that characterize PAH. Absence of Nogo-B in mice causes complete resistance to CH-PAH, while the overall cardiovascular phenotype remains normal. Administration of exogenous Nogo-B mimics hypoxia and induces a PAH cellular phenotype in PASMCs. These findings suggest that Nogo-B may be a useful therapeutic target for PAH. In addition, we have identified a pathway that not only explains several key features of PAH but that offers insights into the role of Nogo during ER stress in general. There is emerging evidence that Nogo is expressed during ER stress as part of a rescue response that contributes to cell survival, whereas the absence of Nogo (or inadequate expression) during sustained ER stress may allow or facilitate apoptosis [24]. The intracellular mechanism underlying these observations remained unknown [24], but our data now provide a direct link between Nogo, ER stress and mitochondrial signaling with broad implications.

Mitofusin 2 (Mfn2) has been proposed to function as a tether, linking the ER with the mitochondria, a contributor to an intact mitochondria-ER unit [45]. The absence

of Mfn2 *in vitro* leads to disruption of the mitochondria-ER unit, decreased $[Ca^{2+}]_m$, mitochondrial hyperpolarization as well as enlarged ER and generalized ER dysfunction [45]. Absence of Mfn2 is embryonically lethal in mice, limiting the exploration of its role in health and disease *in vivo*. We now show that Nogo-B is critical for the function of the mitochondria-ER unit in the pulmonary circulation, but absence of Nogo-A/B is not lethal in mice and does not result in a generalized ER dysfunction under normal conditions. However, absence of Nogo-B may increase the susceptibility of PASMCs to apoptosis under sustained stress conditions like hypoxia or growth factor withdrawal. The presence of Nogo-B at adequate levels during ER stress may allow for restructuring of the ER and disruption of the mitochondria-ER unit, which leads to mitochondrial hyperpolarization, closure of the mitochondrial transition pore and suppression of apoptosis. The decrease in $[Ca^{2+}]_m$ suppresses mitochondrial function and oxidative phosphorylation (see mechanism in Fig. 3-21E). Although the cells can compensate over time by increasing glucose uptake and generating ATP *via* cytoplasmic glycolysis, the short-term effects of this mitochondrial suppression are important for at least two reasons. First, this mitochondrial hyperpolarization is associated with a potentially beneficial decrease in mROS, since oxidative stress exacerbates ER stress. Second, the initial decrease in ATP production might decrease activity of sarco/endoplasmic reticulum calcium-ATPases, and thus limit the Ca^{2+}-overload of the ER another feature of ER stress. However, the rescue of PASMCs from apoptosis during ER stress, which might be beneficial in other tissues or disease states, may come at the expense of a proliferative vascular remodeling and the eventual development of PAH.

Mitochondrial hyperpolarization in PAH has been described in several animal models and human tissues [9, 10, 41]. The important role of mitochondria in PAH is shown by the fact that mitochondrial targeting with dichloroacetate (a small molecule that activates PDH and thus reverses the glycolytic phenotype in PAH, promoting

mitochondria-dependent apoptosis) reverses established PAH in several models [9, 10]. Dichloroacetate, by the same mechanism, can reverse cancer growth in animals [7] as well as in humans [8], conditions also characterized by mitochondrial hyperpolarization, activation of NFATc2 and HIF-1α and down-regulation of Kv1.5 [7, 8]. Disrupting the mitochondria-ER unit during sustained stress may contribute to the pro-survival/anti-apoptotic metabolic changes reported in cancer or PAH. This response would lead to a suppression of mitochondrial respiration and a switch towards the anti-apoptotic glycolytic environment [4, 6]; in that sense, absence of Nogo-B mimics dichloroacetate treatment.

One of the initial events during ER stress, regardless of the specific cause, is the activation of ATF6, which increases Nogo expression [36], supporting the notion that Nogo-B induction is an early event during ER stress. ER stress can be caused by many diverse conditions that lead to PAH in addition to hypoxia, including the unfolded protein response of mutated BMPRII in familial PAH [16], or viral infection of PASMCs with HIV or HSV [12]. Recently, over-expression of Notch3 has been implicated in both the pathogenesis of PAH [13] and ER stress [17]. Sustained ER stress in systemic vascular smooth muscle cells induces the mitochondria-dependent apoptotic pathway [46], in keeping with the fact that Nogo-B appears to be down-regulated in systemic vascular injury [25]. The fact that ATF6 activation may occur only in pulmonary, not systemic, vasculature explains the selective induction of Nogo-B in the pulmonary circulation. This finding strengthens the argument that Nogo-B therapeutic targeting may achieve relative selectivity for the pulmonary circulation in PAH.

Although mice exposed to chronic hypoxia do not completely recapitulate all forms of human PAH, it remains a widely used rodent model. Hypoxia-exposed mice are also directly relevant to the common form of pulmonary hypertension that patients with chronic obstructive pulmonary disease or residents of high altitudes develop, as their

pulmonary circulation is exposed to hypoxia. We did not study PA endothelial cells, which are implicated in PAH [4], although there appears to be some Nogo-B present in the endothelial cells of PAH lungs (Fig. 3-1A) and it remains possible that the effects of Nogo-B in endothelial cells might be different than in PASMC [25]. More work is needed to identify the cellular source(s) of circulating NogoA/B and better define its role as a potential biomarker in larger PAH cohorts. In our small cohort, circulating Nogo/AB levels failed to separate normal controls from patients with early, compensated PAH (i.e. WHO functional class I and II) but were successful in separating advanced and de-compensated PAH (i.e. WHO functional class III and IV) from early compensated PAH (Fig. 3-3).

In summary, Nogo-B targeting represents a potential selective therapeutic strategy for PAH. The link between Nogo-B and mitochondria signaling during ER stress may be relevant to other diseases in which Nogo isoforms are implicated, such as cancer, diabetes and neurodegenerative diseases [24].

Materials and Methods

Breeding of Nogo-A/B$^{-/-}$ mice. *Nogo-A/B*-deficient mice (missing both Nogo-A and Nogo-B isoforms*)* were back-crossed for seven generations to a C57BL/6 background, and used to generate *Nogo-A/B*-deficient, heterozygote and littermate control mice [25, 27].

Blood pressure and heart rate. The CODA2 (Kent Scientific Corporation) mouse-tail cuff system was used to measure systemic blood pressure and heart rate in non-anesthetized mice. Briefly, mice were restrained in a chamber and an occlusion cuff was placed proximally, followed by a volume pressure cuff placed distally on a mouse-tail. The volume-pressure recording was used to obtain the mouse blood pressure and heart rate.

Chronic hypoxic mouse model. All experiments were conduced with the approval of the University of Alberta Policy and Welfare Committee in accordance with the Canadian Council on Animal Care (CCAC) guidelines. Eight-week-old *Nogo*$^{+/+}$, *Nogo*$^{+/-}$ and *Nogo*$^{-/-}$ mice were placed into hypoxic chambers (Reming Bioinstruments; 10% O_2 and 90% N_2) for three weeks, as described [9].

Electrophysiology. With standard whole-cell patch-clamping techniques, cells were voltage-clamped at a holding potential of -70 mV and currents were evoked by 200 ms test pulses from -70 to +70 mV with 20 mV steps, filtered at 1 kHz and sampled at 2-4 kHz, with or without 4-aminopyridine (5 mM Sigma-Aldrich), as described [9, 10].

Right heart catheterization. Mice weighing 25-30g were anesthetized with ketamine (60 mg/kg i.p) and xylazine (20 mg/kg i.p.) and placed in a supine position on a heated table. The right jugular vein was cannulated and right heart catheterization was performed. A sheath was used through which a high-fidelity Millar catheter was advanced (microtip, 1.4F, Millar Instruments Inc., Houston, TX). The sheath was 0.2 mm in inner diameter and 0.58 mm in outer diameter with a specially curved tip to facilitate passage through the right heart and main pulmonary artery. Pressures in the right atrium, right ventricle and pulmonary artery were recorded continuously and mean PA pressure was calculated electronically (Power Lab, using Chart software 5.4, ADInstruments) [9, 10].

Electron microscopy. Hitachi H-7000 Transmission Electron Microscopy (TEM) was used for immunogold (BD Biosciences) conjugated to Nogo (N-18) and non-conjugated images. To estimate the mean distance between the ER and the mitochondria, the minimum distance between the mitochondrial outer membrane and the nearest ER membrane was measured as described [47]. Electron microscopy images of *Nogo*$^{+/+}$, CH-*Nogo*$^{+/+}$, *Nogo*$^{-/-}$ and CH-*Nogo*$^{-/-}$ were loaded in the analysis software Image J. Images were then magnified until the outer mitochondrial membrane and the ER membrane were

clearly visible. Using the Image J software a line was drawn, marking the shortest distance between the outer mitochondrial membrane and the ER by an experimenter blinded to the study. Mean data represent a minimum of 10 images per group with 4-5 mitochondria analyzed per image from the PASMCs of 3 mice.

Echocardiography. Pulmonary artery acceleration time (using pulsed wave Doppler) was measured in the parasternal short axis view using the VeVo 770 imaging system with the 707B probe (30 MHz), as described [9, 42].

Treadmill test. A graded sub-maximal exercise tolerance test was performed on a calibrated, motor-driven treadmill in a Plexiglas cage (Treadmill Simplex II, Columbus Instruments). Incremental increases in treadmill belt speed were made as described: 1 min warm up at 3 m/min, then 1 min at 4 m/min, 2 min at 5 m/min, 2 min at 6 m/min, 6 min at 7 m/min, and finally 8 m/min until the mouse exhibited signs of exhaustion. Exhaustion was defined as the mouse spending >50% of the time or >10 consecutive seconds on the shock grid as described [9].

Cell culture. PASMC, CASMC and RASMCS were freshly isolated from pulmonary arteries, carotid arteries and renal arteries of mice and humans using an enzymatic cocktail containing papin (1 mg/mL), dithiothreitol (0.5 mg/mL), collagenase (0.6 mg/mL) and bovine serum albumin (0.6 mg/mL) (Sigma-Aldrich). Human pulmonary artery smooth muscle cells were established in accordance with University of Alberta ethics approval from resistance PAs isolated immediately after extraction at transplant surgery. Cultured cells were maintained in Dulbecco's modified Eagle's medium (DMEM) supplemented with 10% fetal bovine serum (FBS) and 1% antibiotic/antimycotic (Gibco, Invitrogen) and placed in an incubator set at 37°C in either normoxic conditions (gas perfused incubator with 5.2% CO_2, 21% O_2 and balanced N_2) or hypoxic conditions (gas perfused incubator with 5.2% CO_2, 4% O_2 and balanced N_2). Thapsagargin (600nM, Sigma Aldrich), 4-(2-Aminoethylbenzenesulfonyl fluoride

hydrochloride; AEBSF; 250 uM; Sigma Aldrich) was prepared as aqueous solutions and added to the medium of confluent cells.

Confocal microscopy. Imaging was performed using a Zeiss LSM 510 confocal microscope (Carl Zeiss). Apoptag apoptosis detection kit (TUNEL Serologicals) and the proliferating cell nuclear antigen (PCNA) antibody (DAKO) were used as previously described[9, 10]. Percent of PCNA and TUNEL positive cells and nuclear ATF6 and HIF-1α were measured in 3 different fields/slide; a minimum of 3 slides /experiment were used and 3 independent experiments were performed. Nogo (N-18) (Santa Cruz Biotechnology), ATF6 (Santa Cruz Biotechnology), HIF-1α (Abcam), GRP-78 (Santa Cruz Biotechnology), NFAT-c2 (Novus Biologicals), Kv1.5 (Santa Cruz Biotechnology), tetramethyl rhodamine methyl ester (10nM Molecular Probes) and MitoSOX (5μM Molecular Probes) were used as previously described [9, 10]. FLUO-3 (10μM, Molecular Probes, Invitrogen). TMRM, MitoSOX, FLUO-3, Rhod-2AM (5μM, Molecular Probes, Invitrogen), Nogo-B, GRP-78 and Kv1.5 intensity was measured in 3 different field /slide; a minimum of 3 slides /experiment were used and 3 independent experiments were performed. FITC- and TRITC-conjugated (DAKO) secondary antibodies were used in immunofluorescence.

Media wall thickness: Percent medial wall thickness was measured at the two ends of the shortest external diameter of the distal pulmonary arteries and the average was taken ([2 x wall thickness/external diameter] x 100).

Adenoviral infection. PASMC were grown on poly-L-lysine (Sigma-Aldrich) coated glass coverslips, and infected at a multiplicity of infection of 100 in serum-free DMEM (Gibco, Invitrogen) for 6 h allowing an infection rate of ≈80% as previously described [48]. Medium was then exchanged for DMEM containing 10% FBS.

Mitochondrial calcium imaging. Rhod-2AM (Invitrogen GIBCO) was used to measure mitochondrial calcium as indicated in the commercially available protocol. The cameleon plasmid for mitochondrial FRET-Ca^{2+} and imaging was used as previously described [39]. Briefly, PASMCs were plated on confocal dishes and the plasmid was introduced by electroporation. The method for dual-emission ratio imaging of Ca^{2+} with the use of the cameleon plasmid was a Zeiss LSM 510 confocal microscope in which the excitation was at 458nm and the emission filters used were 480 to 520nm for cyan (when Ca^{2+} is not bound) and 535 to 590nm for FRET (yellow when Ca^{2+} is bound). The ratio of FRET/cyan was used to standardize the rate of infection for each cell.

ATF6 luiferase assay. ATF6 dual-luciferase reporter kit (SA Biosciences) was used to assess the ATF6 activity in human PASMCs and CASMCs as described in the commercially available protocol. Briefly, PASMCs (20,000 cells/well) was plated on a 96 well plate containing the transfection agent (SureFect; SA Biosciences) and the ATF6 Cignal reporter (which contained a control Renilla reporter as well). After 16 h of transfection, the transfection media was replaced with regular PASMC growth media and exposed to normoxia or hypoxia for 48 h. ATF6 activity was assessed using the Promega dual luciferase reporter assay system from Promega (SA Biosciences). Briefly, cells were lysed with the passive lysis buffer (provided in the kit) before luminescence was detected with a illuminometer. ATF6 activity was standardized to the transfection of each cell by normalizing data to Renilla luminescence.

Immunoblotting. Tissues were collected and immunoblotting was performed as previously described [9, 10] (25 μg protein in pooled sample (4 different animals)/lane). The films were digitized and quantified using 1D Image Analysis Software (Kodak). Expression was normalized to α-actin to correct for loading differences. The Nogo 1761 antibody detecting Nogo-B has been described and characterized [49].

α-Ketoglutarate measurements. α-Ketoglutarate levels were measured as described in a commercially available spectro-photometric a-ketoglutarate Assay Kit (BioVision). PASMCs cells were grown to confluency in a T75 flask. Cells were then harvested, lysed and protein concentration was adjusted to equal levels between groups. α-Ketoglutarate levels were measured by measuring OD at 570nm after the kit-based reaction was completed as previously described [8].

PDH activity. PDH activity was measured using the MitoProfile Dipstick Assay Kit (MitoSciences). Protein was collected after cells were homogenized. Protein (50μL of 1μg/mL) was placed in a 96-well dish and incubated with the dipstick containing the PDH complex antibody and then incubated in activity buffer. PDH activity was measured by intensity of band using a flat top scanner as previously described [8].

Quantitative RT-PCR. Samples were added to a micro-well plate, along with TaqMan probes and reagents, and quantitative RT-PCR was performed using the ABI PRISM 7700 Sequence Detector (Applied Biosystems) and 18S RNA was used as a housekeeping gene (Applied Biosystems), identical amounts of RNA was added in each group, (~100ng of RNA per group) as previously described [10].

Phospholipid biosynthesis and functional assessment of mitochondria-ER contacts. PASMCs in 60 mm culture dishes were incubated at 37°C for 7 to 12 h with 15μCi of [3-^{3}H] serine (0.4 mM). The reaction was terminated by the addition of 1mL chloroform/methanol (2:1, v/v) on ice and [^{3}H]-labeled phospholipids were extracted. Phosphatidylserine and phosphatidylethanolomine were isolated by thin-layer chromatography in the solvent system chloroform/methanol/acetic acid/formic acid/water (70:30:12:4:2, v/v), after addition of carrier phospholipids. The phospholipids were identified according to standards with iodine vapor and radioactivity was measured, as described [34].

Whole cell respiration. PASMCs were harvested (5 x 10^6 cells/mL) in Hanks' Balanced Salt Solution (HBSS) supplemented with 10 mM glucose and placed in a sealed glass chamber (Warner Instruments). Cells were kept at a constant temperature of 37°C and continuously stirred. Real-time oxygen consumption was measured by an oxygen electrode (Warner Instruments) connected to a Strathkelvin 782 oxygen meter. Rate of oxygen consumption was calculated using the oxygen meter's software (version 4.0, Strathkelvin instruments LTD.).

siRNA studies. Human donor and iPAH PASMCs were grown to 80% confluence in six-well culture dishes. The transfection agent siPORTamine (Ambion siRNA Transfection II kit 1631) was pre-incubated at room temperature for 10 min at a ratio of 1:12 in OptiMEM1 culture medium (Invitrogen-GIBCO) before being mixed with 50nM ATF6 siRNA (Ambion) or scrambled RNA (Ambion). The culture media was aspirated from the cells, and the transfection agent-RNA complex mixture was allowed to spread over the monolayer of cells. Plates were incubated at 37°C for 48 h.

Statistics. Values are expressed as mean±SEM. Inter-group differences were appropriately assessed by either unpaired Student's t-test or one-way ANOVA with post hoc analysis as indicated (SPSS 19). $P<0.05$ or less was considered significant.

Figures

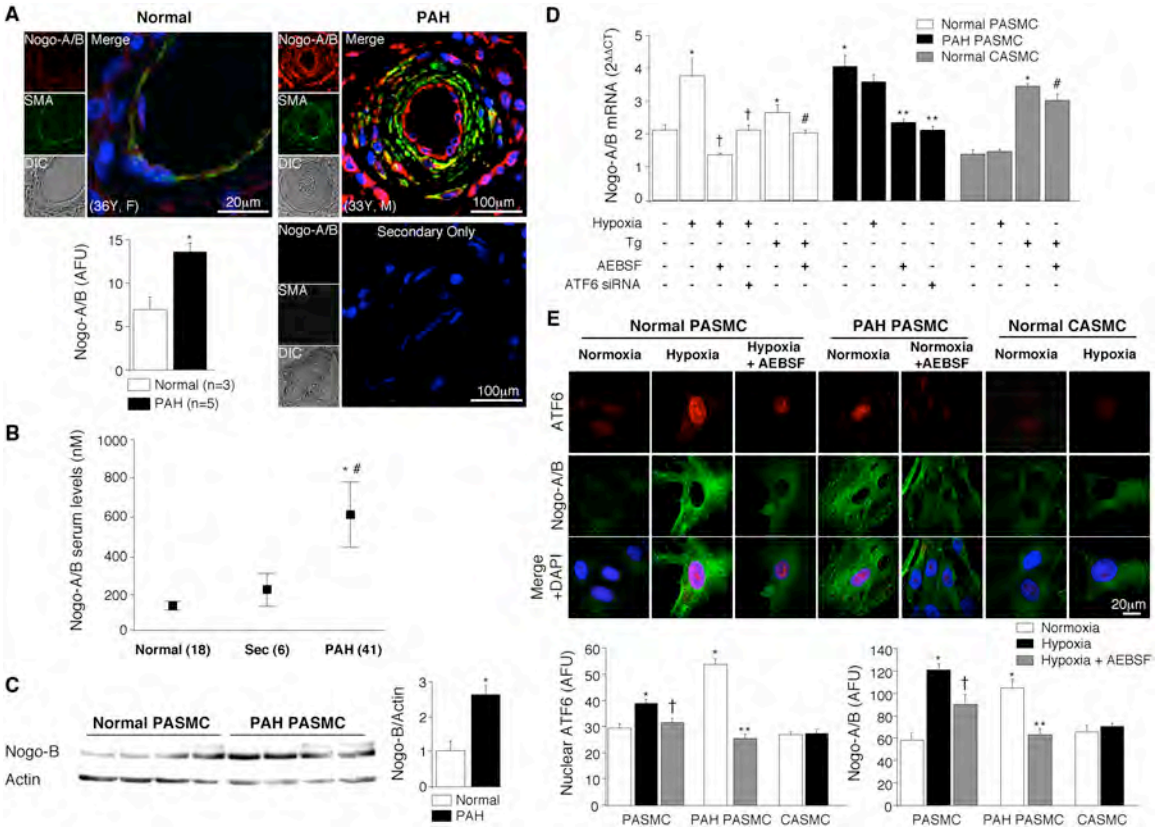

Fig. 3-1. Nogo-B and ATF6 in pulmonary arteries, pulmonary arterial smooth muscle cells and serum from patients with PAH

(A) Resistance pulmonary arteries in the lungs of 5 patients with idiopathic PAH have increased levels of Nogo-B protein (red) compared to normal pulmonary arteries from 3 transplant donors, as shown by immunofluorescence and confocal microscopy (n=7 PAs/patient). *P<0.01, unpaired Student's t-test. Although the antibody detects both Nogo-A and Nogo-B, Nogo-A is not expressed in the lungs [27]. Resistance pulmonary arteries were co-stained with an antibody to smooth muscle actin (SMA; green). Pulmonary artery morphology is shown in the differential interference contrast (DIC) panel. In the merged panel, Nogo-B and SMA colocalization is shown (yellow), along with nuclei stained blue with DAPI. Mean data are presented in arbitrary fluorescence units (AFU). **(B)** Serum levels of Nogo-A/B in PAH patients are increased compared to normal and secondary pulmonary hypertension (thromboembolic disease) patients. Sample sizes are shown in parentheses. *P<0.01 vs. normal, $^{\#}P$<0.01 vs. secondary PAH using ANOVA with Fisher's Least Significant Difference (FLSD) post-hoc analysis. A previously described ELISA method was used [50]. Individual patient values are shown in Fig. 2-2.

(C) PASMCs isolated from resistance pulmonary arteries taken from patients with idiopathic PAH have higher levels of Nogo-B protein (45kDa), than do PASMCs from normal pulmonary arteries as shown by immunoblot (n=4 experiments/group). $^{*}P<0.01$ using unpaired Student's t-test. Although the antibody detects both Nogo-A and Nogo-B isoforms, Nogo-A is known to be absent from vascular and lung tissues; in addition, Nogo-B (45kDa) is separated from Nogo-A (180kDa) based on molecular weight. **(D)** PASMCs from normal donor patients exposed to ER-stress inducers, hypoxia and thapsigargin (Tg), and PASMCs from PAH patients have increased Nogo-B mRNA values compared to normal vehicle-treated PASMCs, as shown by qRT-PCR. Tg, but not hypoxia, increased Nogo-B mRNA in CASMCs from transplant donors. An ATF6 inhibitor (AEBSF) and ATF6 siRNA decrease Nogo-B mRNA in both hypoxia- and Tg-treated PASMC and in PAH PASMCs (n=3 experiments/group). $^{*}P<0.05$ vs. normoxia, $^{\dagger}P<0.05$ vs. hypoxia, $^{\#}P<0.05$ vs. Tg, $^{**}P<0.05$ vs. PAH normoxia using ANOVA with FLSD post-hoc analysis. **(E)** PASMCs from normal donor patients exposed to hypoxia and PASMCs from PAH patients have increased nuclear ATF6 (red) and Nogo-B (green) levels as shown by immunocytochemistry. ATF6 colocalization with the nuclei, stained with DAPI (blue), is shown in pink in the merged panel. Nuclear ATF6 and Nogo-B were decreased by the ATF6 inhibitor AEBSF, in hypoxia-treated normal donor PASMCs and PAH PASMCs. Hypoxia did not increase nuclear ATF6 or Nogo-B levels in CASMCs (n=70 cells/group). $^{*}P<0.05$ vs. normoxia PASMC, $^{\dagger}P<0.05$ vs. hypoxia PASMC, $^{**}P<0.05$ vs. normoxia PAH PASMC using ANOVA with Tukey's post-hoc analysis. Mean data are presented in arbitrary fluorescence units (AFU).

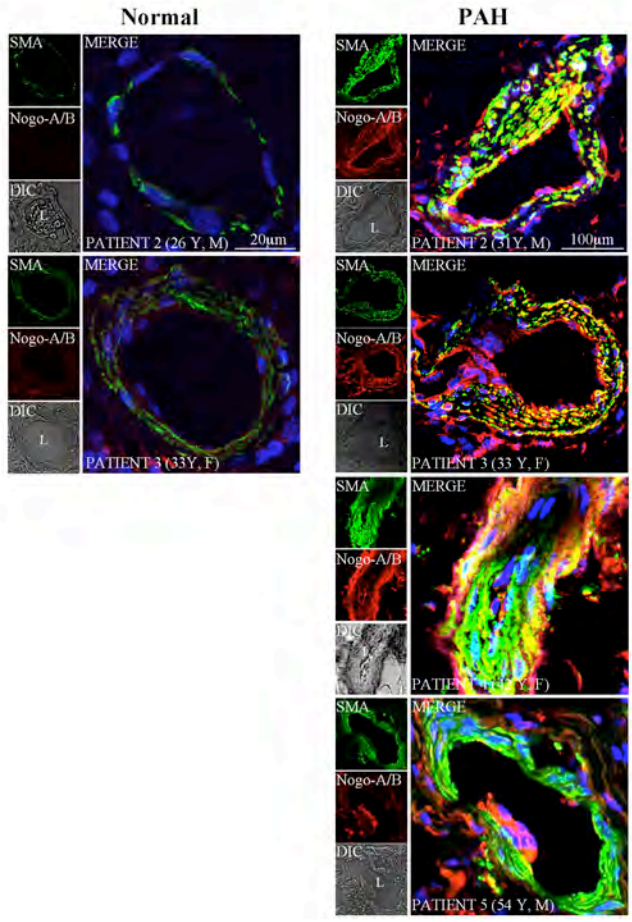

Fig. 3-2. Nogo-B levels are increased in human PAH pulmonary arteries

Resistance pulmonary arteries in the lungs of 5 patients with idiopathic PAH have increased levels of Nogo-B protein (red) compared to normal pulmonary arteries from 3 transplant donors, as shown by immunofluorescence and confocal microscopy. Resistance pulmonary arteries were co-stained with an antibody to smooth muscle actin (SMA; green). Pulmonary artery morphology is shown in the differential interference contrast (DIC) panel. In the merged panel, Nogo-B and SMA colocalization is shown (yellow), along with nuclei stained blue with DAPI. Mean data are presented in arbitrary fluorescence units (AFU).

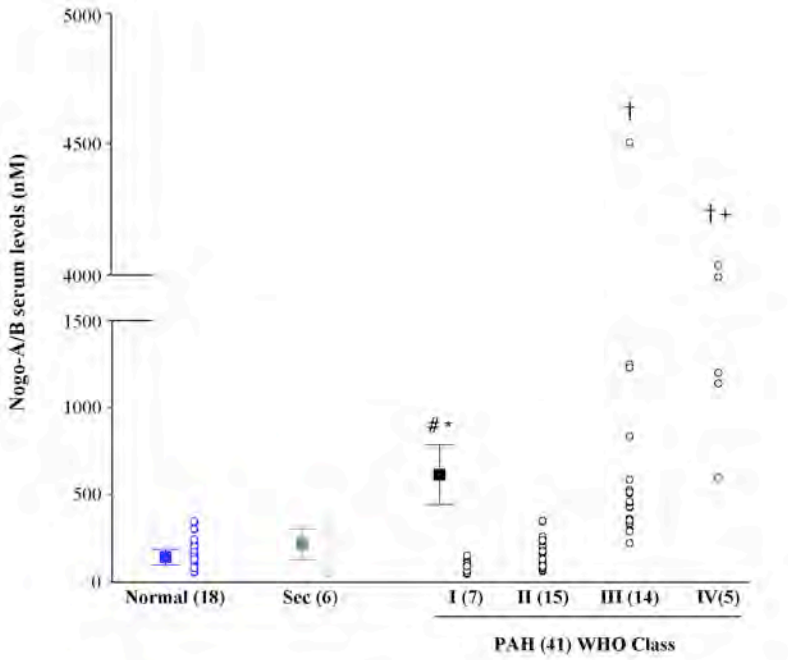

Fig. 3-3. Nogo-B levels are increased in the serum of PAH patients

Serum levels of Nogo-A/B in individual PAH patients (black), normal (blue) and secondary pulmonary hypertension (green) (thromboembolic disease) patients. Mean±SEM are also shown for each group. World Health Organization functional class, a measure of disease severity, further subdivides PAH patients. Sample sizes are shown in parentheses. $^{*}P<0.01$ vs. normal, $^{\#}P<0.01$ vs. secondary PAH, $^{\dagger}P<0.01$ vs. WHO I and WHO II, $^{+}P<0.01$ vs. WHO III using ANOVA with Fisher's Least Significant Difference (FLSD) post-hoc analysis.

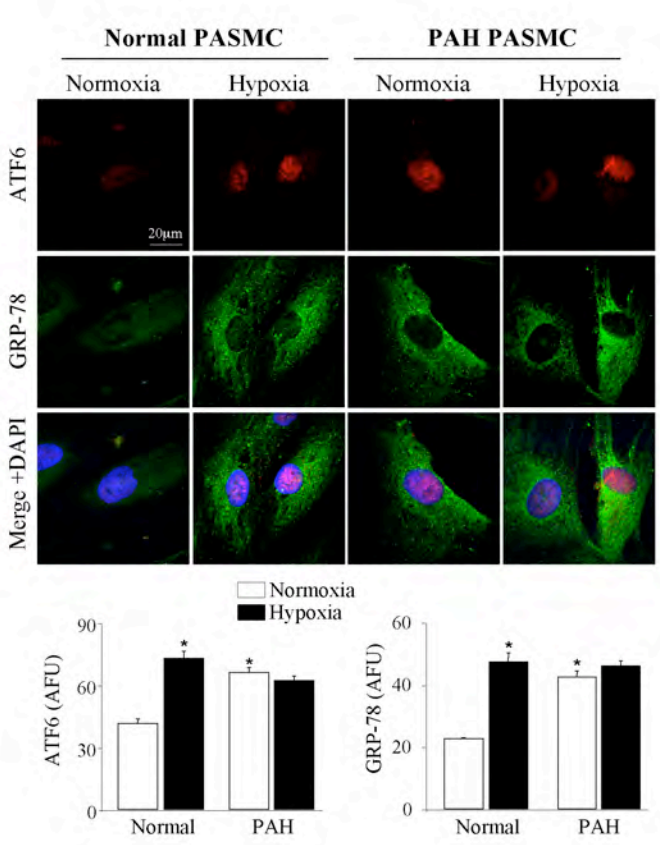

Fig. 3-4. Hypoxia-induced ER stress in normal human PASMCs to levels similar to PAH PASMCs Human normal PASMCs exposed to hypoxia had increased nuclear ATF6 (red) and GRP-78 (green) levels as shown by immunofluorescence. ATF6 colocalization with the nuclear stain DAPI (blue) is shown in pink in the merged panel. Hypoxia did not further increase nuclear ATF6 levels or GRP-78 in PAH PASMCs (n=80 cells/group). *P<0.05 vs. normal normoxia using ANOVA with Tukey's post-hoc analysis. Mean data are presented in arbitrary fluorescence units (AFU).

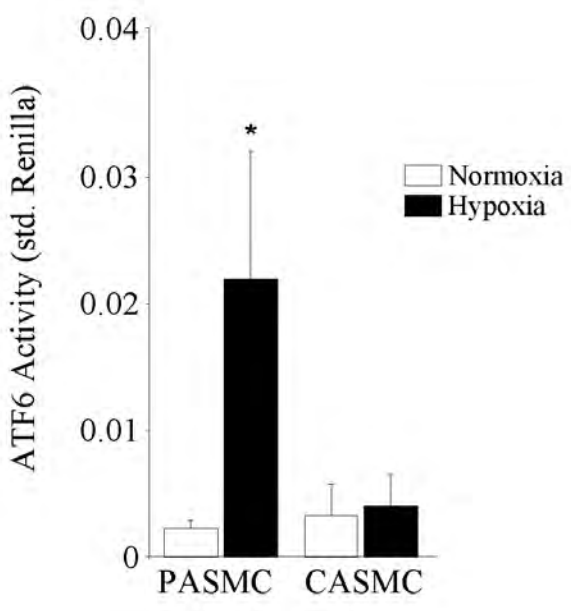

Fig. 3-5. Hypoxia increases ATF6 luciferase activity in human donor PASMCs.

Human normal PASMCs exposed to hypoxia had increased ATF6 activation shown by increased luminescence as measured by dual luciferase reporter assay. Hypoxia did not increase luminescence in CASMCs (n=12 wells/group). *P<0.05 vs. normoxia control using unpaired Student's t-test. Mean data was standardized to the rate of infection based on the constitutively expressed Renilla luciferase.

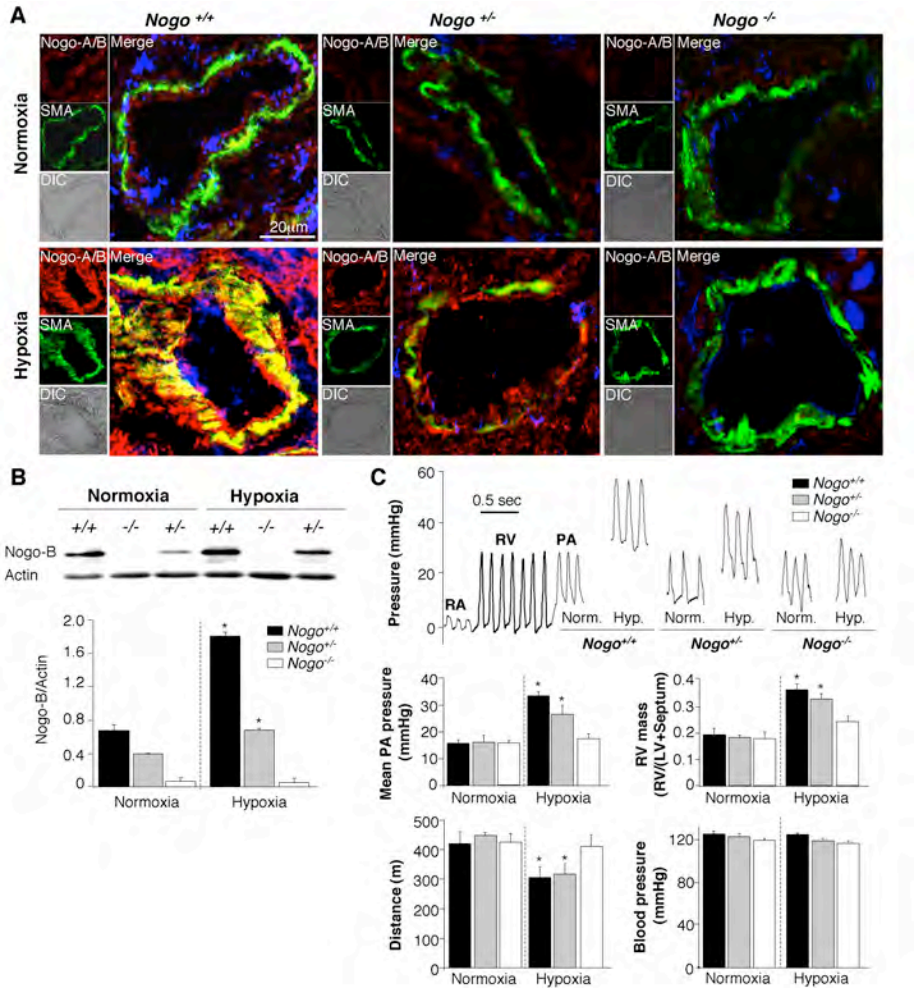

Fig. 3-6. In mice, chronic hypoxia-induced PAH is dependent on Nogo-B

(A) Resistance pulmonary arteries in the lungs of control (*Nogo*$^{+/+}$) and heterozygote (*Nogo*$^{+/-}$) littermates exposed to chronic hypoxia have increased levels of Nogo-B protein (red) compared to normoxia-treated controls, as shown by immunofluorescence and confocal microscopy. Nogo-deficient (*Nogo*$^{-/-}$) mice had no detectable Nogo-B protein in either normoxic or chronic hypoxic pulmonary arteries. Although the antibody detects both Nogo-A and Nogo-B, Nogo-A is not expressed in the lungs [27]. Resistance pulmonary arteries were co-stained with an antibody to smooth muscle actin (SMA; green). Pulmonary artery morphology is shown in the differential interference contrast (DIC) panel. Nogo-B and SMA colocalization (yellow) is shown along with the nuclear stain DAPI (blue) in the merged panel. **(B)** Lungs of *Nogo*$^{+/+}$ and *Nogo*$^{+/-}$, but not *Nogo*$^{-/-}$ mice, exposed to chronic hypoxia had increased levels of Nogo-B protein when compared to those from normoxic mice, as shown by immunoblot (n=5 mice/group). *P<0.05 vs. normoxia controls using ANOVA with FLSD post-hoc analysis. **(C)** (Top) Representative pressure traces obtained by closed chest, right heart catheterization of anesthetized mice with a Millar catheter advanced through the internal jugular vein into the right atrium (RA), right ventricle (RV) and

pulmonary artery (PA). (Bottom) *Nogo*$^{+/+}$ and *Nogo*$^{+/-}$, but not *Nogo*$^{-/-}$ mice, exposed to chronic hypoxia showed increased mean PA pressure, RV mass (RV/LV+septum weight ratio) and decreased functional capacity (distance run on rodent treadmill). Systemic blood pressure was not different among groups (n=8 mice/group). $^{*}P<0.05$ vs. normoxia controls using ANOVA with FLSD post-hoc analysis.

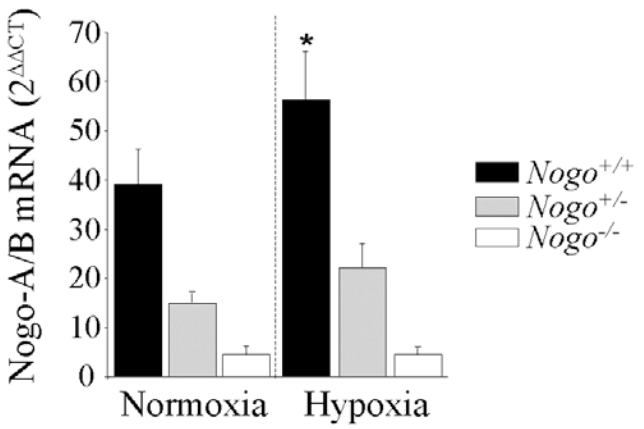

Fig. 3-7. Nogo-B expression is increased in CH-PAH *Nogo*$^{+/+}$ and *Nogo*$^{+/-}$ lungs

Lungs (which includes the pulmonary microvessels) of *Nogo*$^{+/+}$ and *Nogo*$^{+/-}$ mice exposed to hypoxia had higher Nogo-B mRNA expression compared to normoxic controls as measured by qRT-PCR (n=3 experiments from 5 mice/group). *P<0.05 vs. normoxic controls using ANOVA with FLSD post-hoc analysis.

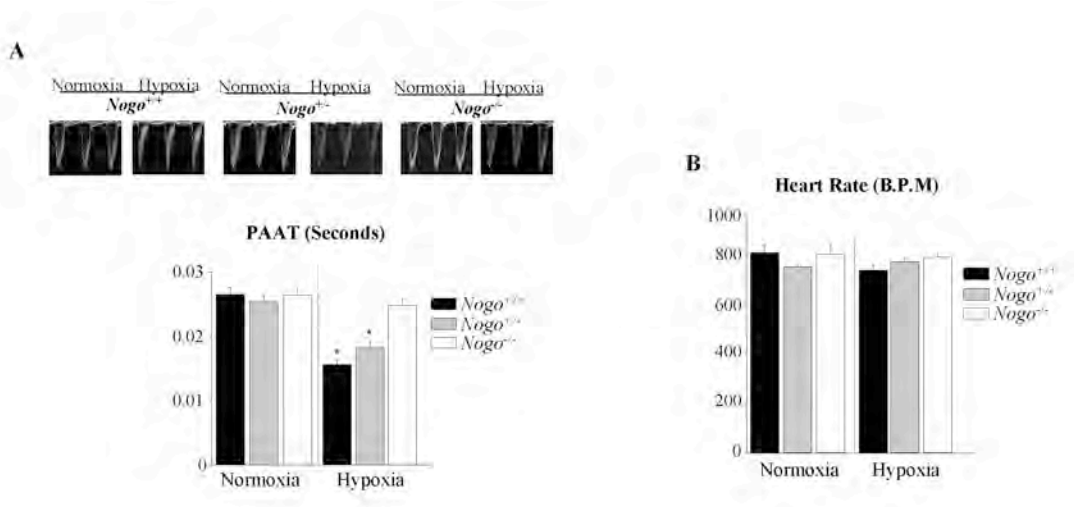

Fig. 3-8. *Nogo*$^{-/-}$ mice are resistant to CH-induced increases in PAAT

(A) (Top) Representative pulmonary artery acceleration time (PAAT, the time from the beginning of the Doppler signal deflection to the peak of the deflection, the shorter the PAAT the higher the PA pressure) top panel of control littermates (Bottom) *Nogo*$^{+/+}$ and *Nogo*$^{+/-}$, but not *Nogo*$^{-/-}$ mice, exposed to chronic hypoxia had decreased PAAT (n=8 mice/group). *P<0.05 vs. normoxia controls using ANOVA with FLSD post-hoc analysis. **(B)** Heart rate did not significantly differ between *Nogo*$^{+/+}$, *Nogo*$^{+/-}$, and *Nogo*$^{-/-}$ mice exposed to normoxia and chronic hypoxia, measured by tail cuff (n=8 animals/group).

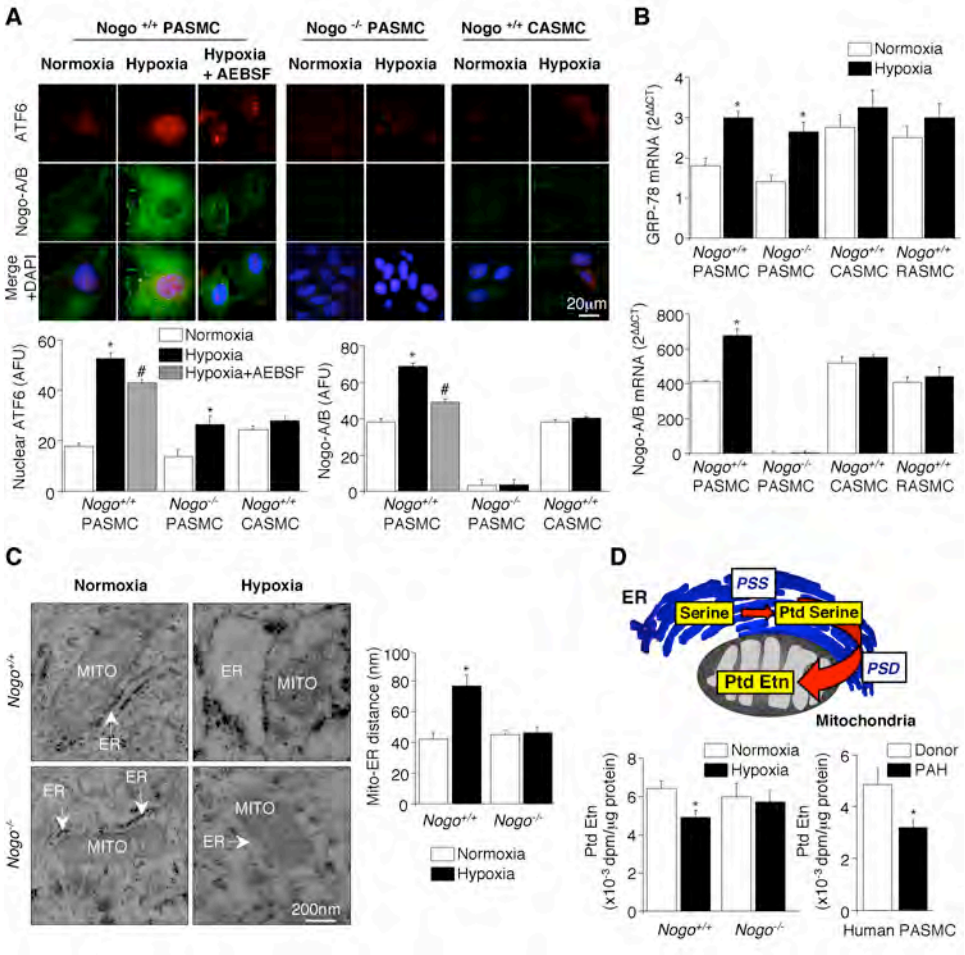

Fig. 3-9. Hypoxia-induced Nogo-B disrupts the mitochondria-ER unit in mice PASMC

(A) *Nogo*$^{+/+}$ PASMCs exposed to hypoxia had increased nuclear ATF6 (red) and Nogo-B (green) levels as shown by immunofluorescence. ATF6 colocalization with the nuclear stain DAPI (blue), is shown in pink in the merged panel. Nuclear ATF6 and Nogo-B were decreased by the ATF6 inhibitor AEBSF in hypoxia-treated *Nogo*$^{+/+}$ PASMCs. Hypoxia-treated *Nogo*$^{-/-}$ PASMCs had increased nuclear ATF6 levels but no detectable Nogo-B. Hypoxia did not increase nuclear ATF6 and Nogo-B levels in *Nogo*$^{+/+}$ CASMCs (n=70 cells/group). $^{*}P<0.05$ vs. normoxia, $^{\#}P<0.05$ vs. hypoxia using ANOVA with Tukey's post-hoc analysis. Mean data are presented in arbitrary fluorescence units (AFU). **(B)** *Nogo*$^{+/+}$ PASMCs, but not *Nogo*$^{+/+}$ CASMCs or RASMCs, exposed to hypoxia had increased Nogo-B and GRP-78 mRNA values, as shown by qRT-PCR. *Nogo*$^{-/-}$ PASMCs exposed to hypoxia had increased GRP-78 mRNA values, while no detectable Nogo-B mRNA values were observed (n=3 experiments/group). $^{*}P<0.001$ vs. normoxia using unpaired Student's t-test.

(C) *Nogo*$^{+/+}$, but not *Nogo*$^{-/-}$, PASMCs exposed to hypoxia had structurally disrupted mitochondria-ER units as shown by the increase in the minimal distance between the mitochondria

and ER in electron microscopy photomicrographs (n=40 contact sites in PASMCs isolated from 3 mice/group). *P<0.001 using unpaired Student's t-test. **(D)** *Nogo*$^{+/+}$, but not *Nogo*$^{-/-}$, PASMCs exposed to hypoxia had functionally disrupted mitochondria-ER units as shown by decreased mitochondrial synthesis of phosphatidylethanolamine (PtdEtn) (n=6/group). *P<0.01 vs. normoxia using unpaired Student's t-test. Human PAH PASMCs had decreased mitochondrial synthesis of PtdEtn as compared to normal donor PASMCs (n=3/group). *P<0.01 using unpaired Student's t-test. Data presented as x10^{-3} disintegrations per minute (dpm)/μg protein.

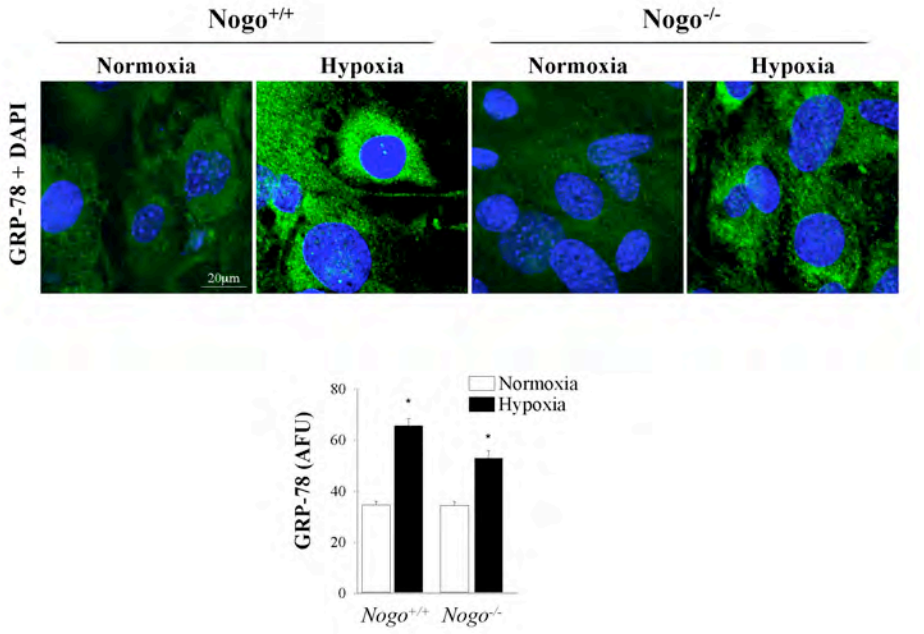

Fig. 3-10. GRP-78 protein is induced in *Nogo*$^{+/+}$ and *Nogo*$^{-/-}$ PASMCs exposed to chronic hypoxia

Nogo$^{+/+}$ and *Nogo*$^{-/-}$ PASMCs exposed to hypoxia had significantly increased levels of GRP-78 (green) shown with nuclear stain DAPI (blue) (n=80 cells/group). *P<0.05 vs. normoxia control using unpaired Student's t-test. Mean data are presented in arbitrary fluorescence units (AFU).

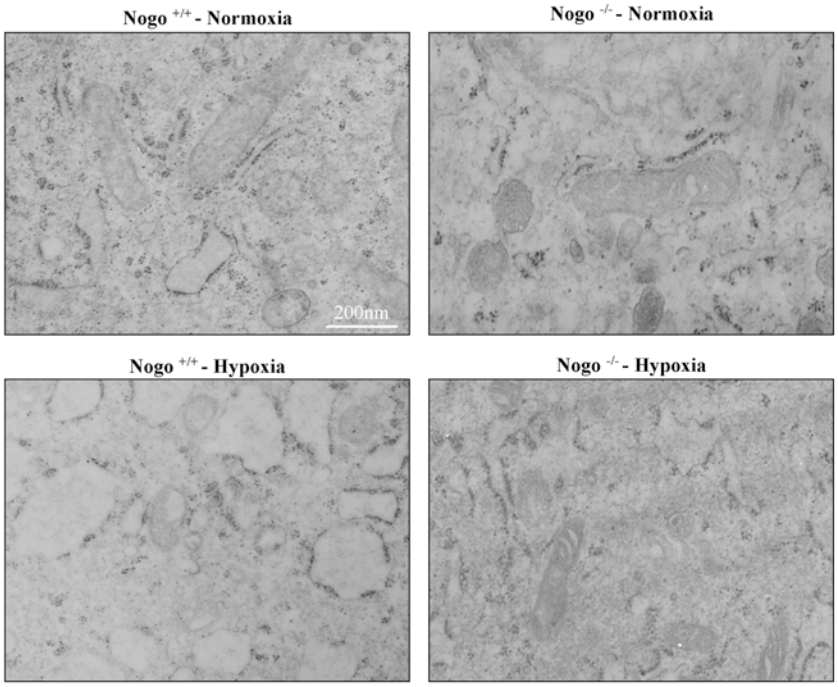

Fig. 3-11. Hypoxia increases the distance between the endoplasmic reticulum and the mitochondria in *Nogo*$^{+/+}$ PASMCs

Nogo$^{+/+}$, but not *Nogo*$^{-/-}$, PASMCs exposed to hypoxia had increased distance between the ER and mitochondria and appeared more swollen and irregular as assessed by electron microscopy photomicrographs.

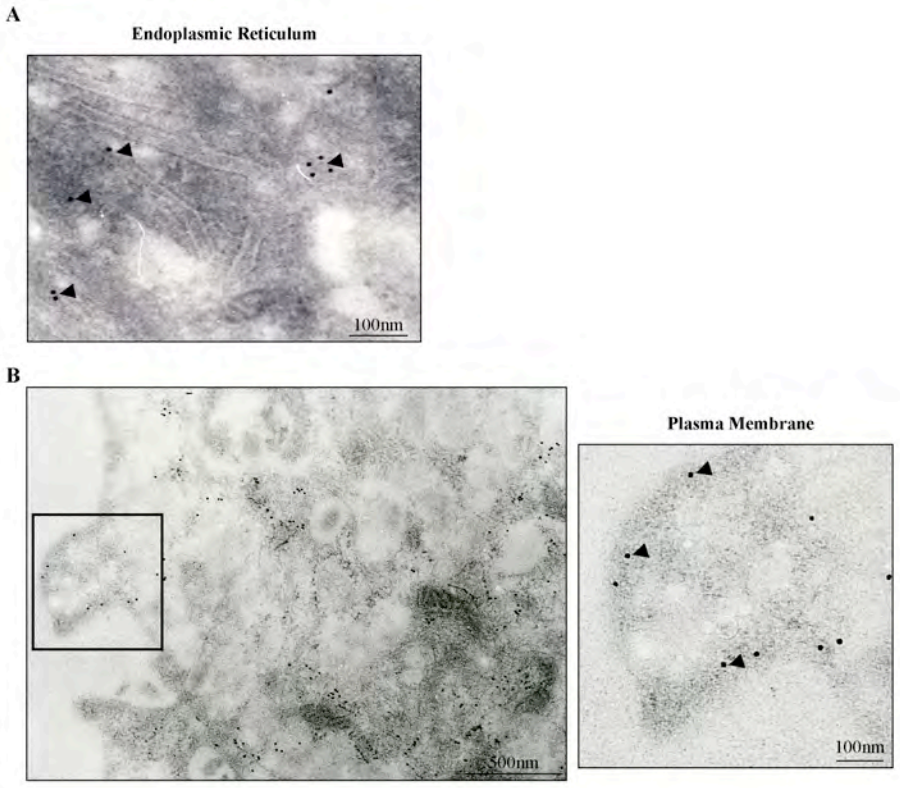

Fig. 3-12. Nogo-B is localized in the endoplasmic reticulum and plasma membrane

(A) Nogo-B is mainly localized in the endoplasmic reticulum shown by immunogold labeling and transmission electron microscopy **(B)** Some Nogo-B localizes on the plasma membrane. Left panel is a low magnification; the inset in black box is expanded in right panel showing a higher magnification.

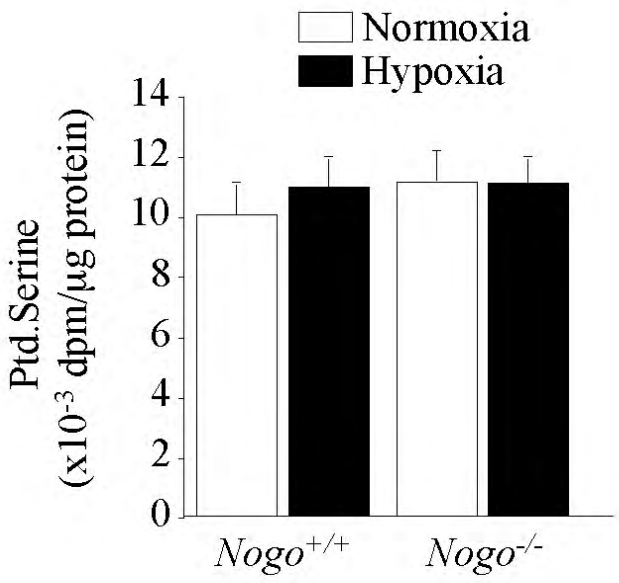

Fig. 3-13. Hypoxia does not change phosphatidylserine synthesis in *Nogo*$^{+/+}$ and *Nogo*$^{-/-}$ PASMCs

Nogo$^{+/+}$ and *Nogo*$^{-/-}$ PASMCs exposed to hypoxia had similar phosphatidylserine (Ptd.Serine) compared to normoxic controls (n=6/group). Data presented as x10^{-3} disintegrations per minute (dpm)/μg protein.

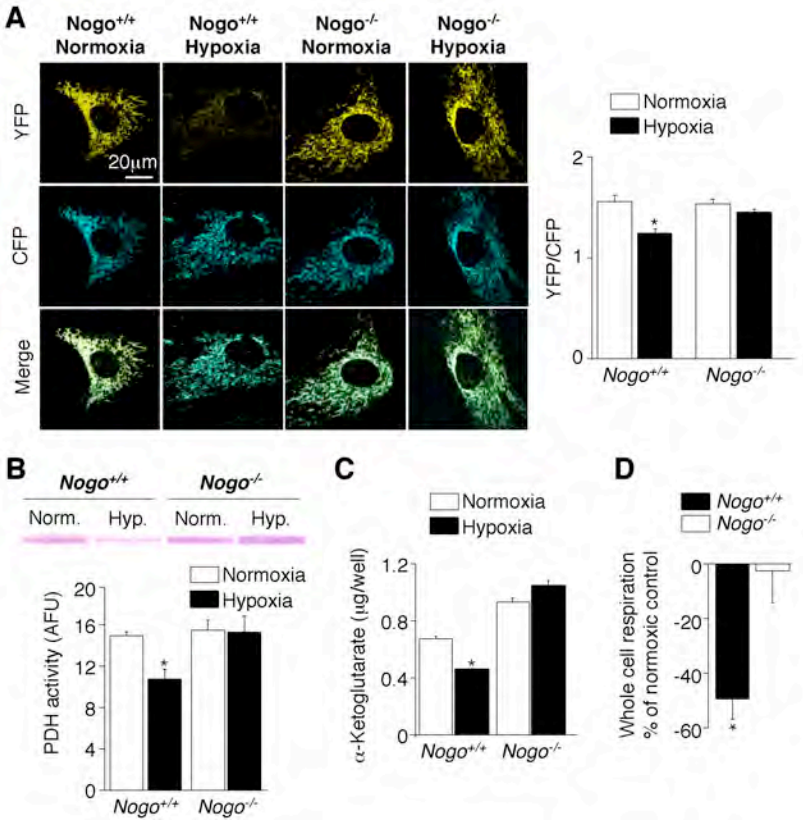

Fig. 3-14. Hypoxia induction of mitochondrial Ca^{2+}, PDH and ICD depends on Nogo-B

(A) *Nogo*$^{+/+}$, but not *Nogo*$^{-/-}$, PASMCs exposed to hypoxia had decreased mitochondrial Ca^{2+} compared to normoxic controls, as shown by the ratio of bound mitochondrial Ca^{2+} (YFP; yellow fluorescent protein, yellow) to unbound mitochondrial Ca^{2+} (CFP; cyan fluorescent protein signal, blue) using the Förster Resonance Energy Transfer (FRET) and confocal microscopy. Mean data are presented as YFP/CFP signal ratio (n=25 cells/group). **P*<0.05 vs. normoxia using unpaired Student's t-test. **(B)** *Nogo*$^{+/+}$, but not *Nogo*$^{-/-}$, PASMCs exposed to hypoxia had decreased PDH activity compared to normoxic controls (n=3 experiments/group). **P*<0.01 vs. normoxia using unpaired Student's t-test. Mean data presented in arbitrary fluorescence units (AFU). **(C)** *Nogo*$^{+/+}$, but not *Nogo*$^{-/-}$, PASMCs exposed to hypoxia had decreased α-ketoglutarate levels, a direct index of isocitrate dehydrogenase (ICD) activity, compared to normoxic controls (n=4 experiments/group). **P*<0.05 vs. normoxia using unpaired Student's t-test. **(D)** *Nogo*$^{+/+}$, but not *Nogo*$^{-/-}$, PASMCs exposed to hypoxia had decreased whole-cell respiration rates (n=5 experiments/group). **P*<0.01 vs. normoxia using an independent one-sample t-test. Mean data are presented as % decrease of hypoxia-treated PASMCs to normoxic control.

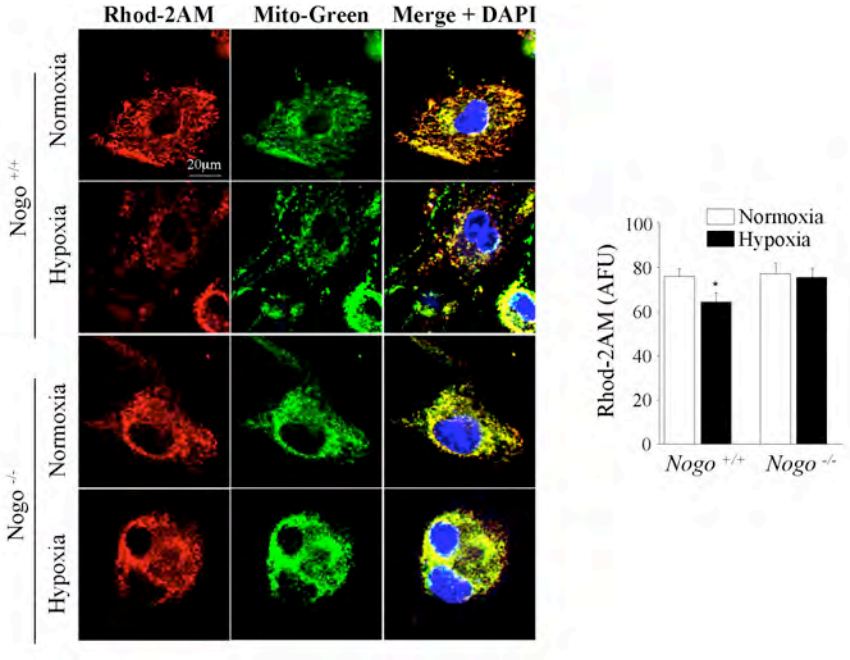

Fig. 3-15. *Nogo*$^{+/+}$ PASMCs exposed to hypoxia have decreased mitochondrial calcium *Nogo*$^{+/+}$, but not *Nogo*$^{-/-}$, PASMCs had decreased mitochondrial calcium as assessed by Rhod-2AM (red) and confocal microscopy (n=70 cells/group). *P<0.05 vs. normoxic control using unpaired Student's t-test. Cells were costained with mitotracker green (Mito-Green, green). Rhod-2AM and Mito-green colocalization (yellow) is shown merged with the nuclear stain DAPI (blue) in the merged panel. Mean data are presented in arbitrary fluorescence units (AFU).

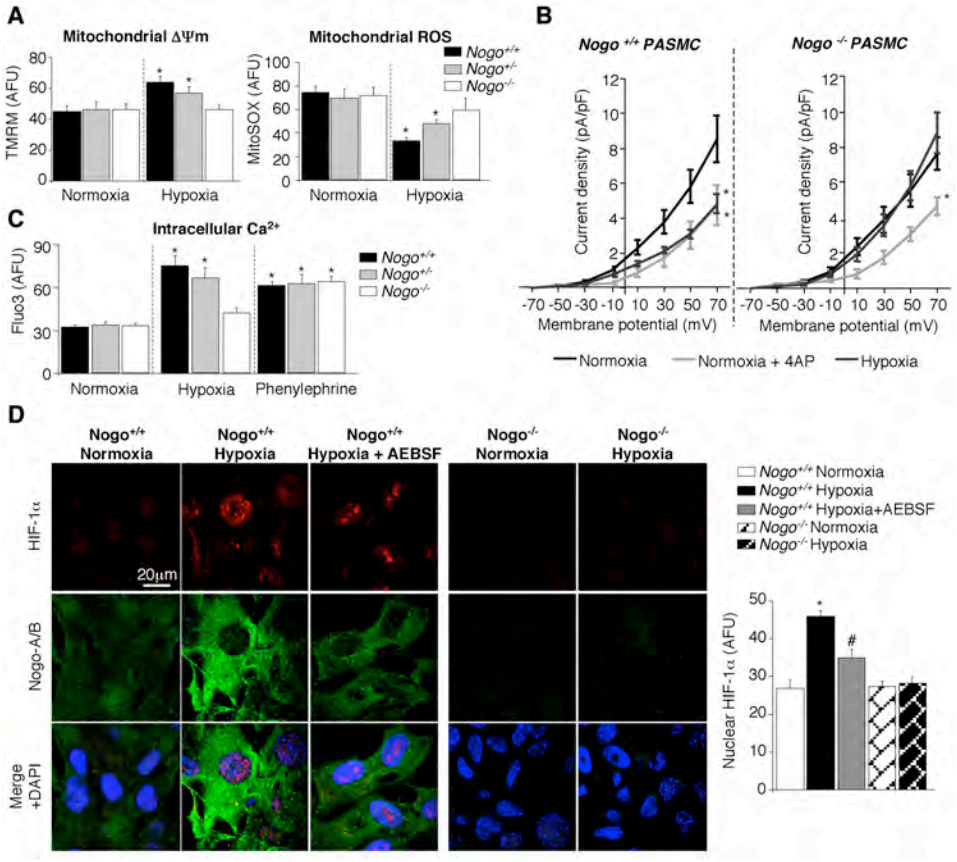

Fig. 3-16. Hypoxia disruption of the mitochondria-mROS-Kv channel axis depends on Nogo

(A) *Nogo*$^{+/+}$ and *Nogo*$^{+/-}$ PASMCs exposed to hypoxia had hyperpolarized mitochondria as assessed by TMRM and decreased mROS production as assessed by MitoSOX, compared to normoxic controls. In contrast, *Nogo*$^{-/-}$ PASMCs exposed to hypoxia had similar mitochondrial potential (ΔΨm) and mROS production as normoxic PASMCs (n=100 cells/group). **P*<0.05 vs. normoxic control using ANOVA with Tukey's post-hoc analysis. **(B)** *Nogo*$^{+/+}$, but not *Nogo*$^{-/-}$, PASMCs exposed to hypoxia had lower outward K^+ current density compared to normoxic controls, measured by whole-cell patch clamping. The K^+ current in normoxic *Nogo*$^{+/+}$ and *Nogo*$^{-/-}$, PASMCs was sensitive to 4-aminopyridine (4-AP) (n=8-10 cells/group). **P*<0.05 vs. normoxia using ANOVA with FLSD post-hoc analysis. Mean data are shown as current density (pA/pF) over membrane potential (mV). **(C)** *Nogo*$^{+/+}$ and *Nogo*$^{+/-}$ PASMCs exposed to hypoxia and phenylephrine had increased intracellular Ca^{2+}, as assessed by Fluo3, compared to normoxic controls. *Nogo*$^{-/-}$ PASMCs showed increased intracellular Ca^{2+} to phenylephrine but not hypoxia (n=100 cells/group). **P*<0.05 vs. normoxic control using ANOVA with Tukey's post-hoc analysis. **(D)** *Nogo*$^{+/+}$ PASMCs exposed to hypoxia had increased nuclear HIF-1α (red) and Nogo-B (green) levels, as shown by immunofluorescence. HIF-1α colocalization with the nuclear stain DAPI (blue), is shown in pink in the merged panel. Nuclear HIF-1α and Nogo-B levels were decreased

by the ATF6 inhibitor AEBSF in hypoxia-treated *Nogo*$^{+/+}$ PASMCs. *Nogo*$^{-/-}$ PASMCs exposed to hypoxia had similar HIF-1α levels compared to normoxic controls and no detectable Nogo-B levels (n=70 cells/group). $^{*}P<0.05$ vs. normoxia, $^{\#}P<0.05$ vs. hypoxia using ANOVA with Tukey's post-hoc analysis. Mean data are presented in arbitrary fluorescence units (AFU).

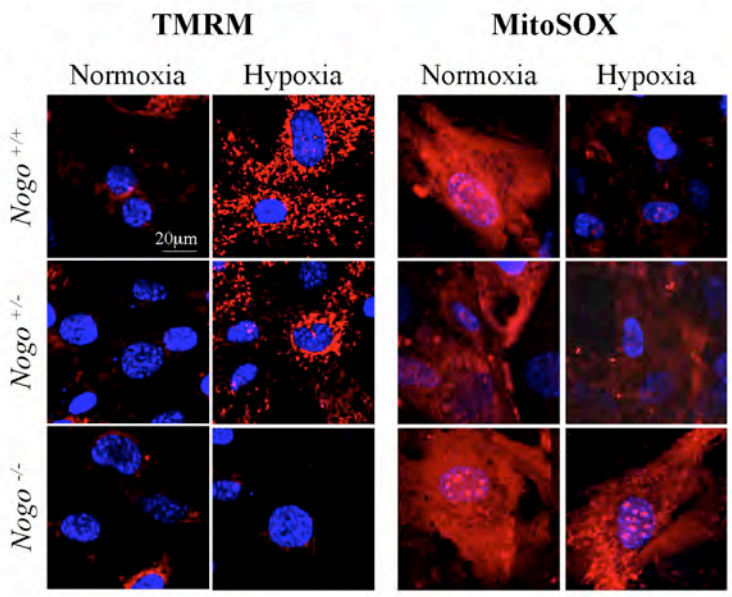

Fig. 3-17. *Nogo*$^{+/+}$ and *Nogo*$^{+/-}$ PASMCs exposed to hypoxia have increased mitochondrial ΔΨm and decreased mROS

Nogo$^{+/+}$ and *Nogo*$^{+/-}$, but not *Nogo*$^{-/-}$ PASMC exposed to hypoxia had hyperpolarized mitochondria (increased red) and decreased mROS production (decreased red) compared to normoxic controls using TMRM staining (left panels; TMRM in red, merged with nuclear stain DAPI in blue) and MitoSOX staining (right panels; MitoSOX in red merged with nuclear stain DAPI in blue), respectively.

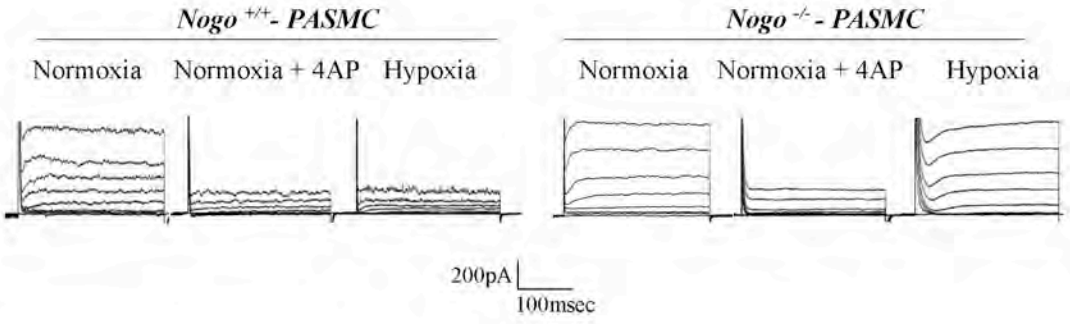

Fig. 3-18. Hypoxia decreases K^+ current in *Nogo*$^{+/+}$ PASMCs

Nogo$^{+/+}$, but not *Nogo*$^{-/-}$, PASMCs exposed to hypoxia had lower whole cell K^+ current than normoxic controls. The outward K^+ current in normoxic *Nogo*$^{+/+}$ and *Nogo*$^{-/-}$, PASMCs was sensitive to 4-aminopyridine (4-AP).

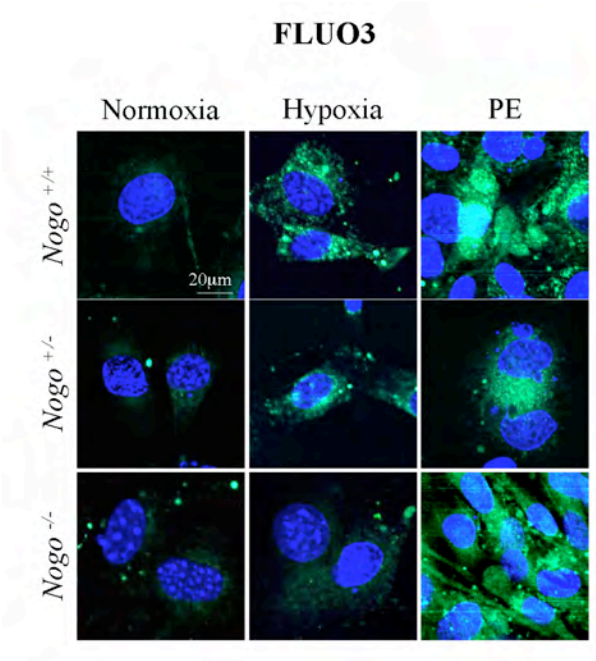

Fig. 3-19. Phenylephrine increases intracellular calcium levels in *Nogo*$^{+/+}$, *Nogo*$^{+/-}$ and *Nogo*$^{-/-}$ PASMCs

Nogo$^{+/+}$ and *Nogo*$^{+/-}$ PASMCs exposed to hypoxia and phenylephrine (PE) had increased intracellular Ca^{2+} as assessed by Fluo3 (green) shown with the nuclear stain DAPI (blue) using confocal microscopy. Intracellular calcium increased with PE but not hypoxia in *Nogo*$^{-/-}$ PASMCs.

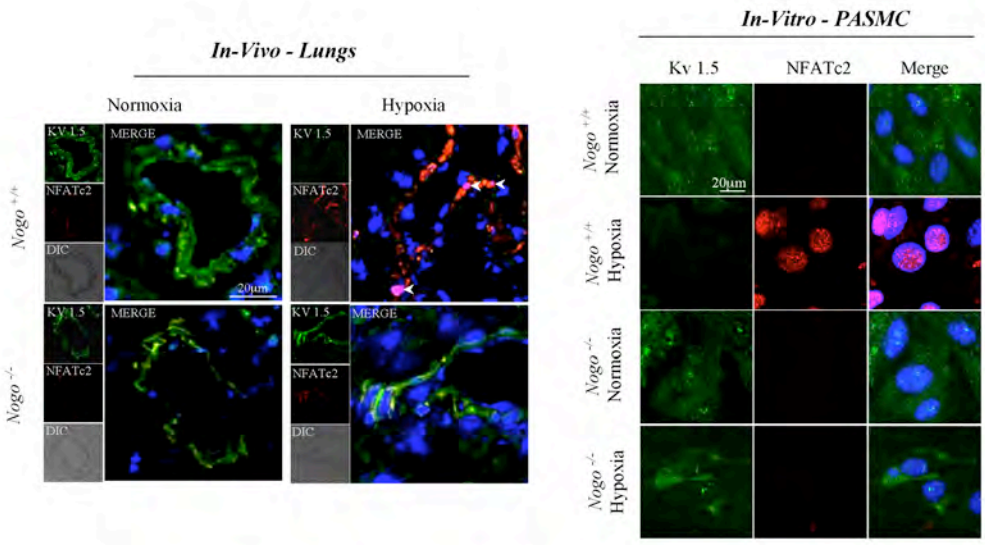

Fig. 3-20. *Nogo*$^{+/+}$ mice exposed to hypoxia have increased activation of NFAT *in-vivo* and *in-vitro*

(Left) Resistance pulmonary arteries from *Nogo*$^{+/+}$, but not *Nogo*$^{-/-}$, mice exposed to chronic hypoxia had increased NFAT (red) and decreased Kv1.5 (green) compared to normoxic controls as shown by immunofluorescence and confocal microscopy. Pulmonary artery morphology is shown in the differential interference contrast (DIC) panel. In the merged panel, NFAT and Kv1.5 are shown with nuclear stained DAPI (blue). (Right) *Nogo*$^{+/+}$, but not *Nogo*$^{-/-}$, PASMCs exposed to chronic hypoxia had increased nuclear NFAT (red) and decreased Kv1.5 (green) compared to normoxic controls. NFAT colocalization with the nuclei, stained with DAPI (blue), is shown in pink in the merged panel.

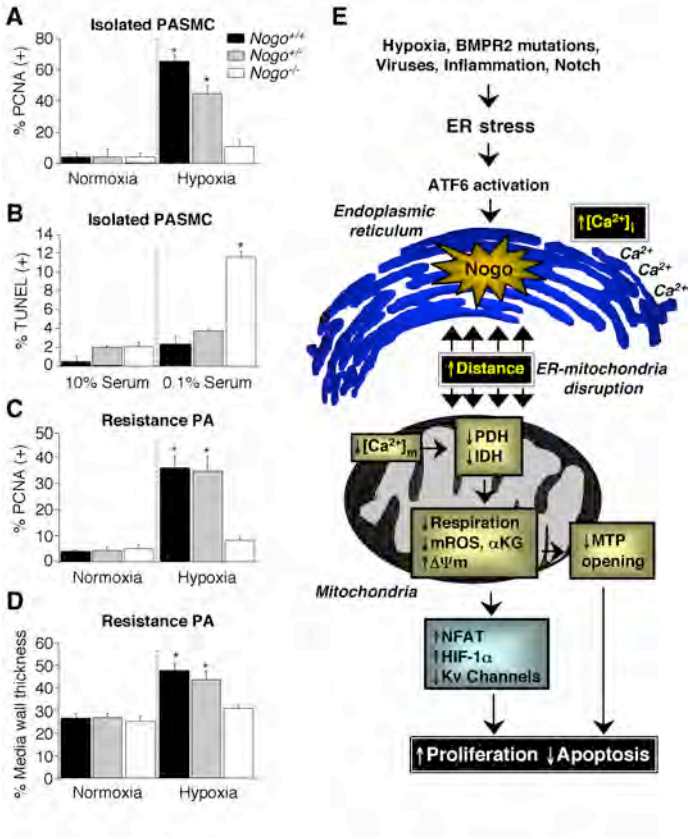

Fig. 3-21. Nogo-B levels correlate positively with the degree of proliferation under hypoxia and the degree of resistance to apoptosis under starving conditions

(A) *Nogo*$^{+/+}$ and *Nogo*$^{+/-}$, but not *Nogo*$^{-/-}$, PASMCs exposed to hypoxia had increased proliferation (%PCNA-positive cells) compared to normoxic controls, using immunofluorescence microscopy (*n*=100 cells/group). **P*<0.05 using ANOVA with Tukey's post-hoc analysis. **(B)** *Nogo*$^{-/-}$, but not *Nogo*$^{+/+}$ and *Nogo*$^{+/-}$, PASMCs exposed to 0.1% serum had increased apoptosis (%TUNEL-positive cells) compared to controls treated with 10% serum, using immunofluorescence microscopy (*n*=100 cells/group). **P*<0.05 vs. controls, using ANOVA with Tukey's post-hoc analysis. **(C)** *Nogo*$^{+/+}$ and *Nogo*$^{+/-}$, but not *Nogo*$^{-/-}$, mice exposed to chronic hypoxia had increased cell proliferation in resistance pulmonary arteries compared to normoxic controls, as shown by %PCNA-positive cells in resistance pulmonary arteries, using immunofluorescence microscopy (*n*=100 cells from 15 PAs/group) **P*<0.05 vs. normoxic control using ANOVA with Tukey's post-hoc analysis. **(D)** *Nogo*$^{+/+}$ and *Nogo*$^{+/-}$, but not the *Nogo*$^{-/-}$ mice exposed to chronic hypoxia had increased %media wall thickness in resistance pulmonary arteries (<300μm) compared to normoxic controls, as assessed by H&E staining and light microscopy. These lungs were obtained from the same mice that underwent hemodynamic assessment in Fig. 3-6 (*n*=40 PAs/group). **P*<0.05 vs. normoxic controls, using ANOVA with Tukey's post-hoc analysis. **(E)** A schematic diagram showing how Nogo links ER stress to mitochondrial function.

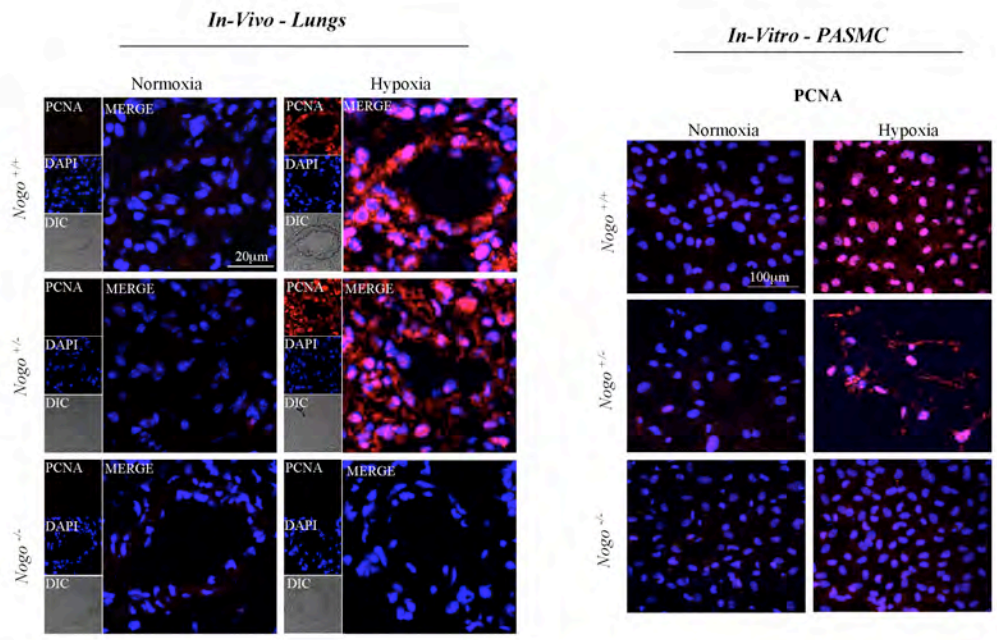

Fig. 3-22. *Nogo*$^{+/+}$ and *Nogo*$^{+/-}$ PASMCs exposed to hypoxia have increased PASMC proliferation *in-vivo* and *in-vitro*

(Left) Resistance pulmonary arteries from *Nogo*$^{+/+}$ and *Nogo*$^{+/-}$, but not *Nogo*$^{-/-}$, mice exposed to chronic hypoxia had increased PCNA (red) compared to normoxic controls as shown by immunofluorescence and confocal microscopy. Pulmonary artery morphology is shown in the differential interference contrast (DIC) panel. In the merged panel, PCNA is shown with the nuclear stain, DAPI (blue). (Right) *Nogo*$^{+/+}$ and *Nogo*$^{+/-}$, but not *Nogo*$^{-/-}$PASMCs exposed to chronic hypoxia had increased nuclear PCNA (red) shown colocalized (pink) with the nuclei stained with DAPI (blue).

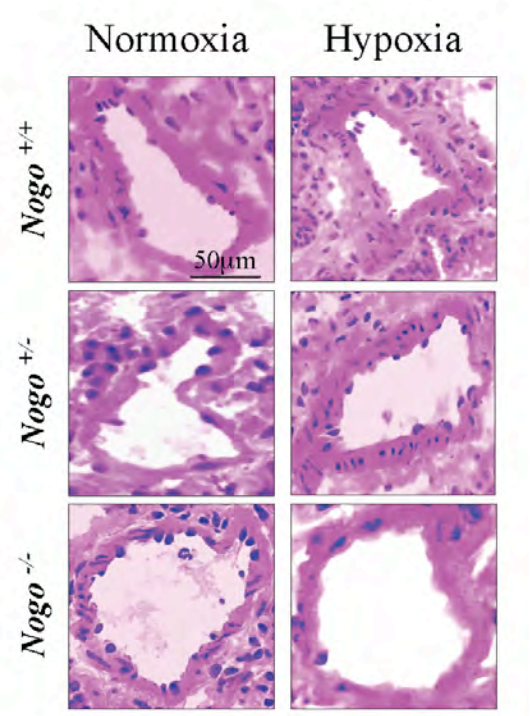

Fig. 3-23. *Nogo*$^{+/+}$ and *Nogo*$^{+/-}$ mice exposed to hypoxia have increased % media wall thickness

Hematoxylin and eosin staining of lungs after exposure to 3 weeks of chronic hypoxia showed a significant increase in the media thickness of resistance pulmonary arteries (<300μm) in *Nogo*$^{+/+}$ and *Nogo*$^{+/-}$ but not the *Nogo*$^{-/-}$ mice.

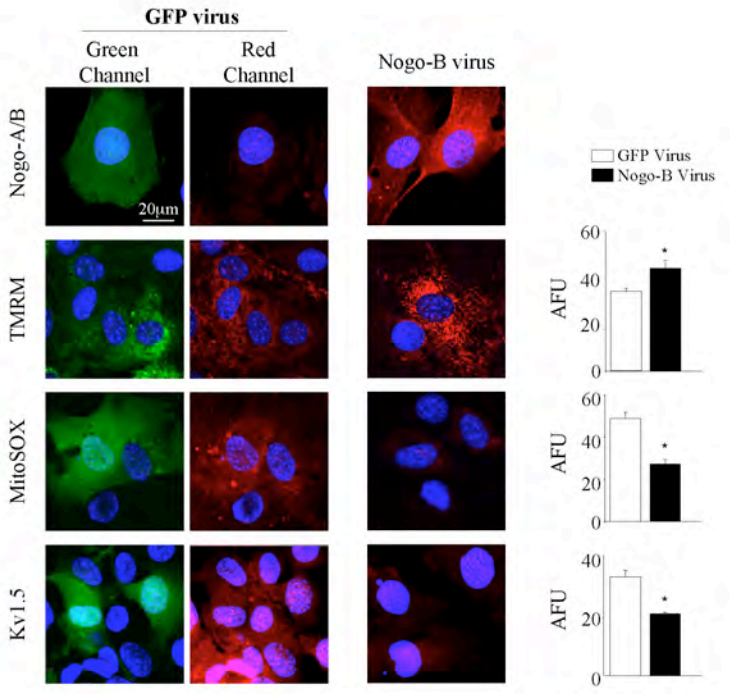

Fig. 3-24. Over-expression of Nogo-B induces a PAH phenotype in normoxic *Nogo*$^{+/+}$ PASMCs

Representative images of Nogo$^{+/+}$ PASMCs infected with a GFP-encoding adenovirus (green, left column showing high infection rate) or a Nogo-B-encoding adenovirus (right column). Compared to GFP-infected cells (middle column) Nogo-B infected cells (right column) had higher Nogo-B levels (red, top row), hyperpolarized mitochondrial membrane potential (TMRM-red, second row), low mROS (MitoSOX-red, third row) and decreased Kv1.5 levels (red, bottom row). (n=40 cells/group). *P<0.01 vs. GFP-infected PASMCs using unpaired Student's t-test. Mean data are presented in arbitrary fluorescence units (AFU).

References

1. McLaughlin VV, Archer SL, Badesch DB, Barst RJ, Farber HW, Lindner JR, Mathier MA, McGoon MD, Park MH, Rosenson RS, Rubin LJ, Tapson VF, Varga J, Harrington RA, Anderson JL, Bates ER, Bridges CR, Eisenberg MJ, Ferrari VA, Grines CL, Hlatky MA, Jacobs AK, Kaul S, Lichtenberg RC, Moliterno DJ, Mukherjee D, Pohost GM, Schofield RS, Shubrooks SJ, Stein JH, Tracy CM, Weitz HH, Wesley DJ (2009) ACCF/AHA 2009 expert consensus document on pulmonary hypertension. Circulation 119: 2250-2294.

2. Macchia A, Marchioli R, Marfisi R, Scarano M, Levantesi G, Tavazzi L, Tognoni G (2007) A meta-analysis of trials of pulmonary hypertension: a clinical condition looking for drugs and research methodology. Am Heart J 153: 1037-1047

3. Macchia A, Marchioli R, Tognoni G, Scarano M, Marfisi R, Tavazzi L, Rich S (2010) Systematic review of trials using vasodilators in pulmonary arterial hypertension: why a new approach is needed. Am Heart J 159: 245-257.

4. Michelakis ED, Wilkins MR, Rabinovitch M (2008) Emerging concepts and translational priorities in pulmonary arterial hypertension. Circulation 118: 1486-1495.

5. Dromparis P, Sutendra G, Michelakis ED (2010) The role of mitochondria in pulmonary vascular remodeling. J Mol Med 88: 1003-1010.

6. Pan JG, Mak TW (2007) Metabolic targeting as an anticancer strategy: dawn of a new era? Sci STKE 2007: pe14.

7. Bonnet S, Archer SL, Allalunis-Turner J, Haromy A, Beaulieu C, Thompson R, Lee CT, Lopaschuk GD, Puttagunta L, Harry G, Hashimoto K, Porter CJ, Andrade MA, Thebaud B, Michelakis ED (2007) A mitochondria-K+ channel axis is suppressed in cancer and its normalization promotes apoptosis and inhibits cancer growth. Cancer Cell 11: 37-51.

8. Michelakis ED, Sutendra G, Dromparis P, Webster L, Haromy A, Niven E, Maguire C, Gammer TL, Mackey JR, Fulton D, Abdulkarim B, McMurtry MS, Petruk KC (2010) Metabolic modulation of glioblastoma with dichloroacetate. Sci Transl Med 2: 31ra34.

9. Sutendra G, Bonnet S, Rochefort G, Haromy A, Folmes KD, Lopaschuk GD, Dyck JRB, Michelakis ED (2010) Fatty acid oxidation and malonyl-CoA decarboxylase in the vascular remodeling of pulmonary hypertension. Sci Transl Med 2.

10. McMurtry MS, Bonnet S, Wu X, Dyck JR, Haromy A, Hashimoto K, Michelakis ED (2004) Dichloroacetate prevents and reverses pulmonary hypertension by inducing pulmonary artery smooth muscle cell apoptosis. Circ Res 95: 830-840.

11. Vander Heiden MG, Cantley LC, Thompson CB (2009) Understanding the Warburg effect: the metabolic requirements of cell proliferation. Science 324: 1029-1033.

12. Voelkel NF, Cool CD, Flores S (2008) From viral infection to pulmonary arterial hypertension: a role for viral proteins? AIDS 22 Suppl 3: S49-53.

13. Li X, Zhang X, Leathers R, Makino A, Huang C, Parsa P, Macias J, Yuan JX, Jamieson SW, Thistlethwaite PA (2009) Notch3 signaling promotes the development of pulmonary arterial hypertension. Nat Med 15: 1289-1297.

14. Hotamisligil GS (2010) Endoplasmic reticulum stress and the inflammatory basis of metabolic disease. Cell 140: 900-917.

15. Sehgal PB, Mukhopadhyay S, Patel K, Xu F, Almodovar S, Tuder RM, Flores SC (2009) Golgi dysfunction is a common feature in idiopathic human pulmonary hypertension and vascular lesions in SHIV-nef-infected macaques. Am J Physiol Lung Cell Mol Physiol 297: L729-737.

16. Sobolewski A, Rudarakanchana N, Upton PD, Yang J, Crilley TK, Trembath RC, Morrell NW (2008) Failure of bone morphogenetic protein receptor trafficking in pulmonary arterial hypertension: potential for rescue. Hum Mol Genet 17: 3180-3190

17. Takahashi K, Adachi K, Yoshizaki K, Kunimoto S, Kalaria RN, Watanabe A (2009) Mutations in NOTCH3 cause the formation and retention of aggregates in the endoplasmic reticulum, leading to impaired cell proliferation. Hum Mol Genet 19: 79-89

18. Smith P, Heath D (1979) Electron microscopy of the plexiform lesion. Thorax 34: 177-186.

19. Michelakis ED, Weir EK (2008) The metabolic basis of vascular oxygen sensing: diversity, compartmentalization, and lessons from cancer. Am J Physiol Heart Circ Physiol 295: H928-H930.

20. L. Sherwood, Kell R (2010) Human Physiology: From Cells to SystemsCengage Learning

21. Voeltz GK, Prinz WA, Shibata Y, Rist JM, Rapoport TA (2006) A class of membrane proteins shaping the tubular endoplasmic reticulum. Cell 124: 573-586.

22. Chen MS, Huber AB, van der Haar ME, Frank M, Schnell L, Spillmann AA, Christ F, Schwab ME (2000) Nogo-A is a myelin-associated neurite outgrowth inhibitor and an antigen for monoclonal antibody IN-1. Nature 403: 434-439.

23. GrandPre TN, F. Vartanian, T. Strittmatter, SM. (2000) Identification of the Nogo inhibitor of axon regeneration as a Reticulon protein. Nature 403: 439-444.

24. Teng FY, Tang BL (2008) Cell autonomous function of Nogo and reticulons: The emerging story at the endoplasmic reticulum. J Cell Physiol 216: 303-308.

25. Acevedo L, Yu J, Erdjument-Bromage H, Miao RQ, Kim JE, Fulton D, Tempst P, Strittmatter SM, Sessa WC (2004) A new role for Nogo as a regulator of vascular remodeling. Nat Med 10: 382-388.

26. Wang H, Yao Y, Jiang X, Chen D, Xiong Y, Mu D (2006) Expression of Nogo-A and NgR in the developing rat brain after hypoxia-ischemia. Brain Res 1114: 212-220.

27. Wright PL, Yu J, Di YP, Homer RJ, Chupp G, Elias JA, Cohn L, Sessa WC (2010) Epithelial reticulon 4B (Nogo-B) is an endogenous regulator of Th2-driven lung inflammation. J Exp Med 207: 2595-2607.

28. Pizzo P, Pozzan T (2007) Mitochondria-endoplasmic reticulum choreography: structure and signaling dynamics. Trends Cell Biol 17: 511-517.

29. Rizzuto R, Duchen MR, Pozzan T (2004) Flirting in little space: the ER/mitochondria Ca2+ liaison. Sci STKE 2004: re1.

30. Szabadkai G, Duchen MR (2008) Mitochondria: the hub of cellular Ca2+ signaling. Physiology (Bethesda) 23: 84-94.

31. Zamzami N, Kroemer G (2001) The mitochondrion in apoptosis: how Pandora's box opens. Nat Rev Mol Cell Biol 2: 67-71.

32. Szanda G, Koncz P, Varnai P, Spat A (2006) Mitochondrial Ca2+ uptake with and without the formation of high-Ca2+ microdomains. Cell Calcium 40: 527-537.

33. Kornmann B, Currie E, Collins SR, Schuldiner M, Nunnari J, Weissman JS, Walter P (2009) An ER-mitochondria tethering complex revealed by a synthetic biology screen. Science 325: 477-481.

34. Vance JE (1990) Phospholipid synthesis in a membrane fraction associated with mitochondria. J Biol Chem 265: 7248-7256.

35. Nadanaka S, Okada T, Yoshida H, Mori K (2007) Role of disulfide bridges formed in the luminal domain of ATF6 in sensing endoplasmic reticulum stress. Mol Cell Biol 27: 1027-1043.

36. Belmont PJ, Tadimalla A, Chen WJ, Martindale JJ, Thuerauf DJ, Marcinko M, Gude N, Sussman MA, Glembotski CC (2008) Coordination of growth and endoplasmic reticulum stress signaling by regulator of calcineurin 1 (RCAN1), a novel ATF6-inducible gene. J Biol Chem 283: 14012-14021.

37. Haze K, Yoshida H, Yanagi H, Yura T, Mori K (1999) Mammalian transcription factor ATF6 is synthesized as a transmembrane protein and activated by proteolysis in response to endoplasmic reticulum stress. Mol Biol Cell 10: 3787-3799

38. Okada T, Haze K, Nadanaka S, Yoshida H, Seidah NG, Hirano Y, Sato R, Negishi M, Mori K (2003) A serine protease inhibitor prevents endoplasmic reticulum stress-induced cleavage but not transport of the membrane-bound transcription factor ATF6. J Biol Chem 278: 31024-31032.

39. Arnaudeau S, Frieden M, Nakamura K, Castelbou C, Michalak M, Demaurex N (2002) Calreticulin differentially modulates calcium uptake and release in the endoplasmic reticulum and mitochondria. J Biol Chem 277: 46696-46705.

40. MacKenzie ED, Selak MA, Tennant DA, Payne LJ, Crosby S, Frederiksen CM, Watson DG, Gottlieb E (2007) Cell-permeating alpha-ketoglutarate derivatives alleviate pseudohypoxia in succinate dehydrogenase-deficient cells. Mol Cell Biol 27: 3282-3289.

41. Bonnet S, Michelakis ED, Porter CJ, Andrade-Navarro MA, Thebaud B, Haromy A, Harry G, Moudgil R, McMurtry MS, Weir EK, Archer SL (2006) An abnormal mitochondrial-hypoxia inducible factor-1alpha-Kv channel pathway disrupts oxygen sensing and triggers pulmonary arterial hypertension in fawn hooded rats: similarities to human pulmonary arterial hypertension. Circulation 113: 2630-2641.

42. Bonnet S, Rochefort G, Sutendra G, Archer SL, Haromy A, Webster L, Hashimoto K, Bonnet S, Michelakis ED (2007) The Nuclear Factor of Activated T cells in Pulmnary Arterial Hypertension can be therapeutically targeted. PNAS 104: 11418-11423.

43. Yuan XJ, Wang J, Juhaszova M, Gaine SP, Rubin LJ (1998) Attenuated K+ channel gene transcription in primary pulmonary hypertension. Lancet 351: 726-727.

44. Weir EK, Lopez-Barneo J, Buckler KJ, Archer SL (2005) Acute oxygen-sensing mechanisms. N Engl J Med 353: 2042-2055.

45. de Brito OM, Scorrano L (2008) Mitofusin 2 tethers endoplasmic reticulum to mitochondria. Nature 456: 605-610.

46. Chin TY, Lin HC, Kuo JP, Chueh SH (2007) Dual effect of thapsigargin on cell death in porcine aortic smooth muscle cells. Am J Physiol Cell Physiol 292: C383-395.

47. Darios F, Muriel MP, Khondiker ME, Brice A, Ruberg M (2005) Neurotoxic calcium transfer from endoplasmic reticulum to mitochondria is regulated by cyclin-dependent kinase 5-dependent phosphorylation of tau. J Neurosci 25: 4159-4168.

48. McMurtry MS, Archer SL, Altieri DC, Bonnet S, Haromy A, Harry G, Bonnet S, Puttagunta L, Michelakis ED (2005) Gene therapy targeting survivin selectively induces pulmonary vascular apoptosis and reverses pulmonary arterial hypertension. J Clin Invest 115: 1479-1491.

49. Yu J, Fernandez-Hernando C, Suarez Y, Schleicher M, Hao Z, Wright PL, DiLorenzo A, Kyriakides TR, Sessa WC (2009) Reticulon 4B (Nogo-B) is necessary for macrophage infiltration and tissue repair. Proc Natl Acad Sci U S A 106: 17511-17516.

50. Rodriguez-Feo JA, Hellings WE, Verhoeven BA, Moll FL, de Kleijn DP, Prendergast J, Gao Y, van der Graaf Y, Tellides G, Sessa WC, Pasterkamp G (2007) Low levels of Nogo-B in human carotid atherosclerotic plaques are associated with an atheromatous phenotype, restenosis, and stenosis severity. Arterioscler Thromb Vasc Biol 27: 1354-1360.

A version of this chapter has been accepted for publication. Sutendra G, Dromparis P, Wright P, Bonnet S, Haromy A, Hao Z, McMurtry MS, Michalak M, Vance JE, Sessa WC and Michelakis ED. The role of Nogo and the mitochondria-endoplasmic reticulum unit in pulmonary hypertension. Sci. Transl. Med. 2011. Jun 22;3(88):88ra55.

Chapter Four

Pyruvate dehydrogenase Inhibition by the Inflammatory Cytokine TNFα Contributes to the Pathogenesis of Pulmonary Arterial Hypertension

Abstract

Pulmonary arterial hypertension (PAH) is a vascular remodeling disease characterized by enhanced proliferation and suppressed apoptosis of pulmonary artery smooth muscle cells (PASMC). This apoptosis resistance is characterized by PASMC mitochondrial hyperpolarization (in part, due to decreased pyruvate dehydrogenase (PDH) activity), decreased mitochondrial reactive oxygen species (mROS), down-regulation of Kv1.5, increased $[Ca^{++}]_i$ and activation of the transcription factor NFAT. Inflammatory cells are present within and around the remodeled arteries and patients with PAH have elevated levels of inflammatory cytokines, including tumor necrosis factor-α (TNFα). We hypothesized that the inflammatory cytokine TNFα inhibits PASMC PDH activity, inducing a PAH phenotype in normal PASMC. We exposed normal human PASMC to recombinant human TNFα and measured PDH activity. In TNFα-treated cells PDH activity was significantly decreased. Similar to exogenous TNFα, endogenous TNFα secreted from activated human $CD8^+$ T-cells, but not quiescent T-cells, caused mitochondrial hyperpolarization, decreased mROS, decreased K^+ current, increased $[Ca^{++}]_i$ and activated NFAT in normal human PASMC. A TNFα antibody completely prevented, while recombinant TNFα mimicked the T-cell-induced effects. *In vivo*, the TNFα-antagonist etanercept prevented and reversed monocrotaline (MCT)-induced PAH. In a separate model, T-cell deficient rats developed less-severe MCT-induced PAH compared to their controls. We show that TNFα can inhibit PASMC PDH activity and induce a PAH phenotype. Our work supports the use of anti-inflammatory therapies for PAH.

Introduction

Pulmonary arterial hypertension (PAH) is a multi-factorial disease that, at its later stages, is characterized by a pro-proliferative and anti-apoptotic diathesis in pulmonary artery smooth muscle cells (PASMC) of the resistant pulmonary arteries (PA). Similar to cancer, PAH PASMCs have a glycolytic phenotype, characterized by increased glycolysis (Gly) and suppressed glucose oxidation (GO)[1-4]. There is now emerging evidence that, by a number of mechanisms, a glycolytic environment promotes a state of apoptosis resistance in both cancer and PAH[1, 5]. The mitochondrial gate-keeping enzyme, pyruvate dehydrogenase (PDH), appears to be critical to this metabolic remodeling in both diseases[3, 4, 6]. PDH regulates the coupling between Gly and GO since it allows the influx of pyruvate (a product of Gly) into the mitochondria, where it is oxidized, completing GO. PDH is tonically inhibited by pyruvate dehydrogenase kinase (PDK) and, while inhibition of PDH shifts metabolism towards Gly and an anti-apoptotic environment, activation of PDH pharmacologically by the PDK inhibitor dichloroacetate (DCA), or molecularly by PDK siRNA, reverses this phenotype[2-4, 6]. The fact that DCA reverses PAH and cancer in several animal models confirms the central role of this enzyme[2-4, 6, 7].

The primary consequence of PDH inhibition includes suppression of mitochondrial function (decreased Krebs' cycle and respiration) which is associated with a mitochondrial hyperpolarization and decreased mitochondria-derived reactive oxygen species (mROS), both of which prevent the opening of the voltage- and redox-sensitive mitochondrial transition pore (MTP), a mega-channel from which pro-apoptotic mediators efflux to induce apoptosis[8]. The decreased mROS inhibits redox-sensitive plasmalemmal voltage-gated K^+ (Kv) channels (like Kv1.5), which control the resting plasma-membrane potential in PASMC[9]. Thus, their inhibition leads to depolarization, opening of the voltage-gated Ca^{++} channels and increase in $[Ca^{++}]_i$, resulting in PASMC

contraction and proliferation[10]. Secondarily, the resulting increase in intracellular K^+ further suppresses apoptosis, since K^+ is a tonic inhibitor of caspases[11].

Another consequence of mitochondrial suppression and the switch towards Gly is the inhibition of the metabolic signaling protein glycogen synthase kinase 3β (GSK3β), which was also recently recognized to play an important role in PAH[4]. When activated, GSK3β phophorylates the voltage-dependent anion channel (VDAC), a component of the MTP[12], preventing its inhibition by the glycolytic enzyme hexokinase-II (HkII)[12]. In other words, GSK3β inhibition will promote VDAC closure, which leads to mitochondrial hyperpolarization (less anions will efflux from the mitochondria via the VDAC) and increases the threshold for MTP opening and apoptosis. Furthermore, inhibition of GSK3β also promotes activation of the transcription factor nuclear factor of activated T-cells (NFAT), which we have previously shown to be activated in PAH and cancer[6, 13]. The activation of NFATc2 causes a down-regulation of plasma membrane Kv channel expression and also promotes mitochondria hyperpolarization, closing a powerful positive feedback[6, 13]. Thus, important features of PAH, like mitochondrial hyperpolarization, decreased mROS, activation of NFAT, inhibition of Kv channels (which all result in resistance to apoptosis) may be secondary to PDH inhibition.

In addition to the metabolic abnormalities, there is strong evidence implicating inflammation in PAH pathology. Human resistance PAs exhibit marked infiltration by many inflammatory cells[14, 15] including T-cells[16]. Moreover, PAH is associated with viral infections, like HIV and HSV[17, 18], and the PAH associated with autoimmune/inflammatory diseases like scleroderma, carries the worst prognosis compared to all other PAH forms[19]. PAH patients have higher serum levels of inflammatory cytokines[14], including tumor necrosis factor-α (TNFα)[20], than healthy or secondary pulmonary hypertension patients. TNFα has been shown to inhibit

myocardial PDH and the resulting metabolic shift is proposed to contribute to the dramatic myocardial dysfunction that characterizes sepsis[21]. We therefore hypothesized that inflammation may worsen or cause PAH through TNFα-mediated inhibition of PDH. We propose that there is a direct link between the inflammatory and metabolic environment in PAH, which could be exploited therapeutically.

Results

4.1. TNFα inhibits PDH activity in normal PASMCs

To determine whether TNFα can directly inhibit PDH, we exposed healthy human PASMCs to recombinant human TNFα (rhTNFα) and measured PDH activity. rhTNFα reduced PDH activity in healthy human PASMCs to levels similar to untreated human PAH PASMCs (Fig. 4-1A). PDH is tonically inhibited by PDK. PDKII is the most ubiquitously expressed isozyme and the one most sensitive to DCA [22]. DCA normalized PDH activity in PAH and rhTNFα treated PASMC to levels comparable to healthy PASMC, suggesting that rhTNFα is inhibiting PDH in a reversible manner (Fig. 4-1A). These effects were mimicked by a PDKII siRNA (Fig. 4-1A, 4-2A), which had no effects on healthy PASMC PDH activity (despite effectively decreasing PDKII expression), suggesting that while PDKII is present, its *activity* may be maximally inhibited in normal PASMC (Fig. 4-2B).

The glycolytic environment that results from PDH inhibition can be associated with inhibition of GSK3β[4] an important regulator of mitochondrial membrane potential ($\Delta\Psi m$) and NFAT. Indeed, healthy human PASMCs exposed to rhTNFα had significantly more phosphorylated (i.e. inhibited) GSK3β (Fig. 4-1B) and HkII-mitochondrial co-localization (Fig. 4-1C).

4.2. $CD8^+$ T-cells inhibits PDH activity and suppresses mitochondrial function in a TNFα−dependent manner in normal PASMCs

To determine whether TNFα produced by activated human immune/inflammatory cells is sufficient to inhibit PDH and induce the cellular PAH phenotype, we co-cultured healthy human PASMCs with activated human $CD8^+$ T-cells, obtained from healthy volunteers, in a Boyden chamber assay. Activated, but not quiescent $CD8^+$ T-cells, caused PASMC mitochondrial hyperpolarization (i.e. increased $\Delta\Psi m$), reduced mROS, increased $[Ca^{++}]_i$ and enhanced proliferation (Fig. 4-3A). Furthermore, activated $CD8^+$ T-cells activated NFAT, resulting in decreased Kv1.5 expression (measured by qRT-PCR and immunocytochemistry) (Fig. 4-3B). Expression of another well-characterized target of NFAT, IL-6, significantly increased, providing additional evidence of NFAT activation (Fig. 4-3B) since normally NFAT decreases the expression of Kv1.5 and increases the expression if IL-6. The effects of activated $CD8^+$ T-cells on mitochondria and $[Ca^{++}]_i$ were blocked by the NFAT inhibitor VIVIT (a competing peptide that inhibits the NFAT-calcineurin interaction) [13](Fig. 4-3A and 4-3B). While co-culture with an antibody to γ-interferon had minimal effects (Fig. 4-4), an antibody to TNFα, which had no effects on normal PASMCs (Fig. 4-5), completely prevented the effects of the activated $CD8^+$ T-cells on PASMC mitochondrial $\Delta\Psi m$, mROS, Kv1.5, $[Ca^{++}]_i$, NFATc2 and proliferation, supporting the concept that the primary effects of $CD8^+$ cells is through secreted-TNFα (Fig. 4-3A, 4-3B). In addition, rhTNFα caused mitochondrial hyperpolarization in a dose-dependent manner (Fig. 4-6) and completely mimicked the effects of activated $CD8^+$ T-cells (Fig. 4-3A, 4-3B, 4-7).

The decrease in mROS and Kv1.5 expression resulted in decreased K^+ current (as measured by whole-cell patch clamping) in healthy human PASMCs co-cultured with activated, but not quiescent $CD8^+$ T-cells (Fig. 4-8A). The effects of $CD8^+$ T-cells on K^+ current were once again reversed with a TNFα-antibody and mimicked with exogenous

rhTNFα (Fig. 4-8A). The majority of the inhibited K^+ current was sensitive to 4-aminopyridine, suggesting it was primarily Kv.

In addition to increased proliferation, activated T-cells induced resistance-to-apoptosis in PASMC. Serum starvation caused increased apoptosis (measured by %TUNEL positive cells) in PASMC; this was inhibited by exposure to activated T-cells, but not by exposure to the control quiescent T-cells (Fig. 4-8B).

4.3. TNFα is expressed in the cytoplasm and mitochondria of PAH PASMCs

Since in T-cells, TNFα expression is driven by NFAT, we speculated that the activation of NFAT may lead to increased levels of TNFα in an autocrine manner in PASMC as well[23]. We found that TNFα was expressed in the cytoplasm of human PAH PASMC both *in vitro* and *in vivo* (Fig. 4-9A, 4-9B). In cultured human PAH PASMC TNFα was expressed in a particulate pattern and some of the TNFα co-localized with mitochondria (co-stained with mitotracker red; Fig. 4-9A). In the PAs of a cohort of 7 patients with iPAH (in which we have previously shown that NFATc2 was activated and Kv1.5 was downregulated in the media[13]), there were variable degrees of infiltration of $CD8^+$ cells (Fig. 4-9B). We found that TNFα was expressed in SMA^+-$CD8^-$ cells (i.e. PASMC), SMA^--$CD8^+$ cells (i.e. $CD8^+$-T-cells) and SMA^--$CD8^-$ cells (i.e. other infiltrating cells and potential sources of TNFα, like macrophages; Fig.4-9B). The induction of TNFα expression in PASMC suggests that, in addition to exogenous, endogenous TNFα could also directly inhibit PDH in the mitochondria and have both autocrine and paracrine effects (i.e. mediated *via* the TNFα receptor in the plasma membrane).

4.4. Etanercept attenuates PAH in monocrotaline-induced PAH animals

We then studied rats that developed PAH after an intra-peritoneal injection of monocrotaline (MCT), a standard PAH model with a strong inflammatory component [24]. MCT-injection resulted in accumulation of $CD8^+$ T-cells around the resistance PAs (<300μm) and elevated levels of serum TNFα (Fig. 4-10A). The accumulation of $CD8^+$ T-cells was often present around PAs at early time points (i.e. between the first and second week post injection), prior to the development of PA medial hypertrophy, suggesting that the T-cell infiltration is an early and not a late event in PAH vascular remodeling (Fig. 4-10A).

We treated MCT-PAH rats with clinically relevant doses of the TNFα inhibitor etanercept [25]. Etanercept therapy was initiated either at the same time as MCT injection (prevention protocol) or 3 weeks later, after PAH is established (reversal protocol). PDH activity was higher *in vivo* in the PAs from etanercept-treated rats compared to the vehicle (saline) treated rats (Fig. 4-10B). Etanercept, in both the prevention and reversal protocol, decreased mean PA pressure (mPAP), pulmonary artery acceleration time (PAAT) and right ventricular hypertrophy (RVH) (Fig. 4-10C, 4-11). The activation of NFATc2 (as assessed by % nuclear localization and decreased expression of its downstream target Kv1.5) in the PA media of vehicle-treated MCT-PAH rats (compared to controls) was prevented and reversed by etanercept therapy (Fig. 4-12A, 4-12B, 4-13). Etanercept treatment, in both protocols, significantly decreased resistant PA vascular remodeling (Fig. 4-12C, 4-14A). The reversal of PA medial thickening was associated with a decrease in proliferation (PCNA expression) and activation of apoptosis (TUNEL) in the reversal protocol (Fig. 4-12D, 4-12E, 4-14B).

4.5. T-cell deficient athymic rats develop less monocrotaline-induced PAH compared to euthymic rats

We then studied a strain of athymic rats that lack mature T-cells ($rnu^{-/-}$) and compared them to their littermate controls (euthymic), which have an intact thymus and

mature T-cells ($rnu^{+/-}$). PAs from euthymic rats with established MCT-PAH had greater inhibition of PDH activity *in vivo* compared to the athymic MCT-PAH PAs (Fig. 4-15A). Euthymic rats developed more severe MCT-induced PAH compared to MCT-PAH athymic rats as assessed by increased mPAP, shorter PAAT, increased RVH and increased resistance PA % medial thickness (Fig. 4-15B, 4-16, 4-17). This was associated with increased activation of NFAT (as assessed by % nuclear localization, decreased expression and downregulation of Kv1.5 and increased expression of IL6) in the PAs of euthymic MCT-PAH rats compared to athymic MCT-PAH rats (Fig. 4-15C, 4-15D, 4-18).

In contrast, when exposed to chronic hypoxia, the euthymic and athymic rats developed similar degrees of pulmonary hypertension, as shown by similar mPAP, PAAT, RVH and PA % medial thickness (Fig. 4-19A). In addition, NFATc2 was activated and Kv1.5 was downregulated in a similar manner between chronic hypoxic euthymic and athymic rats (Fig. 4-19B).

Discussion

Here, we describe a direct and strong link between inflammation, mitochondria and PAH and show for the first time that activated $CD8^+$ T-cells contribute to the pathogenesis of PAH through a TNFα-mediated inhibition of the metabolic enzyme PDH. The TNFα-mediated inhibition of PDH decreases the influx of carbohydrates (pyruvate) into the mitochondria, limiting GO and favoring a switch toward cytoplasmic Gly (Fig. 8). The resulting decrease in mROS as well as the inhibition of GSK3β, results in mitochondrial hyperpolarization, a decrease in Kv current, a subsequent increase in $[Ca^{++}]_i$ and activation of the Ca^{++} and GSK3β-sensitive transcription factor NFATc2. NFATc2 activation potentiates and sustains this phenotype through suppression of Kv1.5

expression. Collectively, all of these changes result in suppressed apoptosis and increased proliferation within the PA wall, a hallmark of PAH (Fig. 4-20).

TNFα has been shown to inhibit myocardial PDH in sepsis [21] but the molecular mechanism of PDH inhibition remains unknown. Classically, TNFα binds the plasmalemmal TNFα receptor, activating transcription factors such as NFκB and the NFAT-cofactor AP-1. TNFα-mediated effects may either inhibit PDH indirectly through downstream signaling from the TNFα receptor or directly through TNFα-mitochondrial interactions, since TNFα expression is induced within the PASMC (Fig. 4-9A). TNFα antibodies would only block the effects of circulating and not endogenously induced TNFα, potentially explaining the only modest PAH in etanercept-treated rats.

The effects of TNFα on the mitochondria and mROS, in addition to the inhibition of Kv channels (Fig. 4-3A, 4-3B, 4-8A) might have additional downstream redox effects. For example, such mitochondria-mROS signals contribute to the normoxic activation of HIF in PAH[26]. HIF increases the expression of PDK in cancer[27] resulting in inhibition of PDH, suggesting another positively reinforcing feedback loop in PAH.

Although there are additional inflammatory cells implicated in PAH, we focused our study to $CD8^+$ T-cells. Our work is in keeping with recent work that showed that intermittent challenge with two different soluble antigens eliciting a $CD4^+$ T-helper type 2 (Th2) response induced severe muscularization in small to medium sized PAs[28]. Others have shown, contradictory to our findings, that T-cells may have a protective role in the development of PAH[14]. However, this was shown in a different model (VEGF receptor antagonist injection in athymic rats) and these inferences remained associative, without a specific mechanism proposed, and no *in vitro* models or appropriate controls (i.e. strain-specific euthymic rats) were used. In addition, it is also possible that depending on the

exact strain of the athymic ($rnu^{-/-}$) animals used there may be differences in their basal immunity, potentially explaining these varied differences. It is quite possible that depending on immunologic stimuli or disease states there may be competing or synergistic signals between $CD4^+$ and $CD8^+$ T-cells.

A recent study showed that etanercept had only a small and non-significant decrease in RV systolic pressure in MCT-induced PAH in Wistar rats[29]. In addition to the difference in the rat strain studied, the authors used 9 fold less (0.03mg/Kg three times a week) etanercept and used an incomplete hemodynamic assessment of the treated rats (i.e. measured RV systolic pressure and not mPAP) potentially explaining these differences. The choice of our dose is based on the dose used in children with rheumatoid arthritis[25]. Furthermore, in a recent case report, the TNFα antibody infliximab reduced pulmonary pressures and improved quality of life in a patient with severe PAH secondary to advanced scleroderma[30].

Our work is in agreement and provides a potential mechanism and explanation to earlier work showing that over-expression of TNFα in transgenic mice causes PAH[31] and is supportive of the emerging theory that inflammation is important in PAH. Other inflammatory cytokine inhibitors, like an IL-1 receptor antagonist, have also been shown to improve experimental PAH, but the mechanism for this was not elucidated[32].

Along with our previous report that NFATc2 inhibition, by the immune-suppressant cyclosporine, reverses rodent PAH[13], our study has a strong and direct translational potential. The greatest benefit for TNFα antagonists may be in PAH associated with autoimmune diseases, particularly those with elevated serum levels of TNFα; this can be easily measured and thus "targeted" clinical trials in patients with high serum TNFα levels are possible. A challenge with this approach however, may be the fact that not all patients with increased TNFα develop PAH. For example, other

inflammatory diseases, like rheumatoid arthritis, where TNFα levels are high, develop PAH much less frequently than patients with scleroderma. The notion that TNFα may, not by itself, be enough to cause PAH is not surprising and is in keeping with the current pathogenesis scheme for PAH, where both genetic predisposition and environmental triggers are required before the disease is expressed. Nevertheless, the recent findings that TNFα levels are high in patients with both familiar and sporadic PAH is in support of the clinical relevance of our work[20].

Finally, our results may also extend beyond PAH, to systemic vascular remodeling, where *in-vivo* blockade of TNFα suppresses neointimal occlusion of coronary arteries, but definitive mechanisms are lacking[33].

One limitation of our study is that we did not measure RV contractility or cardiac output in response to TNFα antagonists. We would predict that an increase in PDH activity and the resulting increase in mitochondrial activity in RVH would increase contractility, since it has previously been shown that an inhibition of PDH by TNFα in sepsis decreases myocardial contractility[21]. The fact that the decrease in mPAP by etanercept was associated with a decrease in PA vascular remodeling suggests that these were effects primarily targeting the pulmonary circulation, leading to the expected secondary regression of RVH. However potential effects of etanercept on the RV, whether beneficial (i.e. increased inotropy) or adverse (i.e. induction of apoptosis) remain unknown and need to be studied before a clinical translation of our findings.

We also did not study the effects of T-cells and TNFα on endothelial cells or other cells within the PA wall, and some of our cells identified as PASMC, based on smooth muscle actin expression, may include fibroblasts or myofibroblasts[34]. However, our work provides a potential link between inflammatory/immune signals and cellular metabolism that may apply to several cell types within the PA wall. For example,

recent data suggest that the PA endothelial cells in PAH have a glycolytic phenotype[35], similar to what we describe in PASMC[1]. In other words, in an inflammatory environment TNFα may inhibit PDH in both PASMC and PA endothelial cells and explain the metabolic remodeling throughout the vascular wall.

Materials and Methods

Cell culture: Human $CD8^+$ T-cells were isolated, maintained and activated as previously described[36]. Briefly, human $CD8^+$ cells were separated from peripheral blood mononuclear cells of healthy donors using the Easy-Sep Human CD8 Positive Selection Kit (Stem Cell Technologies). $CD8^+$ cells were maintained in Royal Park Memorial Institute (RPMI) 1640 medium containing 10% inactivated fetal bovine serum (FBS), beta-mercaptoethanol (10^{-4}M), human recombinant interleukin-2 (60U/mL) and 1% antibiotic/antimycotic (Gibco, Invitrogen, Burlington, ON). $CD8^+$ cells were stimulated with irradiated RPMI 8866 cells. RPMI 8866 cells were maintained in RPMI 1640 medium containing 10% inactivated FBS, beta-mercaptoethanol (10^{-4}M) and 1% antibiotic/antimycotic (Gibco, Invitrogen, Burlington, ON). Resistance PA PASMC freshly isolated from transplant donors and recipients with no pulmonary vascular disease versus idiopathic PAH were handled in an identical manner and maintained as previously described[2], with approval from the University of Alberta Human Ethics Committee.

Boyden chamber Assay: Human $CD8^+$-T-cells (activated/quiescent) were plated in the upper compartment and normal human PASMCs were plated in the lower compartment of a transwell chamber with 0.4μm polycarbonate membrane (Corning Incorporated, Corning, NY) for 48 hours. PASMCs were plated on circular cover slips pre-coated with poly-L-lysine and at the end of the experiment were collected, fixed and stained as described below.

Confocal microscopy*:* Imaging was performed using a Zeiss LSM 510 confocal microscope (Carl Zeiss Canada, Toronto, ON), as previously described[2, 4, 6, 13].

Detection of FITC- was achieved with excitation at 488 nm and detection between 505 to 530 nm. Detection of TRITC- was achieved with excitation at 543 nm and detection between 565 to 615 nm. PCNA (1:50, DAKO, CA); TUNEL (Serologicals, Norcross, GA); NFAT-c2 (1:100, Novus Biologicals, Littleton, CO); Fluo-3 (10μM Molecular Probes, Invitrogen, Burlington, ON); Kv1.5, HkII (both 1:50, Santa Cruz Biotechnology, Santa Cruz, CA); Mitotracker Red (250nM), JC1 (1μg/mL), TMRM (10nM), Mitosox (5μM) (all Molecular Probes, Invitrogen, Burlington, ON); FITC- and TRITC-conjugated secondary antibody (both 1:100, DAKO Canada, Mississauga, ON) were used as previously described[2, 6, 13]. Rat lung sections were prepared and stained with H&E as previously described by a scientist blinded during analysis[2, 6, 13]. Percent of NFAT, PCNA or TUNEL positive cells were measured blindly in 5 random fields/slide; a minimum of 3 slides/experiment was used and 3-5 repetition experiments were typically performed (involving tissues from 3-5 animals/group). All experiments included secondary antibody-only staining, which in all presented experiments showed no signal, supporting the specificity of the antibodies used (see Fig. 4-21). TMRM, JC1, MitoSOX, Fluo3 and Kv1.5 intensity was measured in 5 random fields/slide; a minimum of 3 slides/experiment was used and a minimum of 3 experiments. Fluorescence was quantified as an average of arbitrary fluorescence units (AFU) in individual cells. All the groups were handled in an identical manner allowing the same time for incubation with the dyes and imaging conditions as used previously[2, 4, 6, 13].

Drugs and peptides: PASMCs were pre-incubated with VIVIT, antennapedia (4 μM, ED Biosciences, USA), recombinant human TNFα (0.01, 0.1 and 1μg/mL, Calbiochem, San Diego, CA) and TNFα antibody (2μg/mL, Santa Cruz Biotechnology, Santa Cruz, CA) for 48 hours. They were then fixed and stained as previously described[2, 6, 13]. We used the antennapedia peptide as control to the VIVIT peptide, as previously described[13].

Echocardiography: Pulsed wave Doppler just downstream of the pulmonary valve was used in the parasternal short axis view using the VeVo 770^{TM} imaging system as previously described[2, 4, 13]. Pulmonary artery acceleration time (PAAT) was measured as in clinical echocardiography (PAAT correlates inversely with mean PA pressure).

Electrophysiology: Standard whole-cell patch-clamping was performed on cultured cells as previously described[4, 6, 13].

Immunoblotting: Mitochondria vs. cytoplasmic fractions were separated by differential centrifugation. Briefly, cells were collected and homogenized before an initial centrifugation at 600xg. The supernatant was collected and an additional centrifugation at 7000xg was performed in which the supernatant contained the cytosolic fraction and the pellet containing the mitochondrial fraction. Immunoblotting was performed as previously described with: Kv1.5, HkII, VDACII, and GAPDH, (all 1:500, Santa Cruz Biotechnology, Santa Cruz, CA); GSK3β and PGSK3β (both 1:1000, Cell signaling USA)[3, 4, 6, 13]. The films were digitized and quantified using 1D Image Analysis Software (Kodak, Rochester, NY) and Image J64 imaging software. Expression was normalized to VDACII for mitochondrial fraction and GAPDH for cytosolic fraction to correct for loading differences.

Medial wall thickness: % Medial wall thickness was measured in small (<100μm) and medium (100-300μm) sized pulmonary arteries at the two ends of the shortest external diameter and the average was taken ([2 x wall thickness/external diameter] x 100).

PAH models: Rats were injected with monocrotaline (MCT) (Sigma-Aldrich, St. Louis, MO) and PAH was assessed by echocardiography as previously described[2, 4, 13]. MCT rats were then randomly assigned to Etanercept treatment (0.4 mg/Kg s.c. twice a week) or placebo (saline). For chronic hypoxia induced PAH, rats were placed in a normobaric hypoxic chamber following a short acclimatization phase, as previously described[2, 4].

Right heart catheterization: Rats were anesthetized and catheterized with high-fidelity Millar catheters (microtip 1.4F, Millar Instruments Inc., Houston, TX) as previously described[2, 4, 13]. The catheters were advanced to the PAs and mean PA pressure was recorded using PowerLab/4SP ADconverter (AD Instruments) and measured using Chart 5.4 software (AD Instruments).

PDH Activity: PDH activity was measured using the MitoProfile Dipstick Assay Kit (MitoSciences, Eugene, OR). Protein was collected after cell/tissue was lyzed. Protein (50μL of 1μg/mL) was placed in a 96-well dish and incubated with the dipstick containing the PDH complex antibody and then incubated in the activity buffer, which contained: enzyme/substrate mix, diaphorase and NBT. PDH activity was measured by the intensity of band using a flat top scanner.

Quantitative RT-PCR: Gene expression was analyzed with primers for Kv1.5, interleukin-6 and 18S as a housekeeping gene (all from Applied Biosystems) and expressed using the 2ΔΔCT method, as previously described[3, 6, 13].

Statistics: Values are expressed as the mean±SEM. Unpaired student t-test was used to compare control and treated group. ANOVA was performed with Tukey's test for post-hoc analysis. $P<0.05$ was considered significant (Statview 4.02, SAS Institute, Cary, NC).

Figures

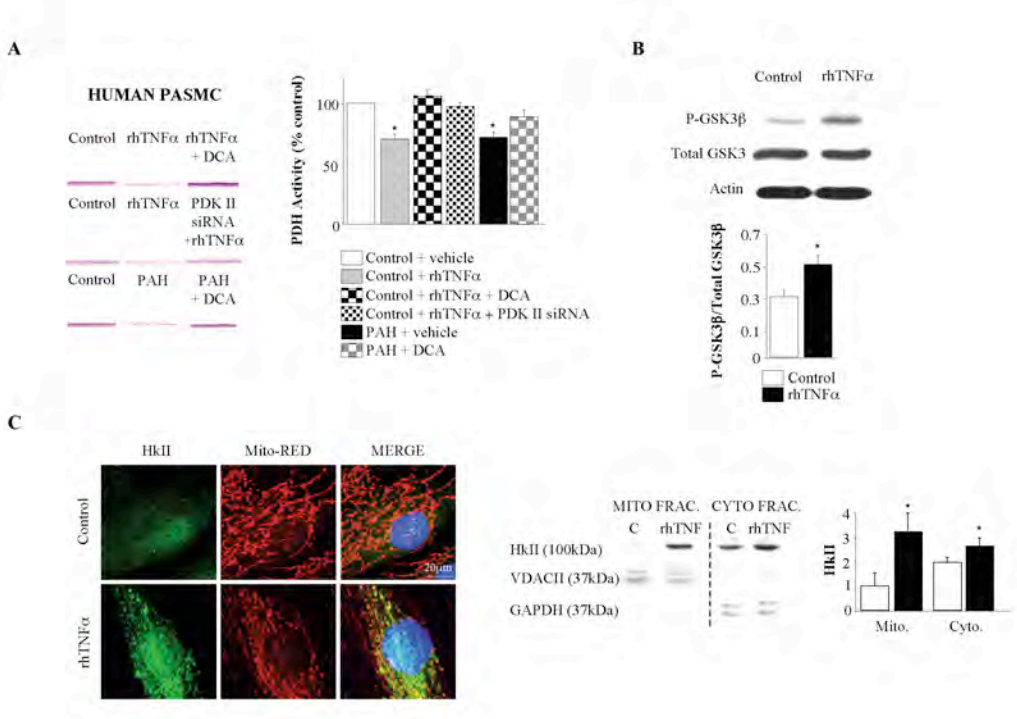

Fig. 4-1. TNFα inhibits PDH activity and decreases GSK3β activity

(A) PDH activity is reduced in both PASMCs exposed to rhTNFα and those isolated from a PAH patient, compared to untreated PASMC from a transplant donor with normal PAs (control). DCA (a PDK inhibitor) and PDKII siRNA completely reversed PDH activity suppression (n=5/group, *p<0.05 vs control). **(B)** Compared to untreated healthy human PASMCs (controls), rhTNFα-treated PASMCS have elevated levels of phosphorylated (inactive) GSK3β (Immunoblot) (n=3, *p<0.05). **(C)** rhTNFα-treated PASMCs also have reduced HkII-mitochondrial association (confocal microscopy Left, Immunoblot Rigt panel, n=3, *p<0.001 vs control).

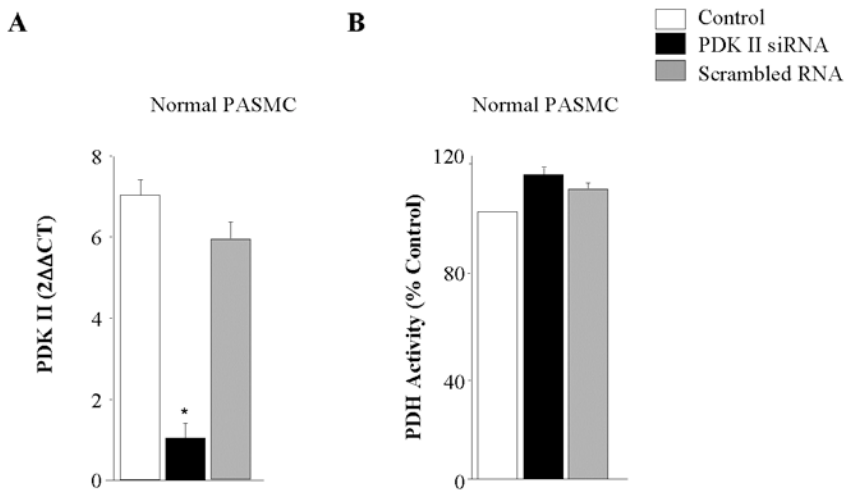

Fig. 4-2. PDKII knockdown does not increase PDH Activity

(A) qrt-PCT analysis of PDKII gene expression. PDKII siRNA effectively knocked down PDKII, whereas scrambled siRNA had no effect. n=3 experiments, *p<0.05 vs control by students t-test. **(B)** PDH activity assay. PDKII siRNA had no effect on PDH activity in healthy PASMCs. Scrambled siRNA also had no effect. n=3 experiments, *p<0.05 vs control by Student's t-test.

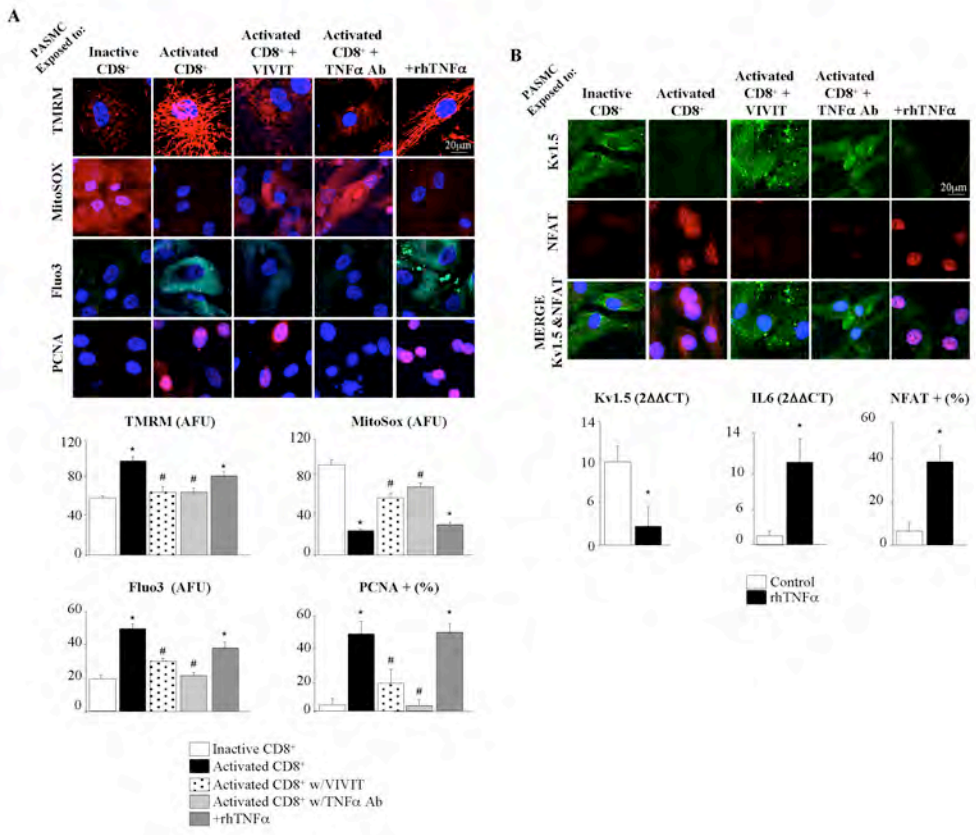

Fig. 4-3. TNFα induces the PAH phenotype *in-vitro*

Compared to quiescent $CD8^+$ T-cell exposure, healthy human PASMCs exposed to activated $CD8^+$ T-cells have; (A) hyperpolarized ΔΨm (measured by TMRM, n=5 experiments, 50 cells/experiment), decreased mROS (measured by MitoSOX, n=5 experiments, 50 cells/experiment), increased $[Ca^{++}]_i$ (measured by FLUO3, n=5 experiments, 50 cells/experiment) and increased proliferation (PCNA expression, n=5 experiments, 50 cells/experiment). (B) increased NFAT activity (% nuclear localization, n=3 experiments, 50 cells/experiment and increased IL6 expression, n=3 experiments) and decreased Kv1.5 expression (n=3 experiments). These effects were reversed by VIVIT (a competing peptide that inhibits NFAT) and a TNFα antibody and mimicked by rhTNFα (confocal microscopy images left, mean data right, *$p<0.001$ vs inactive treated; #$p<0.001$ vs active treated).

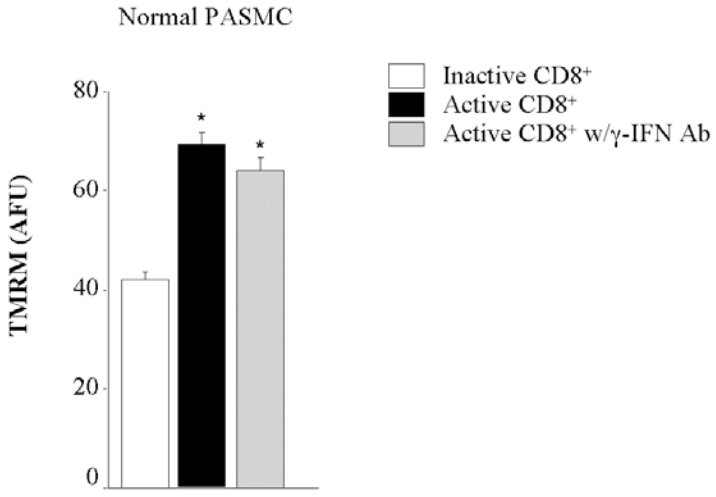

Fig. 4-4. An antibody against γ-interferon does not decrease mitochondrial membrane potential

PASMC exposed to activated $CD8^+$-T-cells displayed mitochondrial hyperpolarization (TMRM) compared to inactive $CD8^+$-T-cells. Treatment of PASMCs with the γ-interferon antibody did not reverse the mitochondrial hyperpolarization induced effects of activated $CD8^+$-T-cells. n=50 cells per group per an experiment, n=3 experiments, *$p<0.05$ by one-way ANOVA (Tukeys post hoc).

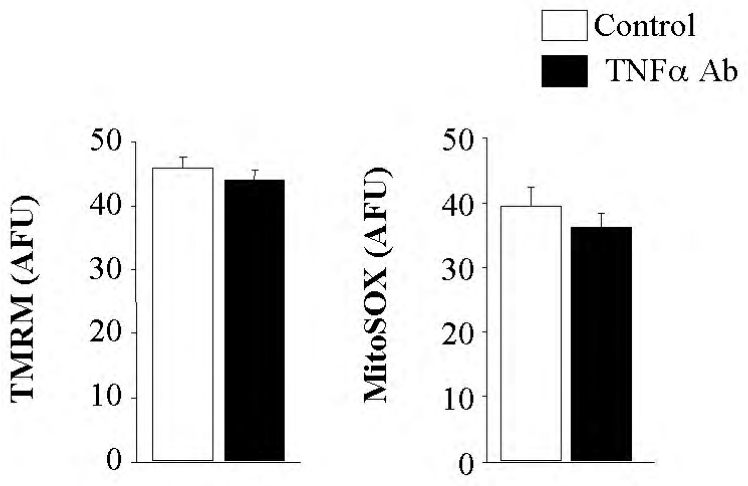

Fig. 4-5. A TNFα antibody does not change mitochondrial function in normal PASMCs

The TNFα antibody (2μg/mL) alone does not change mitochondrial ΔΨm (TMRM) or mitochondrial ROS (mitoSOX) of normal donor PASMCs.

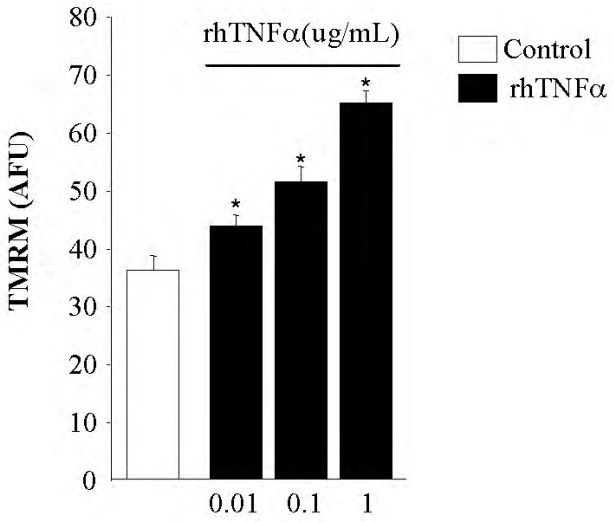

Fig. 4-6. A dose response for rhTNFα on mitochondrial membrane potential

rhTNFα increases mitochondrial ΔΨm (TMRM) in a dose-dependent manner. The dose of rhTNFα used was 0.01, 0.1 and 1 ug/mL. n=3 experiments; 40 cells per experiment from 3 different images; *p<0.05 vs control).

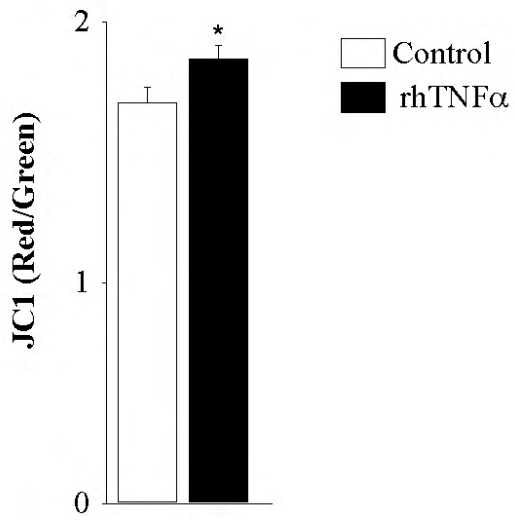

Fig. 4-7. rhTNFα increases mitochondrial membrane potential using JC1

The ratiometic dye JC1 shows that rhTNFα (1ug/mL) significantly hyperpolarizes mitochondrial ΔΨm (n=3 experiments; 40 cells per experiment from 3 different images; *p<0.05 vs control).

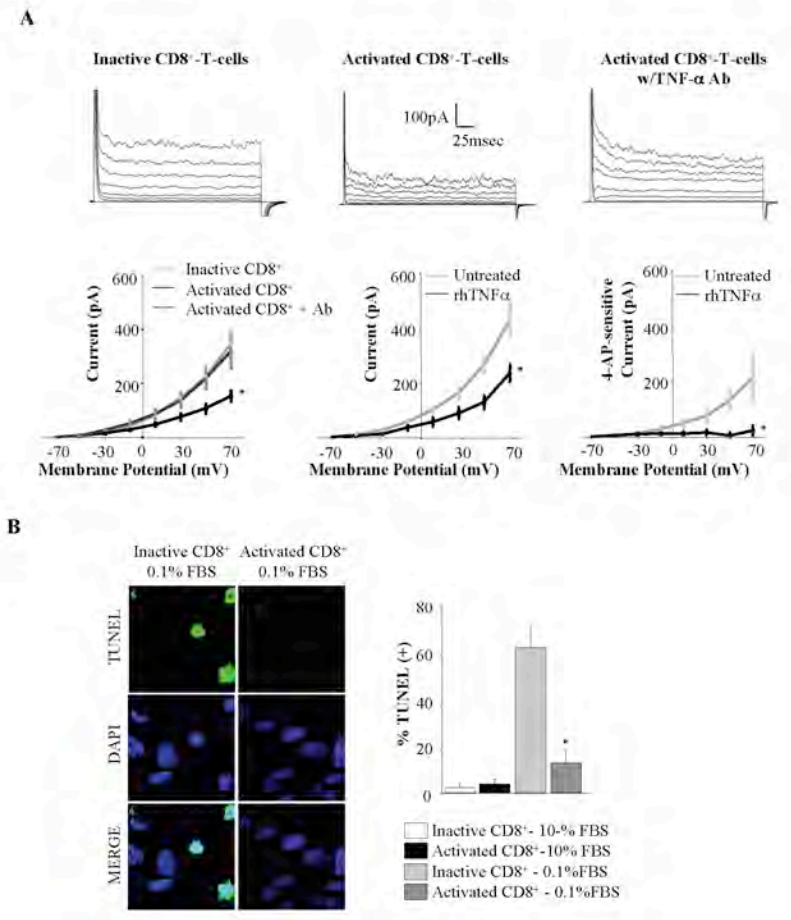

Fig. 4-8. TNFα decreases Kv current and apoptosis resistance

(A) Healthy human PASMCs exposed to $CD8^+$ T-cells and rhTNFα have reduced whole-cell K^+ current, which is reversed by the TNFα antibody (left panel). rhTNFα reduced the whole-cell current to a similar degree with the activated T-cells. The current inhibited by the rhTNFα was 4AP-sensitive, i.e. it was carried by Kv channels (n=8-10 cells per group, *p<0.001 vs inactive treated/untreated). **(B)** Healthy human PASMCs exposed to activated $CD8^+$ T-cells are resistant to serum starvation (0.1 vs 10%) induced apoptosis (TUNEL assay, n=50 cells per group, *p<0.001 vs inactive treated).

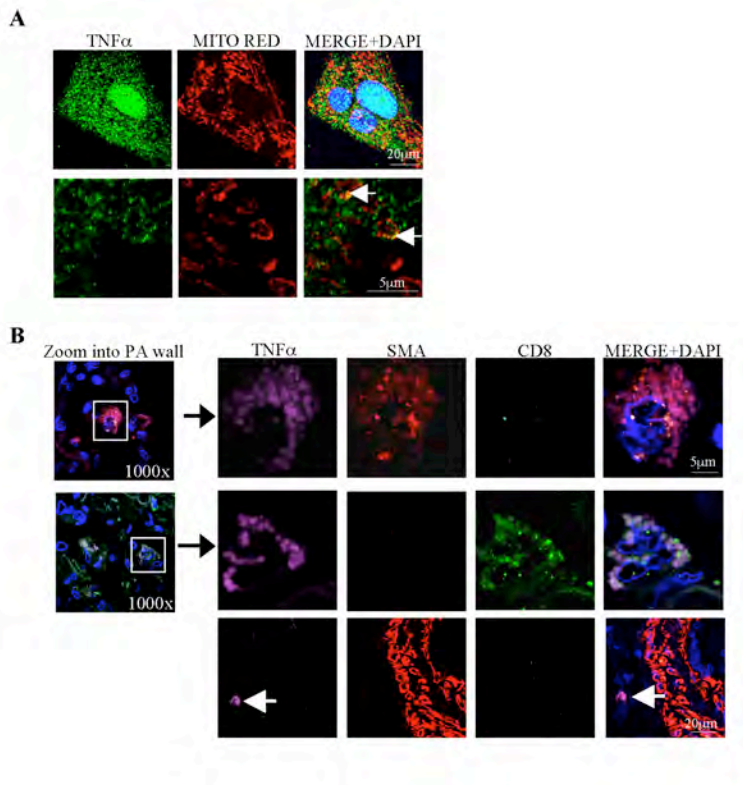

Fig. 4-9. TNFα is expressed in PASMCs both *in vitro* and *in vivo*

(A) TNFα is induced in PAH PASMC *in vitro*. In high magnification confocal images, although most of TNFα (green panel) is in the cytoplasm outside of mitochondria, some also co-localizes with mitochondria (mitoRED in red panel) shown by yellow staining in the merged panel (white arrows). (B) *In vivo* (human PAH tissue), within the PA wall, TNFα (is shown in magenta) is expressed within PASMC (smooth muscle actin, SMA-positive cells), $CD8^+$ cells and other cells (i.e negative for smooth muscle actin or CD8, white arrow in confocal image). Examples of such cells are macrophages, well-known TNFα producers. Nuclei are stained blue with DAPI.

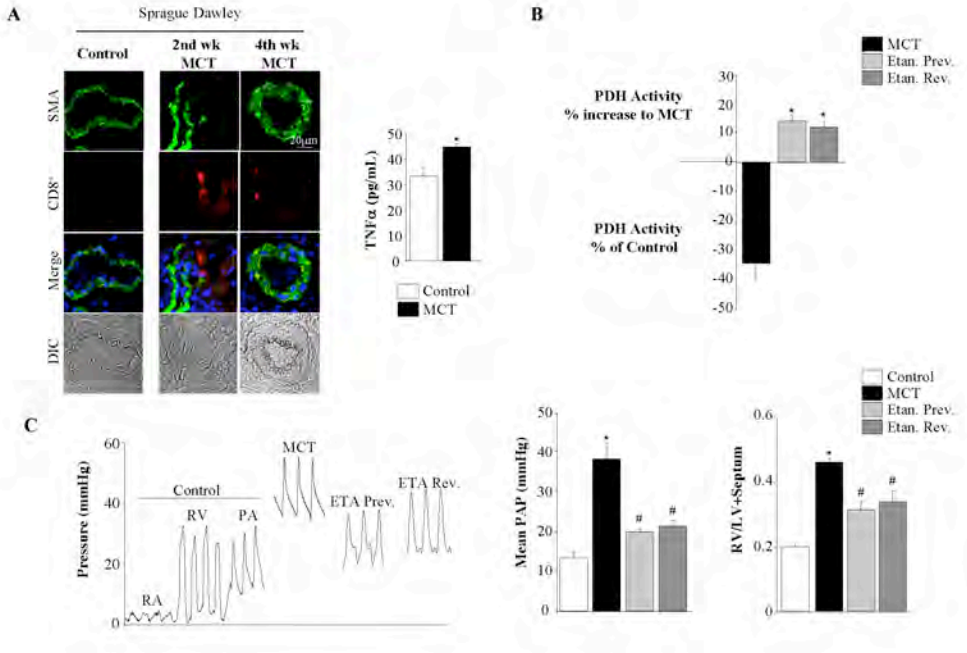

Fig. 4-10. TNFα inhibition with etanercept reverses PAH

(A) Accumulation of $CD8^+$ T-cells around and within the PA wall (left), and elevation of serum TNFα measured by ELISA (right) after MCT-induced PAH, in keeping with MCT being an inflammatory PAH model. There are no $CD8^+$ cells in the PAs of control Sprague Dawley (SD) rats. The middle panel is from an earlier time point (second week post MCT injection, a time that PAH is not significant and significant vascular remodeling is absent) while the right is from a later point (4th week post MCT injection). The presence of $CD8^+$ cells around the PAs prior to significant vascular remodeling suggests that the T-cell infiltration is not a late or secondary event during the PAH development. n=3/group, *p=0.005. **(B)** MCT injection reduced PDH activity in resistance PAs (<300μm). Etanercept prevention and reversal protocols significantly increased PDH activity in MCT-injected SD rats. n=5/group, *p<0.05 vs control. **(C)** Development of MCT-induced PAH as measured by mPAP and RVH. Etanercept treatment in either reversal or prevention protocols significantly attenuated PAH (left; representative hemodynamic tracings are shown). n=8-10 rats per group, *p<0.05 vs group control.

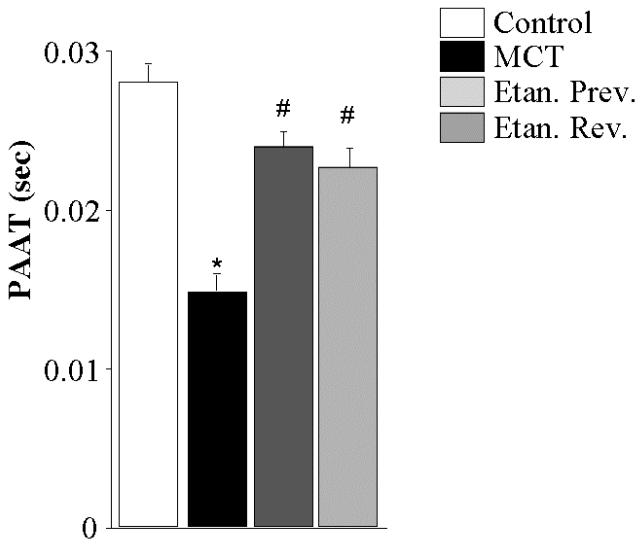

Fig. 4-11. Etanercept treatment increases PAAT

Development of PAH as measured by pulmonary artery acceleration time (PAAT). PAAT was significantly increased in MCT-rats. Etanercept treatment in either reversal or prevention protocols significantly decreased PAAT. These ECHO studies are complimentary to the invasive studies presented in figure 1D and they have the advantage that they were performed in non-anesthetized animals. n=8-10 rats per group, *$p<0.05$ vs control; #$p<0.05$ vs. MCT-injected.

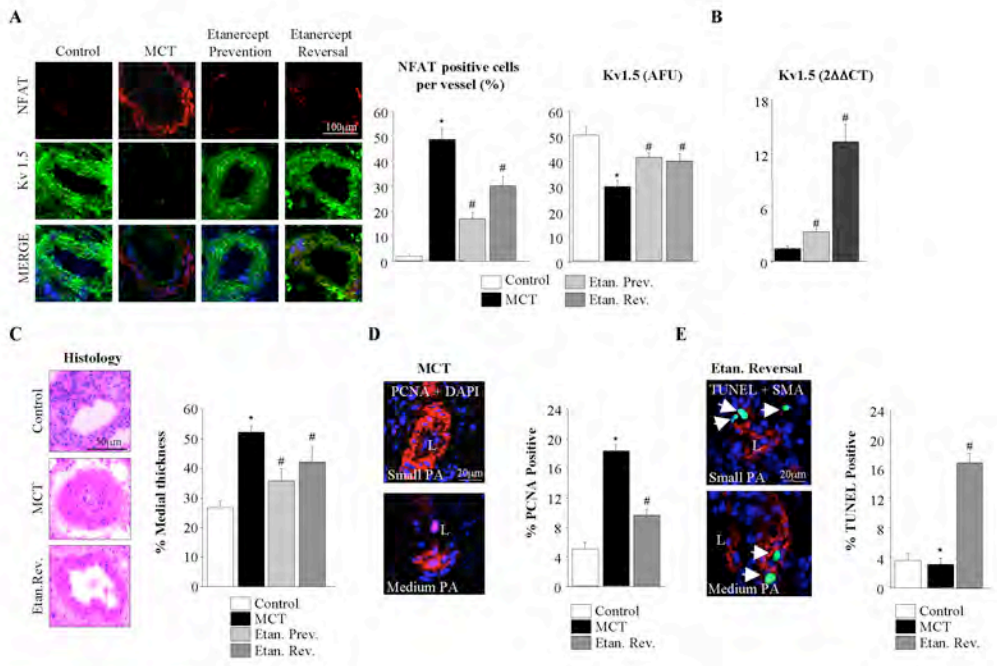

Fig. 4-12. Etanercept reverses PAH vascular remodeling

(A) NFAT activation (nuclear translocation) and Kv1.5 downregulation after MCT injection. Compared to control rats, MCT-PAH rats showed activated NFATc2 (% nuclear localization of cells per vessel) and downregulation of Kv1.5 in resistance PA media. These PAH changes were not present in etanercept treated rats in the prevention or reversal protocol. n=5 animals/group, *p>0.05 vs control; #p<0.05 vs. MCT. **(B)** qRT-PCR shows that Kv1.5 mRNA expression is significantly increased in etanercept treated rats compared to MCT-rats. n=3 animals/group, #p<0.05 vs. MCT. **(C)** Histology images of resistance PAs in control, MCT and etanercept reversal rats with mean data for % medial thickness in resistance PAs (<300μm) are collectively shown. MCT-injected animals developed significantly increased medial wall thickness. Etanercept prevention and reversal attenuated medial wall thickness. n=5 animals/group, *p>0.001 vs control; #p<0.05 vs. MCT. **(D)** Etanercept reversal rats had decreased proliferation (PCNA) in resistance small (<100μm) and medium sized (<300μm) PAs compared to untreated MCT-injected rats. n=5 animals/group, *p>0.001 vs control; #p<0.05 vs. MCT. **(E)** Etanercept administered after established MCT-induced PAH induced apoptosis (TUNEL, green; smooth muscle actin, red). n=5 animals/group, #p<0.05 vs. MCT.

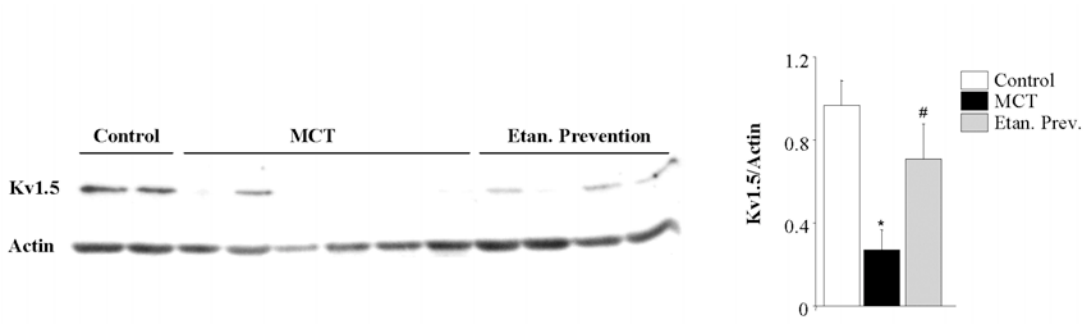

Fig. 4-13. Etanercept treatment increases Kv1.5 protein levels

Immunoblots shows that etanercept treatment (prevention) reverses the downregulation of Kv1.5 that occurs in MCT-vehicle-treated animals. n=3 separate immunoblots with 4-6 rats per group, *p<0.05 vs control; #p<0.05 vs. MCT-injected.

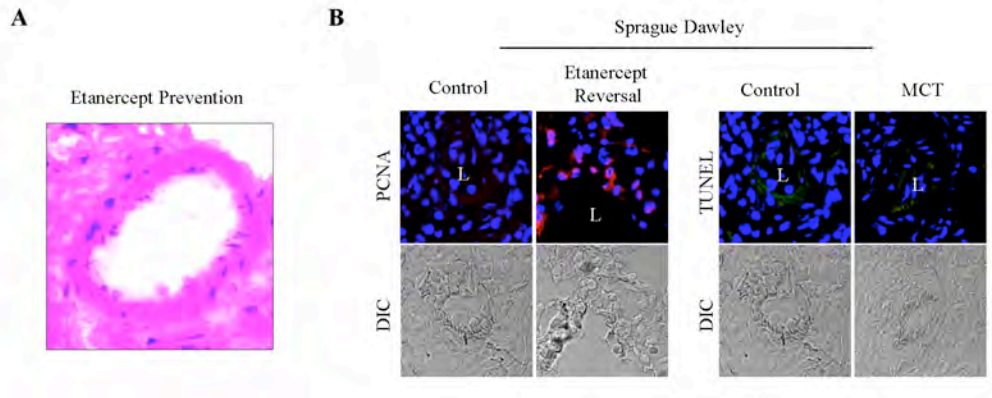

Fig. 4-14. Etanercept treatment decreases medial thickening and proliferation and induces apoptosis of distal pulmonary arteries

(A) Representative H&E image of an etanercept prevention treated lung section. **(B)** Representative immunohistochemistry images with PCNA for control and etanercept reversal animals (left) and TUNEL for control and MCT-treated animals (right). The nuclear stain DAPI is shown in blue.

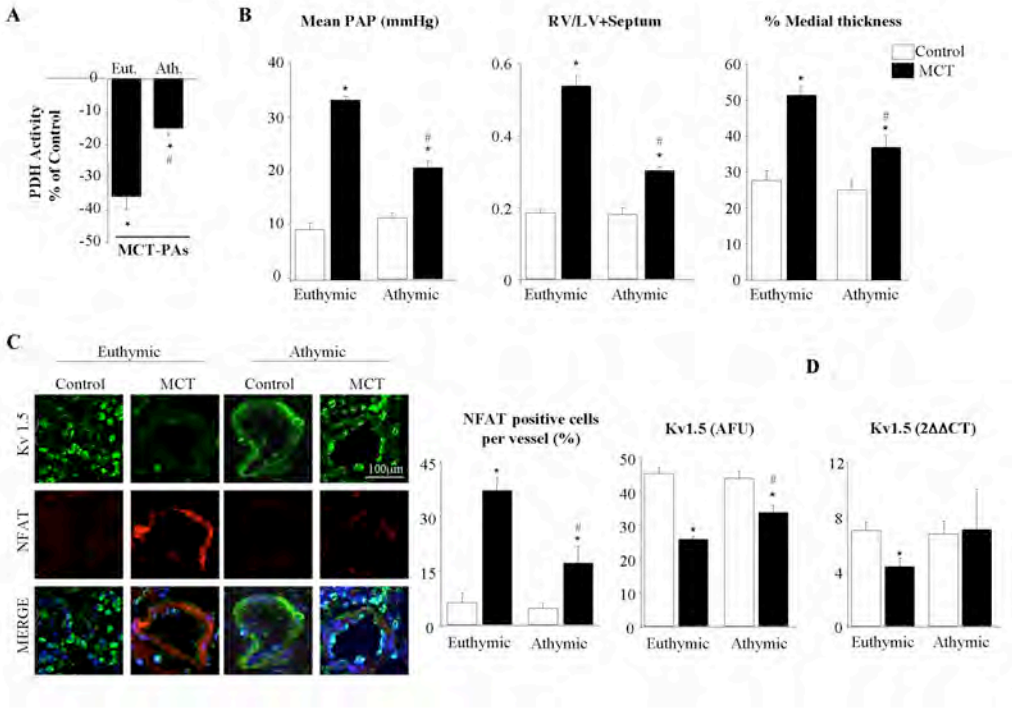

Fig. 4-15. Euthymic rats develop more severe MCT-induced PAH than athymic rats

(A) MCT injection reduced PDH activity in athymic and euthymic rat resistance PAs. MCT-injected euthymic rats have decreased PDH activity compared to MCT-injected athymic rats. *p<0.05 vs control; #p<0.05 vs. MCT-injected euthymic. **(B)** Development of MCT-induced PAH in euthymic and athymic rats, as measured by mPAP, RVH and % medial thickening. MCT injection induced PAH in euthymic and athymic rats. PAH severity was significantly higher in euthymic rats compared to athymic rats. n=8-10 rats per group, *p<0.05 vs control; #p<0.05 vs. MCT-injected euthymic. **(C)** Euthymic rats injected with MCT showed increased NFATc2 activation and Kv1.5 downregulation compared to athymic rats compatible with the fact that they did not develop substantial PAH (n=5 animals per group, *p<0.05 vs control; #p<0.05 vs. MCT-injected euthymic). **(D)** qRT-PCR shows that Kv1.5 mRNA expression is significantly decreased in only the MCT-injected eutymic animals (n=3 animals/group, *p<0.05 vs. control).

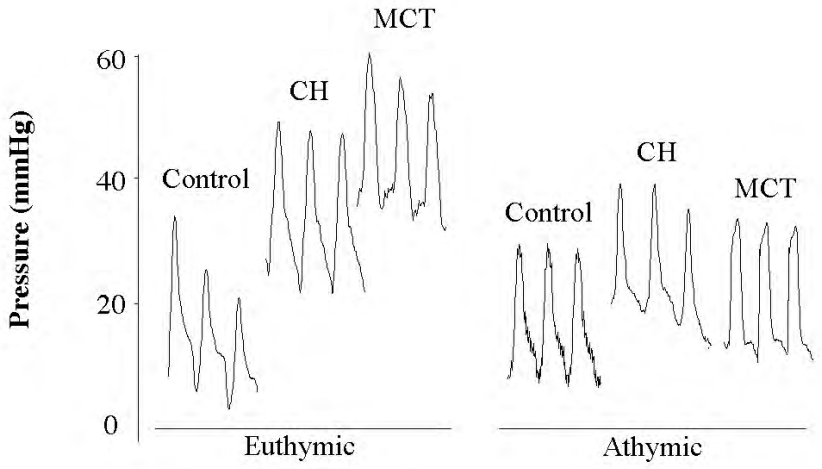

Fig. 4-16. Representative pulmonary artery traces

Traces are representative of pulmonary artery pressures for euthymic and athymic rats. Euthymic MCT rats had increased PA pressure compared to athymic MCT rats, no differences were seen between chronic hypoxic (CH)-euthymic and athymic rats.

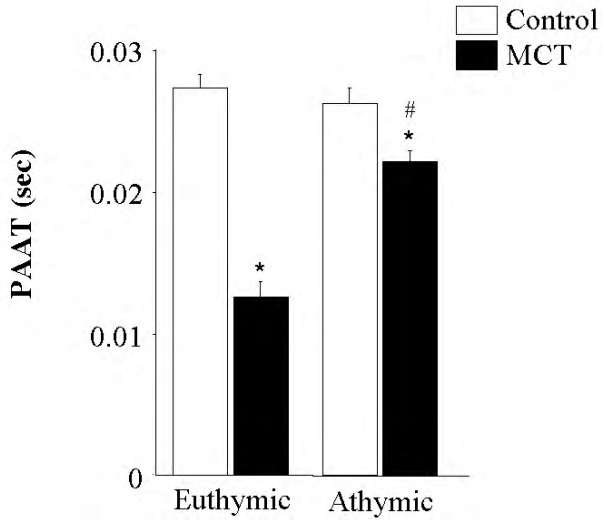

Fig. 4-17. MCT-athymic rats have increased PAAT compared to MCT-euthymic rats Development of PAH as measured by pulmonary artery acceleration time (PAAT). MCT injection caused PAH in euthymic and athymic rats. PAAT was significantly increased in MCT-euthymic vs MCT-athymic rats. n=8-10 rats per group, *$p<0.05$ vs control; #$p<0.05$ vs. MCT-euthymic.

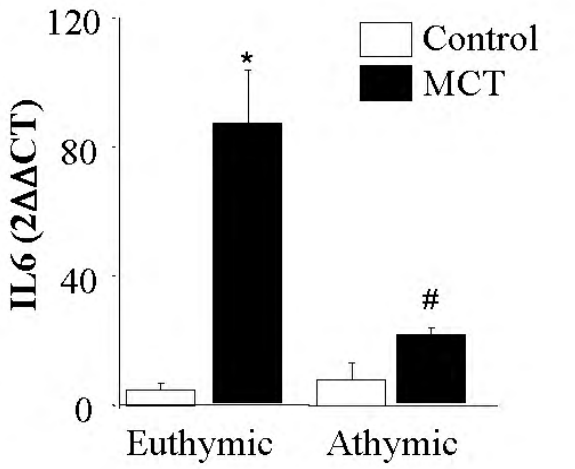

Fig. 4-18. MCT-athymic rats have decreased mRNA levels of IL6 compared to MCT-eutymic rats

NFAT activation was assessed by increased expression of IL6. MCT-euthymic rats had significantly increased IL6 expression in the lungs compared to control rats and MCT-athymic rat lungs. n=3 rats per group, *p<0.05 vs control; #p<0.05 vs. MCT-euthymic.

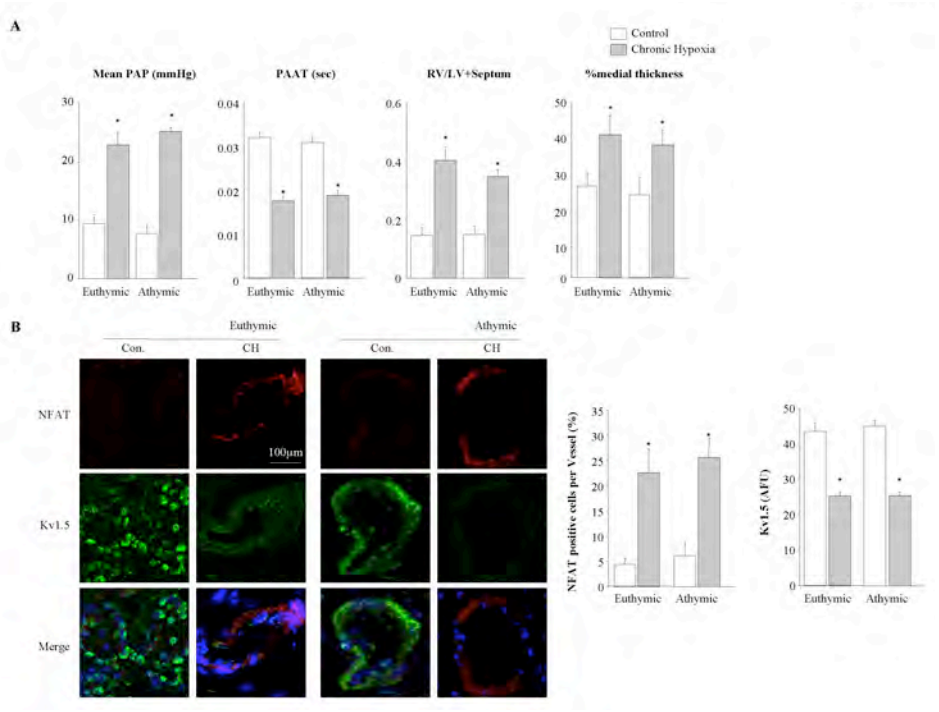

Fig. 4-19. Athymic and euthymic rats develop similar PAH when exposed to chronic hypoxia **(A)** mPAP, PAAT, RVH and %medial wall thickness for athymic and euthymic rats exposed to chronic hypoxia (CH). Euthymic and athymic rats had higher more severe PAH compared to control rats in all parameters studied. n=8=10 rats per group, *p<0.05 vs control by students t-test. **(B)** Immunohistochemistry of distal PAs for euthymic and athymic rats. CH exposure induces NFAT activation and Kv1.5 downregulation, suggestive of the PAH phenotype *in-vivo*.

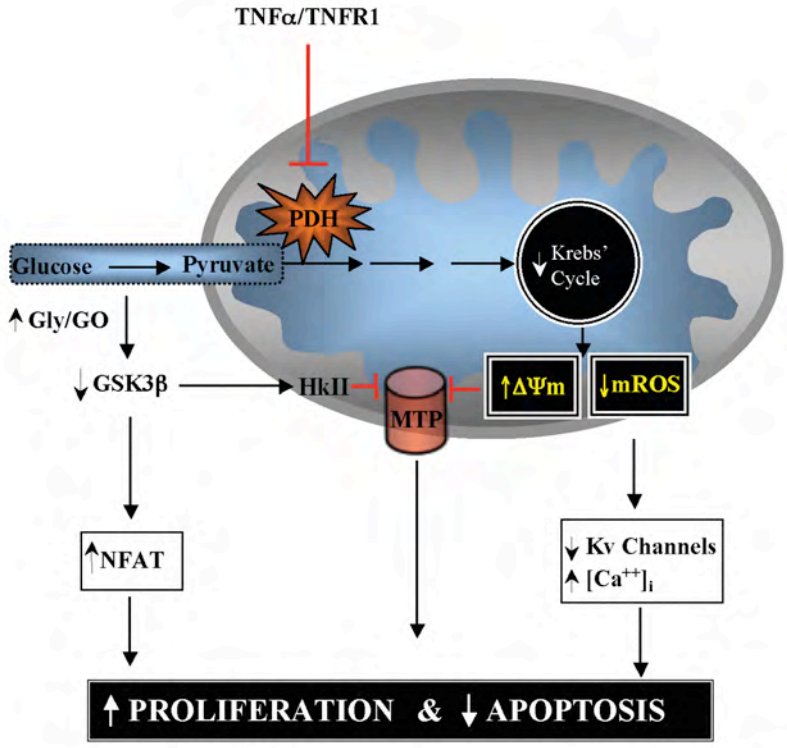

Fig. 4-20. Mechanism of TNFα inducing a PAH phenotype

A mechanism describing how TNFα induces the PAH phenotype. TNFα reduces PDH activity. This results in mitochondrial hyperpolarization and decreased mROS. A decrease in mROS inactivates the redox-sensitive plasmalemal Kv channels (like Kv1.5), which results in plasma membrane depolarization, promoting calcium influx. Elevated intracellular calcium as well as activated GSK3β activates NFAT, which can now suppress Kv1.5 expression and sustain mitochondrial hyperpolarization. The inhibited GSK3β, also directly hyperpolarizes mitochondria. Such positively reinforcing feedback loops might explain the persistence of the PAH phenotype both *in vivo* and *in vitro* and perhaps the difficulty in the treatment of PAH.

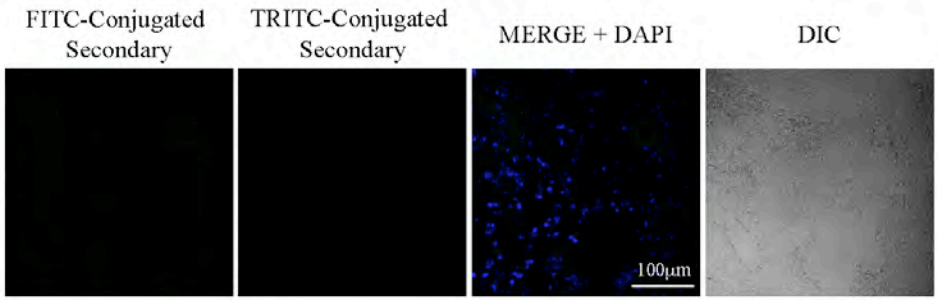

Fig. 4-21. Representative confocal image for secondary only staining

Lack of staining with only the secondary antibody (with either FITC or TRIC conjugated secondary) supports the lack of non-specific staining of these lung tissues. The nuclear stain DAPI is shown in blue.

References

1. Dromparis P, Sutendra G, Michelakis ED (2010) The role of mitochondria in pulmonary vascular remodeling. J Mol Med 88: 1003-1010.

2. McMurtry MS, Bonnet S, Wu X, Dyck JR, Haromy A, Hashimoto K, Michelakis ED (2004) Dichloroacetate prevents and reverses pulmonary hypertension by inducing pulmonary artery smooth muscle cell apoptosis. Circ Res 95: 830-840

3. Michelakis ED, Sutendra G, Dromparis P, Webster L, Haromy A, Niven E, Maguire C, Gammer TL, Mackey JR, Fulton D, Abdulkarim B, McMurtry MS, Petruk KC (2010) Metabolic modulation of glioblastoma with dichloroacetate. Sci Transl Med 2: 31ra34

4. Sutendra G, Bonnet S, Rochefort G, Haromy A, Folmes KD, Lopaschuck GD, Dyck JRB, Michelakis ED (2010) Fatty acid oxidation and malonyl-CoA decarboxylase in vascular remodeling of pulmonary hypertension. Sci Transl Med 2: 44ra58

5. Kim JW, Dang CV (2005) Multifaceted roles of glycolytic enzymes. Trends Biochem Sci 30: 142-150.

6. Bonnet S, Archer SL, Allalunis-Turner J, Haromy A, Beaulieu C, Thompson R, Lee CT, Lopaschuk GD, Puttagunta L, Bonnet S, Harry G, Hashimoto K, Porter CJ, Andrade MA, Thebaud B, Michelakis ED (2007) A mitochondria-K+ channel axis is suppressed in cancer and its normalization promotes apoptosis and inhibits cancer growth. Cancer Cell 11: 37-51

7. Guignabert C, Tu L, Izikki M, Dewachter L, Zadigue P, Humbert M, Adnot S, Fadel E, Eddahibi S (2009) Dichloroacetate treatment partially regresses established pulmonary hypertension in mice with SM22alpha-targeted overexpression of the serotonin transporter. FASEB J 23: 4135-4147.

8. Zamzami N, Kroemer G (2001) The mitochondrion in apoptosis: how Pandora's box opens. Nat Rev Mol Cell Biol 2: 67-71

9. Archer SL, Souil E, Dinh-Xuan AT, Schremmer B, Mercier JC, El Yaagoubi A, Nguyen-Huu L, Reeve HL, Hampl V (1998) Molecular identification of the role of voltage-gated K+ channels, Kv1.5 and Kv2.1, in hypoxic pulmonary vasoconstriction and control of resting membrane potential in rat pulmonary artery myocytes. J Clin Invest 101: 2319-2330

10. Platoshyn O, Golovina VA, Bailey CL, Limsuwan A, Krick S, Juhaszova M, Seiden JE, Rubin LJ, Yuan JX (2000) Sustained membrane depolarization and pulmonary artery smooth muscle cell proliferation. Am J Physiol Cell Physiol 279: C1540-1549

11. Remillard CV, Yuan JX (2004) Activation of K+ channels: an essential pathway in programmed cell death. Am J Physiol Lung Cell Mol Physiol 286: L49-67.

12. Pastorino JG, Hoek JB, Shulga N (2005) Activation of glycogen synthase kinase 3beta disrupts the binding of hexokinase II to mitochondria by phosphorylating voltage-dependent anion channel and potentiates chemotherapy-induced cytotoxicity. Cancer Res 65: 10545-10554

13. Bonnet S, Rochefort G, Sutendra G, Archer SL, Haromy A, Webster L, Hashimoto K, Bonnet SN, Michelakis ED (2007) The nuclear factor of activated T cells in pulmonary arterial hypertension can be therapeutically targeted. Proc Natl Acad Sci U S A 104: 11418-11423

14. Taraseviciene-Stewart L, Nicolls MR, Kraskauskas D, Scerbavicius R, Burns N, Cool C, Wood K, Parr JE, Boackle SA, Voelkel NF (2007) Absence of T cells confers increased pulmonary arterial hypertension and vascular remodeling. Am J Respir Crit Care Med 175: 1280-1289

15. Tuder RM, Groves B, Badesch DB, Voelkel NF (1994) Exuberant endothelial cell growth and elements of inflammation are present in plexiform lesions of pulmonary hypertension. Am J Pathol 144: 275-285

16. Caslin AW, Heath D, Madden B, Yacoub M, Gosney JR, Smith P (1990) The histopathology of 36 cases of plexogenic pulmonary arteriopathy. Histopathology 16: 9-19

17. Cool CD, Rai PR, Yeager ME, Hernandez-Saavedra D, Serls AE, Bull TM, Geraci MW, Brown KK, Routes JM, Tuder RM, Voelkel NF (2003) Expression of human herpesvirus 8 in primary pulmonary hypertension. N Engl J Med 349: 1113-1122

18. Marecki JC, Cool CD, Parr JE, Beckey VE, Luciw PA, Tarantal AF, Carville A, Shannon RP, Cota-Gomez A, Tuder RM, Voelkel NF, Flores SC (2006) HIV-1 Nef is associated with complex pulmonary vascular lesions in SHIV-nef-infected macaques. Am J Respir Crit Care Med 174: 437-445

19. McLaughlin VV, Presberg KW, Doyle RL, Abman SH, McCrory DC, Fortin T, Ahearn G (2004) Prognosis of pulmonary arterial hypertension: ACCP evidence-based clinical practice guidelines. Chest 126: 78S-92S

20. Soon E, Holmes AM, Treacy CM, Doughty NJ, Southgate L, Machado RD, Trembath RC, Jennings S, Barker L, Nicklin P, Walker C, Budd DC, Pepke-Zaba J, Morrell NW (2010) Elevated levels of inflammatory cytokines predict survival in idiopathic and familial pulmonary arterial hypertension. Circulation 122: 920-927.

21. Zell R, Geck P, Werdan K, Boekstegers P (1997) TNF-alpha and IL-1 alpha inhibit both pyruvate dehydrogenase activity and mitochondrial function in cardiomyocytes: evidence for primary impairment of mitochondrial function. Mol Cell Biochem 177: 61-67

22. Bowker-Kinley MM, Davis WI, Wu P, Harris RA, Popov KM (1998) Evidence for existence of tissue-specific regulation of the mammalian pyruvate dehydrogenase complex. Biochem J 329 (Pt 1): 191-196

23. Barath P, Fishbein MC, Cao J, Berenson J, Helfant RH, Forrester JS (1990) Tumor necrosis factor gene expression in human vascular intimal smooth muscle cells detected by in situ hybridization. Am J Pathol 137: 503-509

24. Wilson DW, Segall HJ, Pan LC, Dunston SK (1989) Progressive inflammatory and structural changes in the pulmonary vasculature of monocrotaline-treated rats. Microvasc Res 38: 57-80.

25. Lovell DJ, Giannini EH, Reiff A, Cawkwell GD, Silverman ED, Nocton JJ, Stein LD, Gedalia A, Ilowite NT, Wallace CA, Whitmore J, Finck BK (2000) Etanercept in children with polyarticular juvenile rheumatoid arthritis. Pediatric Rheumatology Collaborative Study Group. N Engl J Med 342: 763-769.

26. Bonnet S, Michelakis ED, Porter CJ, Andrade-Navarro MA, Thebaud B, Bonnet S, Haromy A, Harry G, Moudgil R, McMurtry MS, Weir EK, Archer SL (2006) An abnormal mitochondrial-hypoxia inducible factor-1alpha-Kv channel pathway disrupts oxygen sensing and triggers pulmonary arterial hypertension in fawn hooded rats: similarities to human pulmonary arterial hypertension. Circulation 113: 2630-2641

27. Papandreou I, Cairns RA, Fontana L, Lim AL, Denko NC (2006) HIF-1 mediates adaptation to hypoxia by actively downregulating mitochondrial oxygen consumption. Cell Metab 3: 187-197. 28. Daley E, Emson C, Guignabert C, de Waal Malefyt R, Louten J, Kurup VP, Hogaboam C, Taraseviciene-Stewart L, Voelkel NF, Rabinovitch M, Grunig E, Grunig G (2008) Pulmonary arterial remodeling induced by a Th2 immune response. J Exp Med 205: 361-372

29. Henriques-Coelho T, Brandao-Nogueira A, Moreira-Goncalves D, Correia-Pinto J, Leite-Moreira AF (2008) Effects of TNF-alpha blockade in monocrotaline-induced pulmonary hypertension. Rev Port Cardiol 27: 341-348

30. Bargagli E, Galeazzi M, Bellisai F, Volterrani L, Rottoli P (2008) Infliximab treatment in a patient with systemic sclerosis associated with lung fibrosis and pulmonary hypertension. Respiration 75: 346-349

31. Fujita M, Shannon JM, Irvin CG, Fagan KA, Cool C, Augustin A, Mason RJ (2001) Overexpression of tumor necrosis factor-alpha produces an increase in lung volumes and pulmonary hypertension. Am J Physiol Lung Cell Mol Physiol 280: L39-49

32. Voelkel NF, Tuder RM, Bridges J, Arend WP (1994) Interleukin-1 receptor antagonist treatment reduces pulmonary hypertension generated in rats by monocrotaline. Am J Respir Cell Mol Biol 11: 664-675

33. Clausell N, Molossi S, Sett S, Rabinovitch M (1994) In vivo blockade of tumor necrosis factor-alpha in cholesterol-fed rabbits after cardiac transplant inhibits acute coronary artery neointimal formation. Circulation 89: 2768-2779

34. Stevens T, Phan S, Frid MG, Alvarez D, Herzog E, Stenmark KR (2008) Lung vascular cell heterogeneity: endothelium, smooth muscle, and fibroblasts. Proc Am Thorac Soc 5: 783-791.

35. Xu W, Koeck T, Lara AR, Neumann D, DiFilippo FP, Koo M, Janocha AJ, Masri FA, Arroliga AC, Jennings C, Dweik RA, Tuder RM, Stuehr DJ, Erzurum SC (2007) Alterations of cellular bioenergetics in pulmonary artery endothelial cells. Proc Natl Acad Sci U S A 104: 1342-1347.

36. Atkinson EA, Barry M, Darmon AJ, Shostak I, Turner PC, Moyer RW, Bleackley RC (1998) Cytotoxic T lymphocyte-assisted suicide - Caspase 3 activation is primarily the result of the direct action of granzyme B. Journal of Biological Chemistry 273: 21261-21266

A version of this chapter has been accepted for publication. Sutendra G, Dromparis P, Bonnet S, Haromy A, McMurtry MS, Bleackley RC and Michelakis ED. Pyruvate dehydrogenase inhibition by the inflammatory cytokine TNFα contributes to the pathogenesis of pulmonary arterial hypertension. J Mol Med. 2011 Aug; 89(8):771-83.

Chapter Five

Discussion and Conclusions

Discussion and Conclusions

5.1. Discussion

Current therapies in pulmonary arterial hypertension (PAH) are not selective to the pulmonary circulation and do not address the metabolic complexities associated with this disease (i.e similarities to neoplasia, degenerative diseases and inflammatory diseases). Therefore identifying new targets that would be relatively selective to the pulmonary circulation is critical for evolving therapies in PAH. In chapter 2 of this dissertation we expand on our previous work that mitochondrial suppression is a critical feature in PAH and show that fatty acid oxidation (FAO) may be an important therapeutic target in PAH. Inhibition of FAO either pharmacologically with trimetazidine (TMZ) or by genetic deletion of malonyl-CoA (MCD) in mice resulted in **(1)** increased glucose oxidation (GO) via the "Randle" cycle, **(2)** suppressed hypoxic pulmonary vasoconstriction and **(3)** prevented and reversed chronic-hypoxia (CH)-induced and monocrotaline (MCT)-induced PAH. This study also confirms our previous work that similar to cancer, PAH is associated with decreased mitochondrial function[1-5]. This work also suggests that direct activation of the mitochondrial gate-keeping enzyme pyruvate dehydrogenase (PDH) with dichloroacetate (DCA), which increases GO, may be beneficial to PAH patients. However, this work did not address the underlying factors responsible for the mitochondrial suppression observed in PAH and this was the objective of the next section of this dissertation.

In addition to intrinsic mitochondrial mutations (e.g. cancer), suppression of mitochondrial function can result from disruption of the endoplasmic reticulum (ER)-mitochondria unit. In chapter 3 of this dissertation we provide evidence that many of the triggers associated with PAH, such as inflammation, hypoxia, loss-of-function mutations to BMPRII and viruses are also associated with ER stress. Induction of ER stress results in the activation of the redox-sensitive transcription factor activating-transcription factor

6 (ATF6), which increases the expression of the reticulon protein Nogo. Nogo is a critical protein that can regulate ER shape[6]. Induction of Nogo results in **(1)** increased distance between the ER and mitochondria, **(2)** decreased ER-mitochondrial lipid and Ca^{++} transfer, **(3)** mitochondrial suppression and **(4)** increased proliferation and apoptosis resistance in pulmonary artery smooth muscle cells (PASMCs). Mice with genetic deletion of Nogo were resistant to the development of CH-induced PAH and heterozygous mice developed less severe PAH compared to wild-type mice, suggesting a gene-dose dependent effect of Nogo with PAH.

In chapter four of this dissertation we link inflammation to mitochondrial suppression and the development of PAH. Here, we show that the cytokine tumor-necrosis factor-α (TNFα) caused mitochondrial suppression in PASMCs similar to induction of Nogo (in chapter 3). Antagonizing TNFα pharmacologically with an antibody or the clinically used etanercept (enbrel) resulted in **(1)** increased PDH activity, **(2)** improved mitochondrial function and **(3)** reversed MCT-induced PAH.

5.2. Conclusion

In addition to our previous work with DCA in both PAH [3, 4] and cancer [1, 5], this body of research supports a metabolic paradigm for the etiology of PAH. While primary mitochondrial mutations can result in mitochondrial suppression, this work also emphasizes the importance of ER stress as an additional source for mitochondrial suppression. Therefore, it is possible that all the associated causes for PAH can converge in the ER, resulting in ER stress. Therefore, regardless of the specific cause, targeting this ER-mitochondria unit may prove beneficial as a promising selective therapeutic target in PAH. Potential candidate therapies to increase mitochondrial activity in PAH (summarized in Fig. 5-1) include **(1)** activators of PDH, such as DCA or TMZ, **(2)** inhibitors of ER stress, like 4-phenylbutarate **(3)** inhibitors of Nogo, like anti-Nogo

antibodies and **(4)** inhibitors of inflammatory cytokines, i.e. TNFα inhibitors (e.g. etanercept).

5.3. Future Plans

Currently, DCA is being tried in a Phase I clinical trial for treatment of PAH (NCT01083524) in our center (University of Alberta) in collaboration with Imperial College. In addition, inhibiting ER stress in animal models of PAH is ongoing. Finally, we are currently studying the effects of other inflammatory cytokines on ER stress and mitochondrial function.

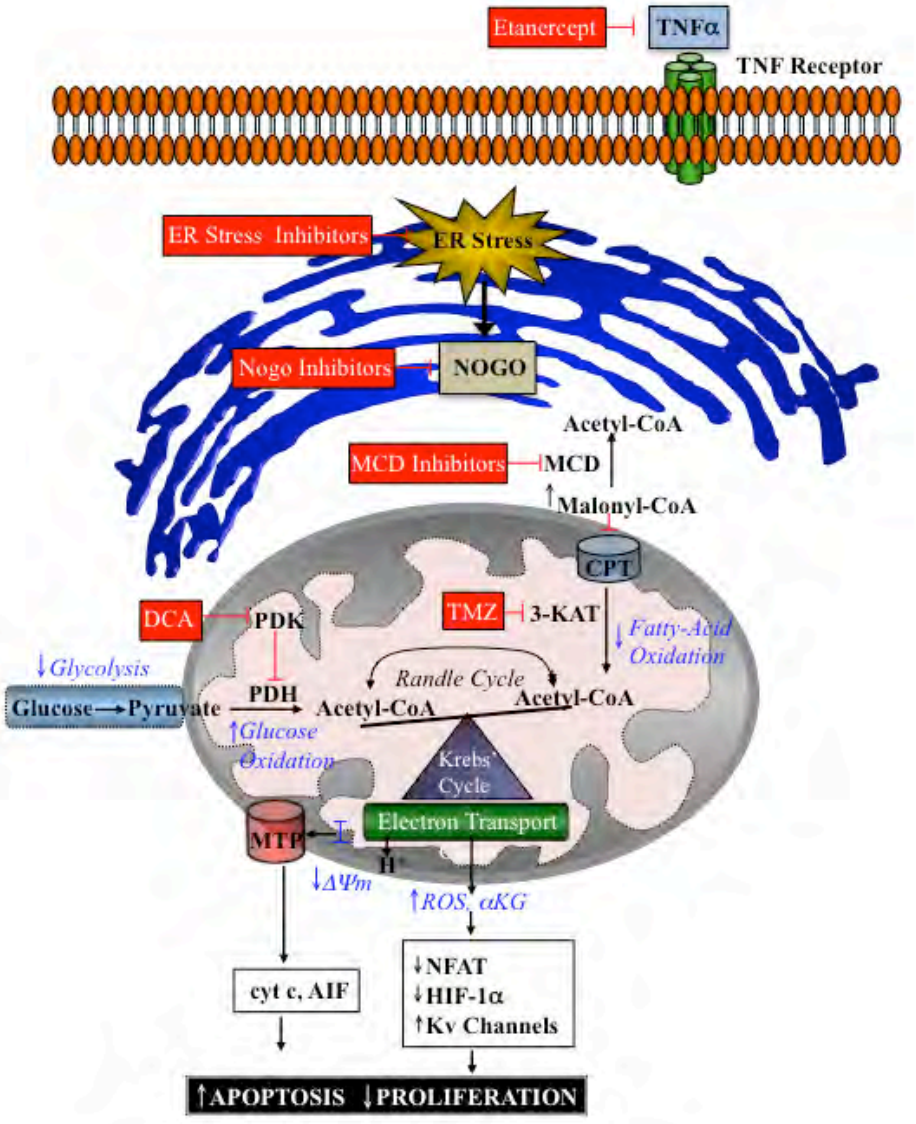

Fig.5-1. Proposed mechanism for potential candidates in PAH therapy

Mitochondrial suppression is a critical feature in PAH pathology. Potential targets to reverse mitochondrial suppression include inhibitors to TNFα, ER stress and Nogo. In addition, drugs that directly activate pyruvate dehydrogenase (PDH), such as MCD inhibitors, DCA and TMZ all would reverse mitochondrial suppression. The downstream effects of all of these targets on mitochondria signaling would lead to reversal of the proliferative and anti-apoptotic diathesis in PAH. TNF; tumor necrosis factor, DCA; dichloroacetate, TMZ; trimetazidine, CPT; carnitine palmityl transferase, MCD; malonyl-CoA decarboxylase, 3-KAT; 3-ketoacyl-CoA-thiolase.

References

1. Bonnet S, Archer SL, Allalunis-Turner J, Haromy A, Beaulieu C, Thompson R, Lee CT, Lopaschuk GD, Puttagunta L, Bonnet S, Harry G, Hashimoto K, Porter CJ, Andrade MA, Thebaud B, Michelakis ED (2007) A mitochondria-K+ channel axis is suppressed in cancer and its normalization promotes apoptosis and inhibits cancer growth. Cancer Cell 11: 37-51

2. Bonnet S, Michelakis ED, Porter CJ, Andrade-Navarro MA, Thebaud B, Bonnet S, Haromy A, Harry G, Moudgil R, McMurtry MS, Weir EK, Archer SL (2006) An abnormal mitochondrial-hypoxia inducible factor-1alpha-Kv channel pathway disrupts oxygen sensing and triggers pulmonary arterial hypertension in fawn hooded rats: similarities to human pulmonary arterial hypertension. Circulation 113: 2630-2641

3. McMurtry MS, Bonnet S, Wu X, Dyck JR, Haromy A, Hashimoto K, Michelakis ED (2004) Dichloroacetate prevents and reverses pulmonary hypertension by inducing pulmonary artery smooth muscle cell apoptosis. Circ Res 95: 830-840

4. Michelakis ED, McMurtry MS, Wu XC, Dyck JR, Moudgil R, Hopkins TA, Lopaschuk GD, Puttagunta L, Waite R, Archer SL (2002) Dichloroacetate, a metabolic modulator, prevents and reverses chronic hypoxic pulmonary hypertension in rats: role of increased expression and activity of voltage-gated potassium channels. Circulation 105: 244-250

5. Michelakis ED, Sutendra G, Dromparis P, Webster L, Haromy A, Niven E, Maguire C, Gammer TL, Mackey JR, Fulton D, Abdulkarim B, McMurtry MS, Petruk KC (2010) Metabolic modulation of glioblastoma with dichloroacetate. Sci Transl Med 2: 31ra34

6. Voeltz GK, Prinz WA, Shibata Y, Rist JM, Rapoport TA (2006) A class of membrane proteins shaping the tubular endoplasmic reticulum. Cell 124: 573-586